

Deliverable 4.1

Report on initial assessments of rock-failure risks for case studies



Organisations	British Geological Survey (BGS), Equinor, Norwegian Geotechnical Institute (NGI), Shell, Geological Survey of Denmark and Greenland (GEUS), Indian Institute of Technology Bombay (IITB), University of Oxford (OX), Alcatel Submarine Networks (ASN), University of Oslo (UiO), NORSAR
Authors	John Williams (BGS), Philip Ringrose, Zoya Zarifi and Nicholas Thompson (Equinor), Kevin Bisdorn (Shell), Tom Kettleby (OX), Susann Wienecke (ASN), Jung Chan Choi and Elin Skurtveit (NGI), Michael Bryld Wessel Fyhn (GEUS), Devendra Narian Singh and Reddi Srinivasa Rao (IITB), Volker Oye (NORSAR, UiO)
Reviewers	Elin Skurtveit and Lars Grande (NGI), Herald Ligtenberg and Kees Hindriks (Shell), Stephen Dee, Rodney Johnston (BP), Daniela Kühn (NORSAR), Malin Torsæter (Equinor), John Hopper (GEUS)
Type of deliverable	Report
Dissemination level	Public
WP	4
Issue date	01 December 2022
Document version	FINAL

Keywords

CO₂ storage, Rock failure, *in situ* stress, seismicity, North Sea, Rajasthan, monitoring

High-level Summary

This report provides an initial assessment of the state of stress and the estimated conditions for rock failure at the study sites being considered in the ACT SHARP Project. The multinational SHARP consortium has the overall objective to improve understanding on:

“Stress history and reservoir pressure for improved quantification of CO₂ storage containment risks”

SHARP Storage is a research project funded under the ERA-NET ACT programme for accelerating Carbon Capture and Storage (CCS). The overall aim is to improve the accuracy of subsurface CO₂ storage containment risk management through the improvement and integration of subsurface stress models, rock mechanical failure and seismicity observations.

In this report we present a preliminary assessment of the state of stress at several case study sites and make initial estimates for tensile and shear failure of reservoirs and caprocks. The intention is to provide an early assessment using currently available data to support research in the SHARP project, and with a view to improving these assessments in future. We refer to this initial work as a ‘round 1’ rock failure assessment. After we have developed novel ways to assess the many aspects of stress and strain in rock systems, we expect to develop updated and improved ‘round 2’ rock failure assessments.

The case studies considered in the ‘Round 1’ rock-failure risks assessment are as follows:

- Norway – Horda/Smeaheia region (mainly released datasets);
- UK Southern North Sea – Bunter storage play (mainly published data, White Rose dataset);
- Netherlands – Aramis site, Rotliegend pre-salt (relatively mature dataset);
- Denmark – Lisa Structure (few wells, more of a ‘greenfield’ site);
- India Rajasthan – Bhagewala Heavy Oil Field (mature field with no CCS assessment).

Before reporting the case study assessments, we present an overview of the scientific and technical challenges involved in making rock failure assessments, which can also act as a general guide for future CO₂ storage studies and site assessments.

The portfolio of case studies described in the report includes a range of potential storage sites with a wide variation in the degree of storage development maturity. While detailed site characterisation and rock failure studies have been conducted for the Horda/Smeaheia region and parts of the UK Southern North Sea (SNS) Bunter storage play, rock failure characterisation studies at the Aramis site and Lisa Structure are limited to regional studies. The Bhagewala Heavy Oil Field in India is the least mature of the case studies considered in the SHARP project. While the field operator has developed extensive understanding of the field throughout its productive history, detailed studies of its CO₂ storage potential are not available in the public domain. As a result, no pre-existing evaluations of the *in situ* stress state, seismicity, rock mechanical properties or rock failure risk are currently available to the SHARP consortium. Where detailed studies are not available, publicly available sources have been used to develop an initial understanding of *in situ* stress and regional seismicity.

One aim of the SHARP project will be to further develop on the initial understanding of rock failure risks outlined in this report.

Table of Contents

1	Scientific Basis	5
1.1	Assessing the state of stress around a site of interest	5
1.2	Making initial estimates for rock failure	7
1.3	North Sea seismicity overview	9
1.4	Summary of conventional site monitoring methods	13
1.4.1	Overview on current state of the art in induced seismicity monitoring	16
1.4.2	Current state of the art in fibre-optic sensing.....	17
1.5	Suggested workflows for initial rock-failure assessments	18
2	State of knowledge at Case Study sites.....	20
2.1	Horda/Smeaheia region	20
2.1.1	Structural and basin setting	20
2.1.2	In situ stress conditions	22
2.1.3	Seismicity data currently available.....	22
2.1.4	Rock failure studies	25
2.2	UK SNS Bunter storage play	28
2.2.1	Structural and basin setting	28
2.2.2	In situ stress conditions	31
2.2.3	Seismicity data currently available.....	35
2.2.4	Mechanical properties.....	38
2.2.5	Rock failure studies	40
2.3	Aramis site	43
2.3.1	Structural and basin setting	45
2.3.2	In situ stress conditions	48
2.3.3	Seismicity data currently available.....	51
2.3.4	Mechanical properties.....	53
2.3.5	Rock failure studies	55
2.4	Lisa Structure.....	57
2.4.1	Structural and basin setting	57
2.4.2	In situ stress and seismicity data	60
2.4.3	Rock mechanics and rock failure	61
2.5	Rajasthan region.....	63
2.5.1	Structural and basin setting	63
2.5.2	In situ stress conditions	65

2.5.3	Seismicity data currently available.....	66
3	Important issues for further work.....	68
4	References.....	72

Corresponding authors

1.	Scientific Basis	
1.1	Assessing the state of stress around a site of interest.....	Philip Ringrose
1.2	Making initial estimates for rock failure.....	John Williams
1.3	North Sea seismicity overview	Tom Kettlety
1.4	Summary of conventional site monitoring methods	Philip Ringrose
1.5	Suggested workflows for initial rock-failure assessments	Elin Skurtveit
2.	State of knowledge at Case Study sites	
2.1	Horda/Smeaheia region	Nicholas Thompson
2.2	UK SNS Bunter storage play	John Williams
2.3	Aramis site	Kevin Bisdom
2.4	Lisa Structure	Michael Bryld Wessel Fyhn
2.5	Rajasthan region	Devendra Narian Singh
3.	Important issues for further work	John Williams
4.	References	

1 Scientific Basis

As a general introduction to the scientific and technical challenges we are addressing in this report, this section reviews the current state of knowledge on:

- How to assess the state of stress around a site of interest;
- How to make initial estimates for reservoir and caprock tensile and shear failure;
- A summary of conventional site monitoring methods.

While most of this discussion concerns the large-scale site setting (reservoir, caprock, structural geology, etc.), some discussion concerns very site-specific well measurements. The issue of scaling between the near-wellbore region and far-field behaviour is beyond the scope of this study, but is an issue warranting further consideration.

1.1 Assessing the state of stress around a site of interest

The geomechanical response to CO₂ injection is a key topic in developing and operating a CO₂ storage project. Key considerations involved are ensuring that significant rock failure is avoided (e.g., fracturing of sealing formations), and ensuring that levels of induced seismicity are kept very low. To set a framework for assessing these issues, we briefly review the principles controlling rock stress and fluid pressures in sedimentary basins. Figure 1 illustrates the main underlying principles.

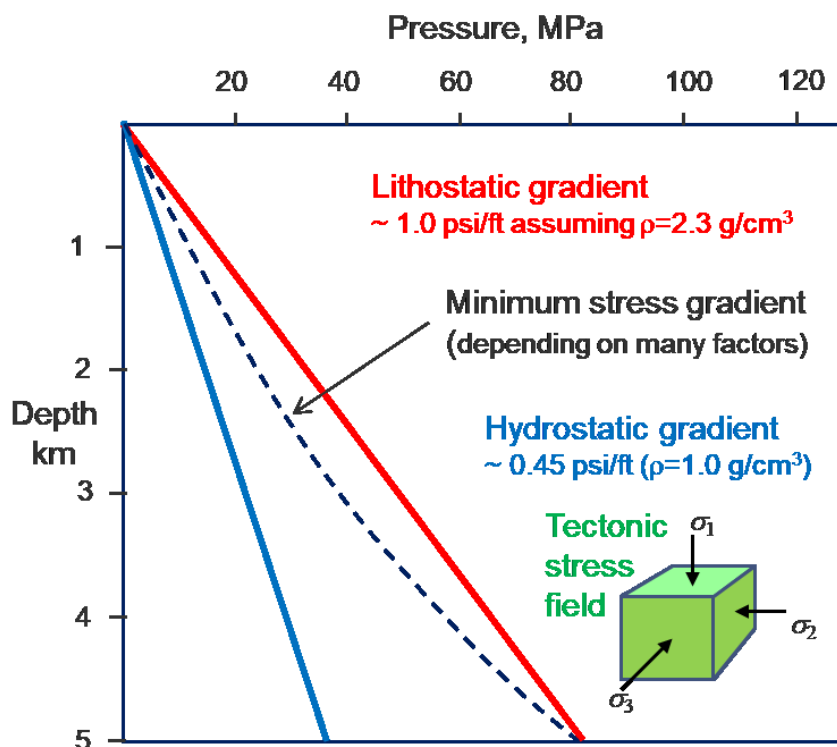


Figure 1. Simple schematic of rock stress and fluid pressure in a sedimentary basin.

The following aspects should be noted:

- Rock stress is mainly controlled by the overburden weight, S_v (which can be estimated from rock density), which in extensional basins is generally equal to the maximum stress vector, σ_1 .

However, this may not be the case in all tectonic settings, particularly where influenced by salt tectonics. The other principal stress components, σ_2 and σ_3 , are determined by the far-field tectonic stresses and the rock strength. In strike-slip tectonic regimes the intermediate stress σ_2 vector is vertical, and in thrust tectonic regimes it is the minimum stress, σ_3 , that is vertical;

- In the shallower parts of sedimentary basins, the fluid pressure is usually in hydrostatic equilibrium, meaning the pressure is equal to the weight of water beneath a reference point close to the earth's surface (i.e. sea level or the water-table level). However, at some depth a situation of overpressure can occur – meaning pressures can become significantly higher than hydrostatic;
- The point at which rocks fracture, often termed the fracture gradient, is related to the minimum stress, σ_3 , controlled by the stress field but also varying with depth in the basin. As rocks become hotter with depth there comes a point where the fracture pressure becomes very close to the maximum stress value (because rocks become less rigid and more plastic at these depths).

A key objective in a CO₂ storage project is to ensure that the injection pressure does not exceed the fracture pressure. While this sounds like a simple objective, determining exactly what the limiting pressure should be can be complicated. Most CO₂ injection projects are likely to target the depth interval of 1–4 km. Projects generally need to be deeper than around 800 m to ensure CO₂ is maintained in the dense phase, and at depths deeper than about 4 km the porosity and permeability of rocks are often too low to maintain sufficiently high rates of injection.

To illustrate the workflow for estimating the state of stress for a CO₂ injection site, Chiaramonte *et al.* (2013; 2015) offer a useful case study (Figure 2). In this example the vertical stress (S_v) is estimated by integrating density logs down to the target injection formation. There is a small uncertainty in this estimate, but it is generally a well-constrained parameter. However, horizontal stresses are much more difficult to estimate. The approach suggested by Chiaramonte *et al.* (2015) is to use available formation tests such as extended leak-off tests (XLOT) to estimate the lower bound for S_{hmin} , and then to use a geomechanical model to estimate an upper bound for S_{Hmax} . The actual magnitude of S_{Hmax} must fall between the magnitude of S_{hmin} and the upper bound S_{Hmax} estimated from the geomechanical model. In their study, the available stress orientation data for the Snøhvit region were also reviewed, including assessment of measurement errors to estimate the likely true variability in stress orientation (Chiaramonte *et al.*, 2015). Subsequently, different scenarios were tested to assess the hydro-fracture or fault leakage potential for different levels of overpressure. The study concluded that fault leakage was unlikely if the injection pressures remained within the operating limits. The workflow adopted offers a useful framework for assessing fault leakage risk within the context of significant uncertainties in stress data, which is typically the case.

Other factors that need to be considered when assessing the state of stress in a storage unit are the effects of temperature changes and geochemical reactions. A thermal stress is caused by heating or cooling of the rock by the injected fluid (CO₂). The thermo-elastic effect can be estimated using rock mechanics theory (see Fjær, 2008). For example, for the Snøhvit injection case, Chiaramonte *et al.* (2013) estimated the thermal stress to be always less than 0.5 MPa if the injected CO₂ is 60–70°C cooler than the formation temperature of 95°C. This thermal stress is much smaller than the poroelastic stress and was therefore not considered to be a significant risk for leakage assessments. In fact, the thermo-elastic effect can be beneficial for improved injectivity by creating small fractures near the wellbore. With regard to possible geochemical effects on fracture risk for CO₂ storage projects, the main issue

to consider is the potential effect of cementation in causing harder and more brittle rocks than would be expected without that cementation. Mostly this effect would be captured by *in situ* measurements of the geomechanical properties of the rock units concerned. However, it is possible that CO₂ injection, via gradual precipitation of carbonate minerals, could alter the rock strength during the injection period. Nguyen et al (2016) have argued that after long periods of CO₂ injection, mineralogical changes could significantly modify the elastic rock properties leading to a lower pressure margin to avoid fracturing. Such long-term geochemical effects may therefore need to be considered in risk assessments.

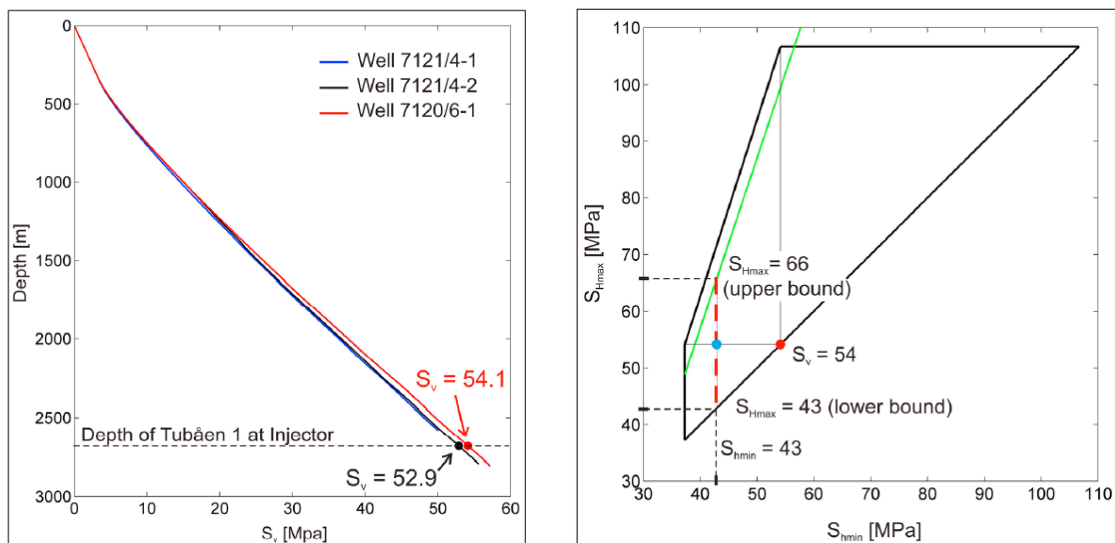


Figure 2. Examples published by Chiamonte et al. (2015) explaining how the stress tensor was estimated for the Snøhvit CO₂ injection site (Tubåen Fm). The left-hand image illustrates vertical stress profiles calculated by integrating density logs from three wells in the vicinity of the injection well. The red and black dots indicate the values of S_v , calculated at the main injection interval depth. The right-hand image is a representation of a stress polygon illustrating the possible magnitudes of S_{Hmax} (red dotted line) for a given value of S_{hmin} (43 MPa) at the top of the reservoir (2683 m), for a given pore pressure (29.6 MPa) and assumed coefficient of friction of 0.6. The green line corresponds to the possible magnitudes of S_{Hmax} as a function of S_{hmin} that is required to generate drilling-induced tensile fractures in a vertical well, considering temperature and mud-weight effects.

1.2 Making initial estimates for rock failure

Mohr circles provide a convenient graphical representation of the state of stress and how it relates to the likelihood of failure for a given set of conditions (Figure 3). The Mohr circle is defined by the magnitudes of the effective principal stresses, with the differential stress ($\sigma_1 - \sigma_3$) determining the size of the circle. Each point on the circle therefore represents the magnitudes of the normal and shear stress components acting on the rotated coordinate system. Changes to pore pressure resulting from injection or production activities modify the effective normal stress, moving the Mohr circle along the X-axis of the diagram. During CO₂ injection, a pore pressure increase is generally expected, which would shift a Mohr circle towards the left of the chart. Poroelasticity can also lead to changes in the magnitude of the horizontal stresses, such that the size of the Mohr circle may increase or become

reduced (Figure 3b). The degree of poroelastic coupling will determine the stress path, which can be illustrated by the common tangent of the Mohr circles shown in Figure 3b.

Poroelastic effects are generally limited to the injection reservoir which experiences the majority of the pressure change and can be estimated from Biot's coefficient (α) and Poisson's ratio (ν) using a simple analytical equation (Equation 1, after Brown *et al.*, 1994; Streit and Hillis, 2004).

$$\Delta S_{Hor} = \alpha \frac{(1-2\nu)}{(1-\nu)} \Delta P_p \quad \text{Equation 1}$$

Where ΔS_{Hor} is the change in horizontal stress magnitude and ΔP_p is the change in pore pressure.

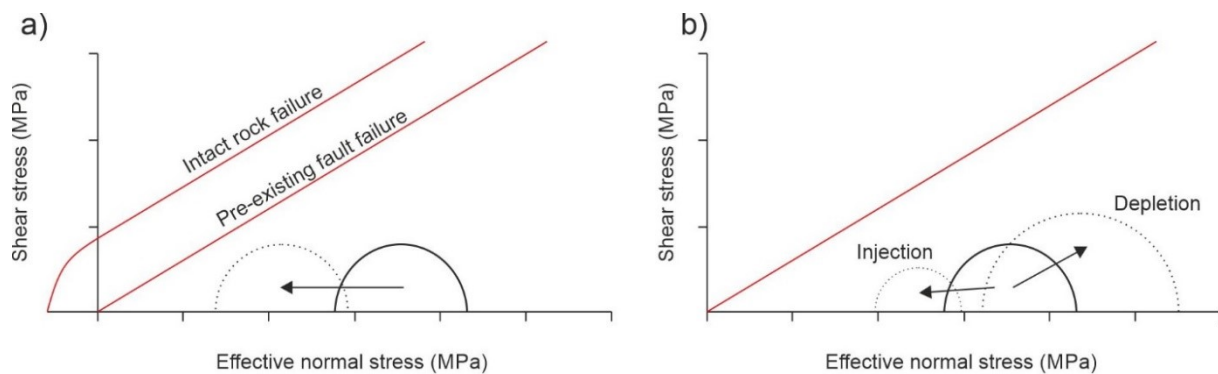


Figure 3. (a) Illustration of Mohr Coulomb diagram representing state of stress and failure envelopes. (b) Mohr Coulomb diagram illustrating common poroelastic stress changes resulting from injection and production activities. See Orlic (2016) for a discussion on geomechanical impact of CO₂ storage in depleted reservoirs. BGS © UKRI (2022).

Rock failure can be expected if the Mohr circle contacts the failure envelope for the material in question. The failure envelope provides a simple constitutive model delineating between areas of stable (to the right) or unstable (to the left) states of stress for a given material. The intact rock failure envelope illustrated in Figure 3a suggests that rock failure is most likely to occur in tension, as the illustrated Mohr circle is small enough that it can only contact the failure envelope in a scenario with negative effective normal stress. This scenario is likely to represent the likely failure mode for intact reservoir rocks in extensional CO₂ storage settings, because poroelastic effects are likely to reduce the differential stress as shown in Figure 3b. A strong poroelastic response will therefore limit the potential for shear failure. The pre-existing fault failure envelope shown in Figure 3a is representative of a cohesionless fault material. Contact of the Mohr circle with this failure envelope would result in shear failure, or reactivation of the existing fault. Faulted materials may not necessarily exhibit zero cohesion, so this failure envelope represents a worst-case (weak) scenario in which pre-existing faults would be expected to be the primary mode of rock failure (i.e. the Mohr circle will contact the pre-existing fault failure envelope before it can exceed the strength of the intact rock).

The Mohr Coulomb model can therefore be used to provide initial failure estimates using available information or assumptions on the *in situ* stress field as defined using methods outlined in the previous section. An example of such an approach using stress magnitude gradients derived from compilation of regional leak-off test datasets is presented by Williams *et al.* (2014). While this approach can provide an initial first-look, site-specific rock property variations are neglected. As such, initial models should be refined as further data and information becomes available. Further studies that consider poroelastic, thermo-mechanical models, geochemically-induced changes to mechanical properties,

and coupled flow-geomechanical modelling should be used to inform risk assessments as projects mature.

1.3 North Sea seismicity overview

The North Sea is located in a relatively stable tectonic environment. It is far (>1500 km) from the North Atlantic plate boundary, and the African-Eurasian plate boundary is 700 km to the south. Large scale tectonic stress patterns are controlled primarily by post-glacial rebound and ridge push forces from these two distant tectonic plate boundaries. As a result, measures of seismic hazard (e.g., earthquake recurrence rates, peak ground velocity/acceleration) in the region are relatively low when compared to more tectonically active regions globally, though some large (~M6) events have been recorded. This section will discuss the overall pattern of seismicity in the North Sea as relevant to the SHARP case study sites.

The geologic structure of the North Sea is primarily associated with the triple plate collision that occurred around 450 Ma ago (Late Ordovician to Early Silurian) during the Caledonian Orogeny. However, many of the largest structures in the North Sea that generate present day seismic hazard were created in the Permian and Triassic. Volcanic rifting 250 to 150 Ma ago created horst and graben structures bounded by a series of large normal faults, which are spread across the north of the study region forming the Viking Graben. The graben is now oriented N–S and is located around 100 km to the west of Norway. Further rifting in the Late Jurassic through to the Early Cretaceous (160 to 140 Ma ago) created additional extensional structures further to the south, forming the Central Graben. Thermal subsidence in the Cretaceous, uplift of the basin margins in the Cenozoic, and continued uplift and glacial erosion through to the Quaternary resulted in a thick series of sedimentary deposits that buried the Jurassic and Cretaceous rocks that sourced the considerable North Sea oil and gas reserves. More recently (in the last 2.5 Ma), changes in river sediment deposition and sea level, broadly associated with changes in glaciation, have produced thick sedimentary sequences in the south of the North Sea. This has given rise to shallow seas over a large area off the east coast of England, in particular the Dogger Bank bathymetric high.

Despite seismic hazard in the North Sea being comparatively low, it is still critical to assess the rate and size of local earthquakes as CO₂ storage operations are being developed. Seismicity can highlight the location of faults and other pre-existing structures (e.g., dominant fracture trends) near prospective storage sites, some of which could act as hydraulic conduits for CO₂ migration. The faulting style of seismic events also directly relates to the *in situ* stresses, which can help in constraining the state of stress at potential storage sites. Stress measurements inferred from faulting style (i.e., stress inversion) can be compared to the results of borehole stress indicators and measurements (compiled for the North Sea by Fellgett *et al.*, 2022), and other seismological methods such as stress drop or anisotropy analysis. Using these measures can provide a more robust and complete assessment of the regional and local state of stress.

The risk of injection-induced seismicity is also present for these operations. Both operators and regulators therefore require a clear understanding of the rate of natural seismicity, to identify and distinguish induced events, and also to assess the likelihood of induced fault reactivation. This requires a sufficient background monitoring programme, with detection rates and location uncertainty low enough to identify any faulting which could affect the CO₂ storage complex.

An ongoing activity within the SHARP project (Work Package 2, Task 2.1) is concerned with aggregating, homogenising, and eventually re-analysing seismicity data for the North Sea. Seismicity catalogues and focal mechanisms from each of the relevant national and international seismic monitoring agencies are being aggregated and quality controlled to produce the most complete set of earthquake observations for the region. Preliminary results from this data aggregation activity (Weemstra *et al.*, 2022) will be discussed in this report and should provide the most recent picture of the general North Sea seismicity pattern (Figure 4).

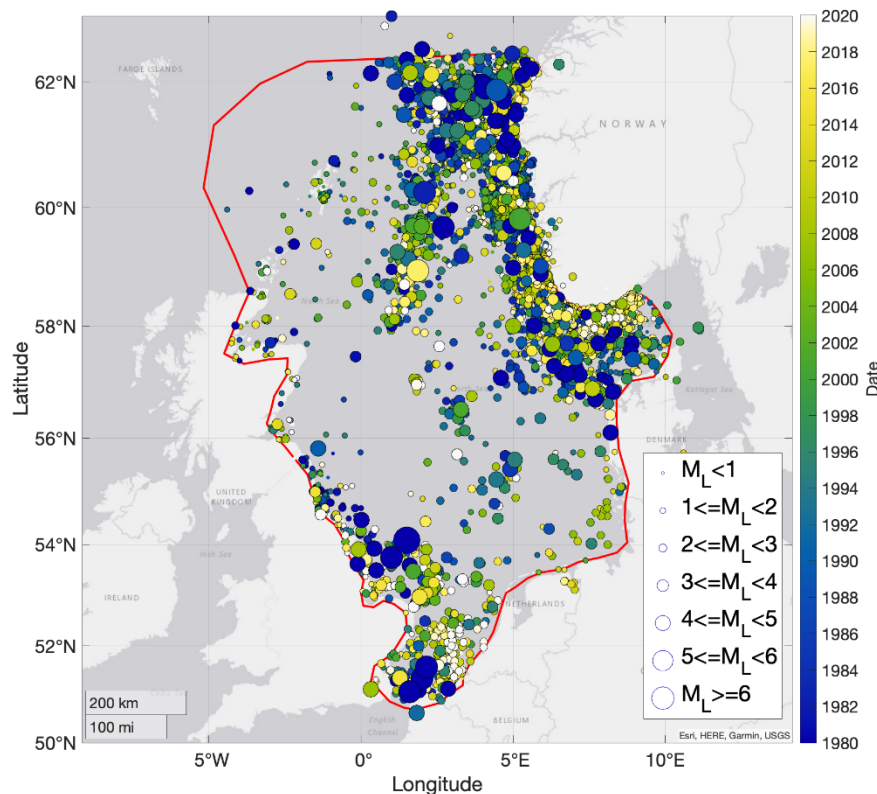


Figure 4. Map of seismicity produced from the data amalgamation being conducted in SHARP Work Package 2. The red outline denotes the study area of the Work Package 2 data aggregation. Event epicentres are shown as circles coloured by time and sized by local magnitude (ranging from -1 to 6.1). Though the colour scale is truncated at 1980, the catalogue contains events dating back to 1382. The catalogue from around 1985 is most likely complete for events with $M_L > 4$ (as shown in Figure 5), though there are clear spatial variations in detection thresholds within the study region. Image reproduced from Weemstra *et al.* (2022).

In general, the more frequent larger magnitude seismic events are concentrated in the north, between Norway and the north of Great Britain, around the Viking and Central grabens. As this area borders the Horda Platform, seismic hazard is relatively high for this case study area compared to other areas of interest of the project. In addition, there is relatively frequent moderate seismicity in the Skagerrak between northern Denmark and southern Norway. Despite this, historically the largest events in the study area are located in the Southern North Sea, closer to the Endurance CO₂ storage site, and toward the Dover Strait. Little felt seismicity has been recorded (so far) to the immediate west of Denmark or in the north of the Netherlands.

Figure 5 shows the size of earthquakes in the North Sea study region through time. Magnitudes of historical (pre-1900) seismicity do not originate from any instrumental recordings of ground motion and are instead inferred from written records of shaking and damage. The catalogue would not be

considered complete to a local magnitude M_L of 3 to 4 until around 1980, when instrumentation coverage, detection methods, and reporting mechanisms were more advanced. The degree of completeness is significantly variable across the study area. Though a thorough completeness analysis will be undertaken in future work. Further, differences in the measurement of M_L in the different jurisdictions within the study region are not yet reflected in the catalogue.

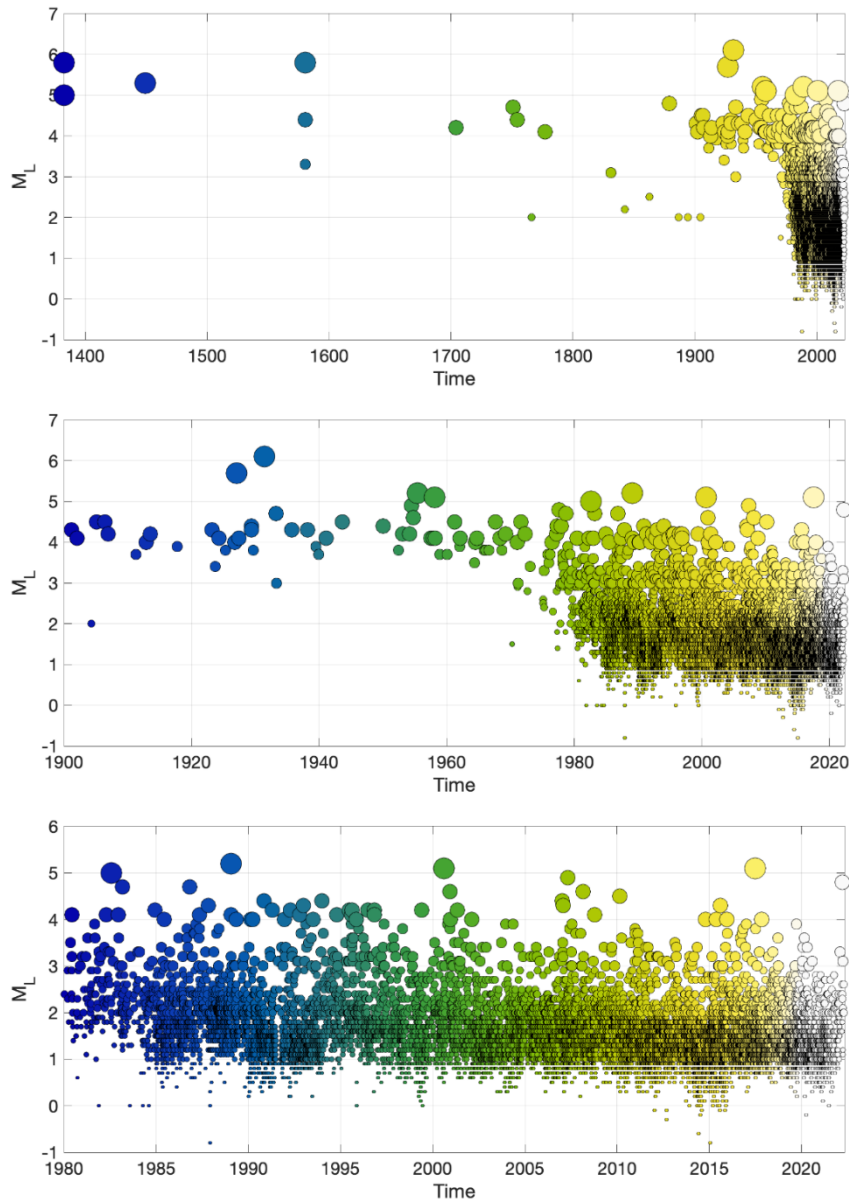


Figure 5. Local magnitude of North Sea events through different time periods. The upper figure shows from the earliest events in the catalogue (May 1382). The central image shows from 1900, when instrumental measurements of earthquakes began in earnest in the region. The lower figure shows from 1980, when earthquake detection improved to routinely detect $> M3$ events. Image reproduced from Weemstra et al. (2022).

Examining the distribution of earthquake magnitudes within the catalogue (Figure 6) gives a Gutenberg-Richter b-value of 1 ± 0.2 , typical of tectonic earthquake sequences. However, a slight kink in the magnitude-frequency distribution below the magnitude of completeness M_{min} is visible. This could result from the variation in completeness magnitude through space and time or the differing magnitude scales used by the contributing agencies. If small events ($M < 4$) are under-reported in the

catalogue relative to larger events, which is likely, this would result in a decrease of the measured b -value at lower magnitudes. The process of homogenising the magnitudes within the catalogue and studying the spatiotemporal variation in M_{\min} will continue throughout Work Package 2.

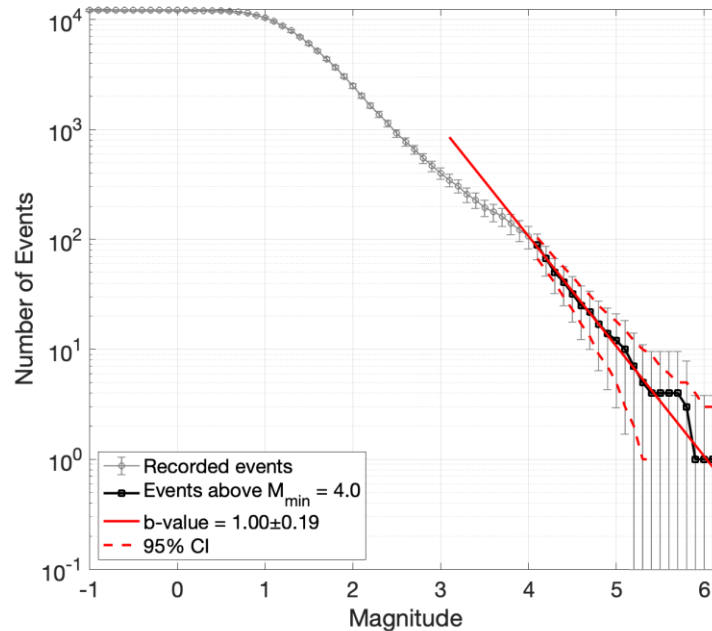


Figure 6. The magnitude-frequency distribution for the prime entries in the bulletin using local magnitude M_L . Gutenberg-Richter b -value was calculated here with defined realistic estimate of magnitude of completeness: M_L 4. Figure reproduced from Weemstra et al. (2022).

The focal mechanisms aggregated in Work Package 2 are shown in Figure 7. As is clear, there are many, mostly historical, large events for which focal mechanisms do not exist. However, the regions surrounding each of the case studies exhibit broad trends in faulting style that can be observed. The Central Graben shows mostly reverse and some dip-slip mechanisms, as expected for the fault structures present in the region. To the west of Norway, events are mostly reverse and strike-slip, though thrust faulting dominates in the north. A diverse mix of mechanisms occur around the Skagerrak, though the largest events are reverse and dip-slip. Though only two mechanisms are present, the central North Sea appears to exhibit a normal faulting regime. Whilst there are few mechanisms shown in Figure 7 on the east coast of Britain, strike-slip mechanisms are common, though normal faulting has been observed to occur further offshore. To the south, the few Dover Strait mechanisms are mostly thrust with a slight dip-slip component. Thus, reverse faulting regimes are common in the North Sea region, indicating the least principal stress to be vertical, though there are events showing more strike-slip and normal faulting. More mechanisms will be computed in Work Package 2, and the trends, especially for events with good depth measurements, will be investigated further.

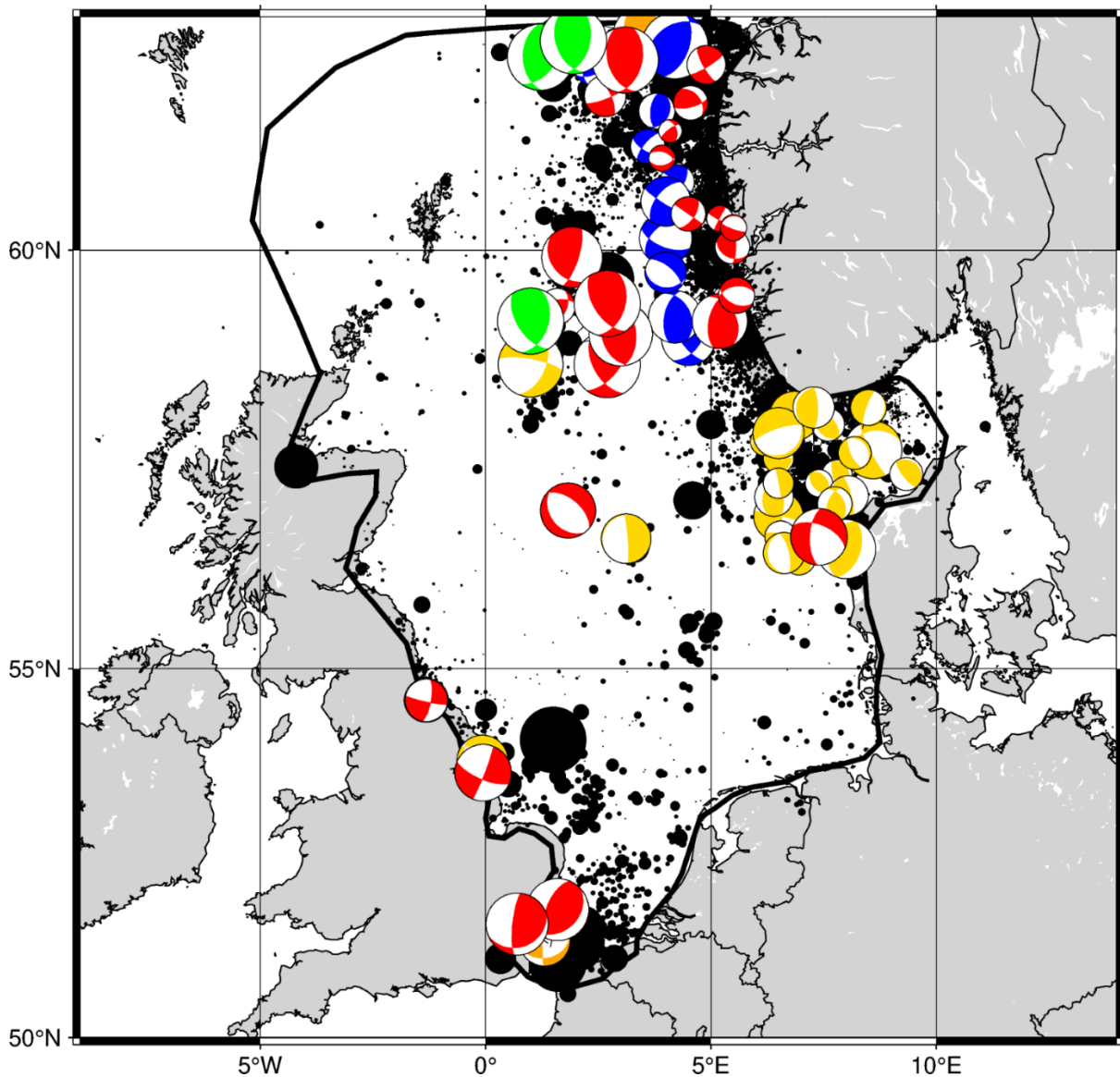


Figure 7. Initial focal mechanism catalogue for the North Sea area from SHARP Work Package 2. Colours mark reporting institutions: green – GCMT; red – ISC; yellow – GEUS; blue – NNSN; orange – GEOFON. Catalogued earthquake epicentres are shown as black dots and are sized by local magnitude. Focal mechanisms are sorted chronologically (i.e., more recent overlay older mechanisms). Figure reproduced from Weemstra et al. (2022).

1.4 Summary of conventional site monitoring methods

There are now many projects around the world where monitoring systems for CO₂ storage have been developed and implemented. The choice of monitoring methods and systems varies from site to site, but some general learnings are evident. There is also a continual push for advances in technology, including tool development, improvements to use of monitoring data, and optimisation and targeting of monitoring systems. The overall objective of a Monitoring, Measurement and Verification (MMV) programme is to verify storage and minimise the risk of leakage, as outlined in European Directive (EC, 2009). Note, that jurisdictions outside the European Union/European Economic Community may have different legal terms but will generally use the same conceptual framework.

The overall monitoring objective can be subdivided into two main goals for a monitoring programme:

- *Conformance*: Verify storage performance;
- *Containment*: Ensure the CO₂ is contained within the storage complex.

The first of these is more targeted at the reservoir (or injection interval) while the second involves more surveillance of the overburden and surface. A third important aspect of an MMV programme is the concept of *Contingency*: the ability to respond to anomalies and potential leakage events. There are also various regulatory requirements, including:

- Reporting to the competent authority at least once a year (EC, 2009);
- Environmental Protection, especially to protect underground sources of drinking water (e.g., US Environmental Protection Agency regulation of Underground Sources of Drinking Water) or to protect the marine environment (e.g., London and OSPAR conventions);
- Liabilities for post-closure monitoring and transfer of responsibility.

For further discussion on regulatory and legal aspects see Dixon and Romanak (2015) and Dixon *et al.* (2015). Jenkins *et al.* (2015) provide a detailed review of monitoring methods applied at various sites.

Another key question is what type of monitoring is necessary or prudent at a specific site. Each site is different, and there are several stakeholder viewpoints that need to be considered in designing MMV programmes for specific sites. It is necessary to consider what is needed:

- From an operational point of view;
- From a regulatory perspective;
- Concerning matters of public interest.

To address these questions, CO₂ storage projects have developed a range of fit-for-purpose approaches to monitoring. Examples are summarised for a few selected sites in Table 1.

Table 1. Overview of monitoring methods applied at five CO₂ storage projects (Note that the table provides a summary of the main technologies applied, and does not document all technologies deployed at these sites).

Monitoring Technology	Sleipner (offshore)	In Salah (onshore)	Snøhvit (offshore)	Decatur (onshore)	Quest (onshore)
Wellhead monitoring	✓	✓	✓	✓	✓
Down-hole fluids	✓	✓	✓	✓	✓
4D surface seismic	✓	✓	✓	✓	✓
4D VSP seismic (DAS)				✓	✓
4D gravity	✓		✓		
Microseismic		✓		✓	✓
Down-hole gauges			✓	✓	✓
Seabed surveys	✓		✓		
Satellite (InSAR)		✓			
Surface/shallow gas	✓	✓		✓	✓
Groundwater sampling		✓		✓	✓

Some general observations can be made from this operational experience:

1. Wellhead and downhole measurement of pressure, temperature and fluid composition can be regarded as a routine monitoring activity;

2. Time-lapse (4D) surface seismic monitoring of CO₂ plumes is widely demonstrated as a valuable tool for monitoring, mainly towards the conformance objective but also supporting the containment objective (e.g., Furre *et al.*, 2017);
3. There are many ways of reducing the cost of 3D/4D seismic surveys, and application of time-lapse vertical seismic profiling (4D VSP) and 4D VSP using distributed acoustic sensing (DAS) has been shown to be especially valuable and cost effective (e.g. Harvey *et al.* 2022);
4. Some technologies have been found to be valuable only at selected sites, such as 4D gravity surveys at Sleipner (Alnes *et al.*, 2011) and satellite InSAR monitoring at In Salah (Vasco *et al.*, 2010), and so can be considered as site specific options;
5. Some degree of environmental monitoring (at surface or in groundwater wells) is usually necessary or required, but the detailed requirements are very site specific;
6. Microseismic or regional earthquake monitoring is usually needed, but the level of and intensity of monitoring required is very site specific.

A full review of experience and options for the monitoring of CO₂ storage sites is beyond the scope of this report, and is covered elsewhere (e.g., Chadwick *et al.*, 2010; Ringrose *et al.*, 2013; Jenkins *et al.*, 2015; Furre *et al.*, 2017; Harvey *et al.*, 2022).

For this report, and in support of the objectives of the SHARP project, it is useful to summarise the monitoring objectives and identify the key challenges for technology development. Figure 8 illustrates the likely components of an idealised CO₂ storage site monitoring programme. In summary we can say that an 'ideal CO₂ monitoring portfolio' is likely to encompass most of the following:

- Good geological characterisation of the site, as a basis for site operation and monitoring;
- A set of standard and mainly continuous wellhead and downhole measurements (i.e., flow rate, pressure, temperature, and changes in composition);
- A sequence of cost-effective time-lapse seismic acquisitions to monitor the CO₂ plume;
- A system for passive seismic (microseismic) monitoring and/or strain monitoring to assess geomechanical response of the rock system to modified fluid pressures;
- Consideration of complementary geophysical surveys (such as gravity or electromagnetic field monitoring) that could provide additional value;
- An approach for surface and environmental monitoring, either using remote sensing or direct measurements.

Important developments in CO₂ storage site monitoring include a stronger focus on monitoring the geomechanical response to CO₂ injection. This can be done using a mix of microseismic monitoring and downhole measurement of pressure and strain. It also requires a set measurements of rock mechanical properties and stress field measurements (see following section). Another major emerging field in monitoring technology is the use of distributed fibre optic (FO) sensing both at surface or downhole. Distributed Acoustic Sensing (DAS) using FO systems allows seismic events (for both active and passive seismic event detection) to be recorded, potentially at lower cost than for conventional geophone systems. Other important fields in FO sensing include Distributed Temperature Sensing (DTS) and Distributed Strain Sensing (DSS), such that FO systems can have multiple uses as part of monitoring systems.

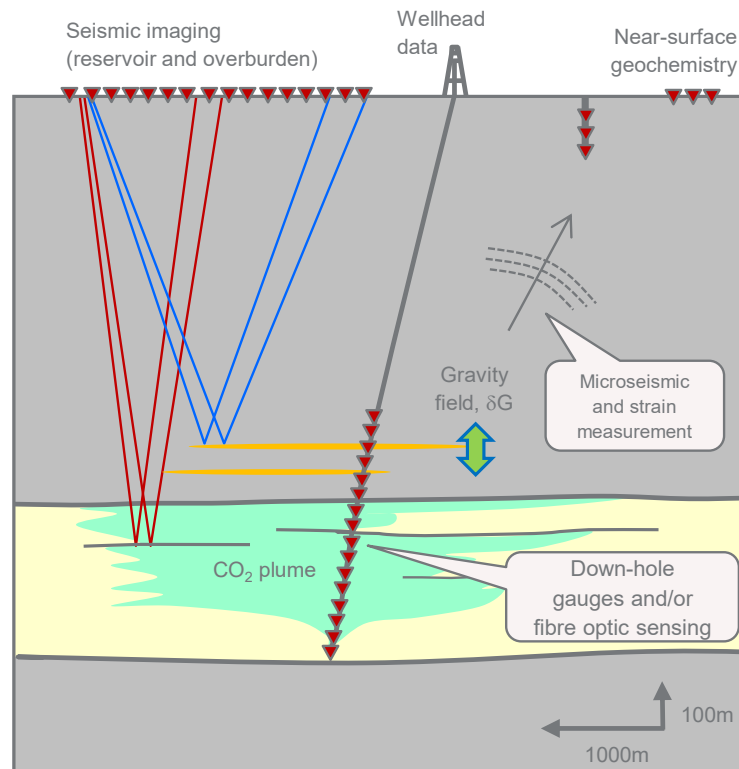


Figure 8. Idealised sketch of a CO₂ storage site monitoring programme (modified from Ringrose, 2020).

1.4.1 Overview on current state of the art in induced seismicity monitoring

Continuous monitoring of microseismicity within a larger region around CO₂ storage sites provides insights on potential areas of sudden stress-releases. Adequate instrumentation is required to capture and characterise the active regions of microseismicity at local scales. For onshore CO₂ storage sites, some level of dedicated microseismic monitoring has usually been deployed. Monitoring with downhole geophones close to the storage interval provides the best possibilities to detect microseismic events down to the smallest magnitudes (e.g., in the range of magnitudes -2 to 0). By also deploying supplementary seismic nodes on the surface, good location estimates can be achieved through advanced processing (e.g., Goertz-Allmann *et al.*, 2022). The actual design of a monitoring network requires a cost-benefit analysis to assess the relative benefits of deep downhole sensors, shallow borehole sensors, surface sensors or surface nodal arrays, as well as potentially including the various options for dedicated FO cable deployments. System performance depends on the spatial placement of the sensors, quality of individual sensors, placement method, and the number of individual sensors. Use of advanced processing methods is also important to optimise the station detection system. Stage-wise and upgrading/down-sizing options of sensor deployment should also be considered, accounting for extensions of the storage site, moving from background seismic characterisation through injection phase monitoring to post-injection phase verification monitoring.

The above-mentioned considerations are certainly also valid for any offshore storage site. However, costs related to offshore installation are significantly higher, which practically excludes certain deployment options simply due to high costs. A cost-effective monitoring approach for offshore sites is to deploy high-quality seismometers in array configuration on land, if nearby coastal regions can be accessible. One example of this is the first deployment of the HolsNøy Array (HNAR) in western Norway

to establish a high-quality baseline of background seismicity within the larger Horda Platform region (Oye *et al.*, 2021; Zarifi *et al.*, 2022b). Other options to monitor local, injection-related seismicity are likely to include dedicated offshore installations, which might include ocean bottom seismometers, sparse Permanent Reservoir Monitoring (PRM) networks or FO cables on the seafloor or along wellbores. Fibre-optic sensing for earthquake detection is covered in the following section.

For all seismic monitoring methods alike, the use of adequate, likely 3D velocity models, will help to reduce location uncertainties. As such, appropriate wave propagation codes need to be applied, which then also allow for estimations of earthquake source mechanisms, which in turn provide causal relationships between the stress field and fault rupture to be determined. This then allows assessment of the potential effects of pressure changes associated with CO₂ injection in inducing seismicity.

Integration of seismicity data with regional stress data and geomechanical datasets for specific sites is a complex topic which will be addressed in the SHARP project. However, the overall objective is to understand the nature of natural seismicity and the potential for induced seismicity.

1.4.2 Current state of the art in fibre-optic sensing

Use of FO technology for reservoir monitoring has been steadily growing over the last decade or so, and applications of FO sensing to CO₂ storage monitoring have been implemented over the last five years. The Ekofisk field provides a useful demonstration, where Folstad *et al.* (2015) demonstrated the benefit of using FO technology for PRM, where ASN's PRM system was installed in 2010. Streamer data were used in the past, and positive time shifts between 3–4 ms were observed (2006–2008) as the reservoir responded to water injection. However, these observed changes in the velocity are very small and within the range of positioning error. ConocoPhillips decided in 2010 to proceed with FO technology to increase repeatability, which became a game changer, enabling time shift interpretations below 1 ms. Velocity changes around 0.4 ms could then be observed (2012–2014), correlating with increased reservoir pressure caused by water injection and reservoir depletion/compaction around the producing wells. Ridder *et al.* (2015) also showed how the anisotropic seismic wave velocities measured at the Ekofisk PRM system could be used for stress field estimation of the overburden. They applied seismic tomography and investigated fast and slow Scholte wave phase velocities. It was observed that the (anisotropic) velocity field forms a large circular pattern with high velocities in the centre, pointing towards extensional stresses due to subsidence that weaken the overburden. These results correlated well with an observed seafloor subsidence bowl (>9 m) caused by pressure depletion of the reservoir due to hydrocarbon production.

Although the use of FO technology for oilfield PRM has shown large benefits, the application for CCS requires reduction of deployment costs and identification of solutions that are more fit-for-purpose. Several onshore CO₂ injection projects have now demonstrated and deployed FO sensing, such as use of DAS in injection wells for time-lapse seismic monitoring. Both the Aquistore (Harris *et al.*, 2016) and Quest (Bacci *et al.*, 2017) projects in Canada have demonstrated successful monitoring of the CO₂ plume using time-lapse DAS VSP (vertical seismic profiling using FO cables as detectors). Application of FO sensing offshore is more challenging, and Ringrose *et al.* (2018) presented the potential for cost-effective monitoring of CO₂ storage offshore using DAS FO cables located in wells. They showed the advantage of using pressure gauges in combination with DAS to monitor pressure and strain close to the injector well.

One of the main challenges for CO₂ storage monitoring is that operators need to monitor large areas/volumes over long time periods. One solution to tackle these challenges could be to use infrastructure that is already in place, such as telecom and power cables. New uses of DAS technology using multi-use FO cables are quickly emerging and show great potential. Rønnekleiv *et al.* (2019) demonstrated the use of DAS for submarine cable protection and integrity monitoring of infrastructure. The technique offers novel opportunities for detection of potential threats to the cable and activities near cable suspension areas.

Another advantage of DAS is that it offers broad band measurements, ranging from 0.01 to 600 Hz (and higher frequencies depending on the signal-to-noise ratio and length of the cable that is interrogated). Walter *et al.* (2020) investigated the potential of DAS for seismic monitoring and detecting microseismic events near a glacier. However, they showed that with DAS the frequency content fades out very quickly above 100–200 Hz due to coupling issues of the FO cable to the ground. However, they concluded that the DAS system is very capable of recording seismogenic glacier flow and even small Alpine mass movements. Hudson *et al.* (2021) discussed how DAS has limitations for microseismic detection and source localisation compared to conventional seismic instruments, but on the other hand that DAS outperforms conventional geophones for source spectra and full-waveform source mechanism inversion. Additionally, they proposed the use of 2D array geometries capable of measuring shear-wave splitting used for subsurface stress field estimations.

Another benefit of using DAS is the increased spatial resolution. Wienecke *et al.* (2022) showed the importance of the choice of the DAS acquisition gauge length which determines the spatial resolution. The choice of a small gauge length below 8 m is crucial to detect surface waves from passive and active sources used to investigate the geomechanical properties of the subsurface. Such investigations using DAS on FO cables could be important input to risk management. Rørstadbotnen *et al.* (2022) showed how DAS measurements from active and passive sources can be used to monitor geomechanical changes in the subsurface and how velocity depth estimations can be inferred. However, more investigations and research are needed to understand the effect of coupling, burial depth, and temperature variations on DAS measurements.

Recent results from field trials show the benefit of DAS on submarine FO cables for subsurface imaging and monitoring, including PRM. Pedersen *et al.* (2022) concluded that while DAS on submarine cables may not provide all the advantages of a PRM system, it offers an alternative cost-effective monitoring method to conventional seismic because of the high quality of the data. The increased spatial resolution (due to a small gauge length choice) improves the seismic imaging capabilities. Small-scale faults can be imaged in the overburden, that compared to a PRM system (with a typical distance of 50 m between seismic stations), would fall below the seismic resolution and would not therefore be detectable.

In conclusion, new emerging DAS technologies using FO cables show great potential but still have some limitations for microseismic detection and source localisation. More field trials and research are needed to fully understand how DAS and other FO sensing methods can be effectively used for qualitative and quantitative interpretations at CO₂ storage sites.

1.5 Suggested workflows for initial rock-failure assessments

An example of a workflow for fault stability assessment is presented in Figure 9 after Choi and Skurtveit (2021). The workflow highlights two levels of detail for the analysis to be performed. Firstly, a

simplified or preliminary screening using an analytical Mohr Coulomb failure assessment is performed (e.g., Skurtveit *et al.*, 2018). Fault geometry, *in situ* stress, pore pressure and frictional properties are key inputs for this initial screening of fault stability. Secondly, for a more detailed analysis of critical stress changes on a fault, a geomechanical model is advised. The geomechanical model can address global stress changes at the reservoir or fault-block scale as a first approach. Subsequently, a detailed modelling study can be performed using local and detailed fault models for selected fault sections or orientations where the global screening assessment indicates critical stress and strain during the injection. In the final stage, the injection-induced stress changes (both magnitude and orientation) on the fault are compared with relevant failure criteria for the fault zone to address how close the fault is to failure. Detailed information about the fault strength and applicable failure criteria (cohesion and friction) is usually associated with high uncertainties and should be carefully addressed in risk assessments. A full geomechanical analysis requires multidisciplinary inputs, including a detailed geological model for geometries (2D or 3D), a reservoir simulation for saturation and pore pressure distribution (and temperature if applicable), petrophysical properties, stiffness, and strength for the reservoir and the surrounding over-, under- and side-burden in the model area. Recent work, comparing fault stability calculations from a simple screening approach (e.g., uniaxial strain assumptions) and a full 3D geomechanical model, highlights the variation in stress changes along faults depending on the modelling approach. Recommendations are also provided for identifying the suitable level of detail for various types of reservoirs and faults (Choi *et al.*, 2022). It is worth noting that the workflow presented in Figure 9 provides a general guideline and the level of detail and complexity of the analysis should be tailored to specific reservoir and fault characteristics. Additionally, uncertainties are caused by natural spatial variations, inhomogeneity of geological systems, and scaling properties from lab to field scale. Therefore, a probabilistic approach, which is being studied through Work Package 5, can be useful for treating uncertain parameters in a systematic way and relating them to the risk of failure.

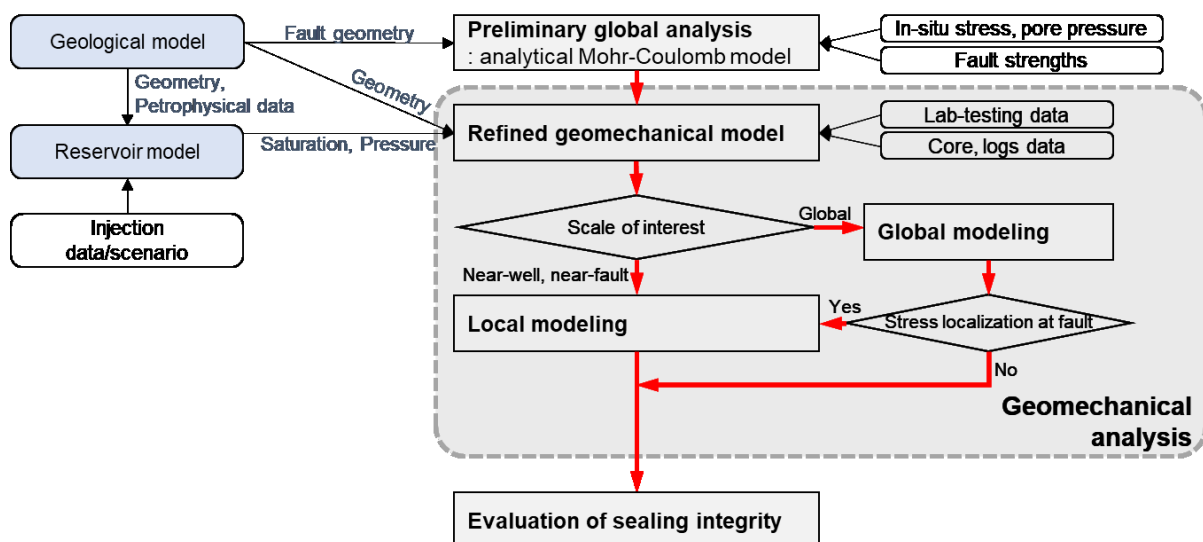


Figure 9. Example of workflow for fault stability assessment (Choi and Skurtveit, 2021).

2 State of knowledge at Case Study sites

2.1 Horda/Smeaheia region

2.1.1 Structural and basin setting

The Horda Platform is a region of N–S trending tilted fault blocks situated on the eastern margin of the North Viking Graben rift zone, in the North Sea to the west of Norway (Figure 10). The structural features and tectonic evolution of this region are well documented in the literature (e.g., Færseth and Ravnas, 1998; Fossen *et al.*, 2017) and have recently been reviewed in terms of the implications for CO₂ storage (Mulrooney *et al.*, 2020; Wu *et al.*, 2021; Holden *et al.*, 2022; Osmond *et al.*, 2022). In terms of the tectonic history, the region was affected by two major extensional events:

- Permian to Triassic rifting;
- Late Jurassic to Early Cretaceous rifting.

The first phase resulted from the break-up of Pangaea and affected the entire North Sea Basin. This Permian to Triassic rifting event resulted in the formation of a series of eastward-tilted half-grabens bounded by large N–S trending normal fault systems (Phillips *et al.*, 2019), including the Brage, Vette and Øygarden Faults in the Horda Platform region (Wu *et al.*, 2021). These offshore N–S trending Permian to Triassic faults were driven by a dominantly E–W extension during this rifting event.

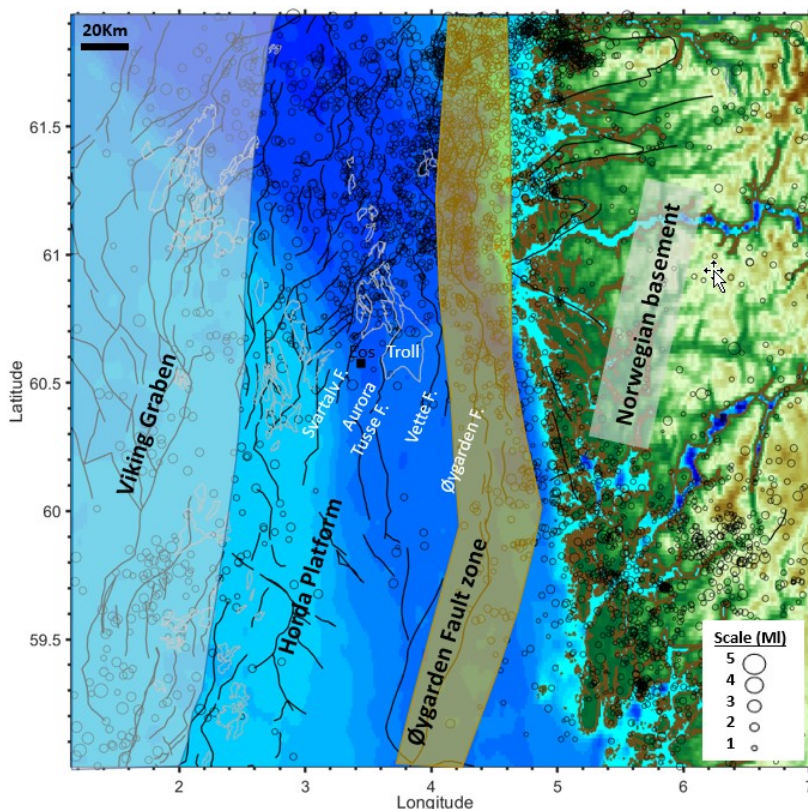


Figure 10. Seismotectonic map of offshore and onshore region of western Norway around the Horda Platform. Symbols show recorded seismicity over the last 30 years (from Zarifi *et al.*, 2022b).

The Late Jurassic to Early Cretaceous rifting event involved several episodes of extension, including formation and development of the Viking Graben. In the Horda Platform region, several faults were active during this time, including the Troll Fault System, and the Svartalv, Tusse, Vette and Øygarden faults. The tectonic extensional direction during this second phase was mainly in a NE–SW direction, with the newly formed intra-block faults striking mainly NW–SE. During this phase, some of the Permian to Triassic faults were reactivated, but many new faults were also developed. These faults were dominated by several NW–SE trending normal faults (Mulrooney *et al.*, 2020; Wu *et al.*, 2021), implying extension towards the NE–SW.

Synrift sedimentary packages are associated with these two extensional tectonic episodes, termed Synrift 1 (Permian to Triassic age) and Synrift 2 (Upper Jurassic to Lower Cretaceous). The post-rift phase was dominated by thermal subsidence and deposition of the Upper Cretaceous Shetland Group and the Paleogene Rogaland and Hordaland Group sediments, and included continued fault movement on the Øygarden fault in addition to movement on a few NW–SE trending faults within the Horda Platform region (Wu *et al.*, 2021). During the Neogene (23 Ma to 2.6 Ma), the whole continental margin was uplifted and eroded (Færseth and Ravnas, 1998; Fossen *et al.*, 2017; Baig *et al.*, 2019), and subsequently, the region was exposed to a series of glacial and interglacial episodes as part of the global Quaternary (Pleistocene) glaciation, which began 2.58 Ma.

In terms of the depositional environments, the main storage reservoirs (of Jurassic age) were deposited during the relatively stable and quiescent tectonic phase following the first rifting episode, during which several fluviodeltaic to shallow-marine systems were deposited, including the Statfjord Group, the Dunlin Group, the Brent Group and the Viking Group. During the second phase of rifting (Late Jurassic–Early Cretaceous) these sedimentary packages were disrupted mainly by fault reactivation along pre-existing N–S trending faults to form several half-graben depocentres (Bell *et al.*, 2014; Whipp *et al.*, 2014; Duffy *et al.*, 2015). The Draupne Formation, which is composed of deep-marine mudstones, was deposited during the early phase of this second rifting event. This tectonic history provides the basis for the main seismotectonic zones identified within the region (Figure 10; Zarifi *et al.*, 2022b):

- a) The Viking Graben – a deep paleo-rift zone with continuing levels of low to moderate present-day seismicity;
- b) The Horda Platform – a series of tilted fault blocks with continuing (mainly low levels) of present-day seismicity;
- c) The Øygarden fault zone – a major basement-margin fault with a long history of tectonic movements and characterised by a relatively higher frequency of present-day seismicity;
- d) The Norwegian basement – an ancient cratonic basement with low levels of seismicity.

There are several storage prospects within the Horda Platform region, including the Aurora injection site (at Dunlin Group level) currently being developed by the Northern Lights Joint Venture. Future storage prospects include the Alpha Structure at Viking Group (Figure 11) and Dunlin Group level. A key storage risk for this region is the potential for brine or CO₂ leakage along the basement bounding fault to the east of the Beta Prospect (Figure 11).

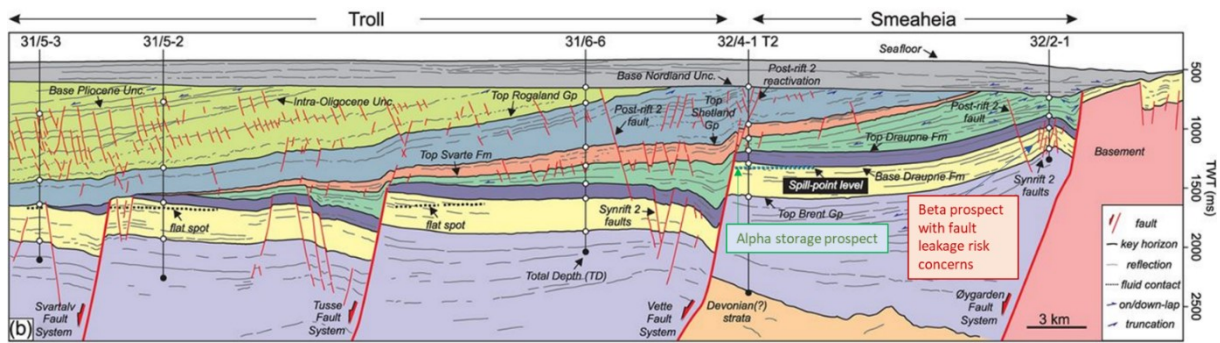


Figure 11. Interpreted profile with well controls and seismic stratigraphic framework for a cross-section of the Horda platform region (from Wu *et al.*, 2021). The Alpha CO₂ storage prospect is indicated as well as the Beta Prospect. Vertical scale in two-way travel time (TWT).

2.1.2 In situ stress conditions

The regional stress field trend in the Horda Platform area is a dominantly NW–SE direction of S_{Hmax} driven by North Atlantic ridge-push tectonic stress (Müller *et al.*, 1992). However, significant variations in stress field orientation occur with S_{Hmax} varying from NW–SE to E–W, probably due to second order effects including effects of Neogene uplift on the Norwegian continental margin, and loading and unloading of ice sheets during 3 million years of Northern Hemisphere glaciation (Heidbach *et al.*, 2007). Analysis of well data in this region shows that the stress state in the sedimentary basin package is under a normal-faulting stress regime, where the vertical stress is greater than the horizontal stresses (De Lesquen *et al.*, 2020). However, at deeper levels in the basement, stress field estimation from earthquake focal mechanism analysis indicates that the maximum principal stress is horizontal, and oriented between a NW–SE to E–W trend (Zarifi *et al.*, 2022a). Further work is needed to improve understanding of the stress state in region; however, it is most probable that at the levels targeted for CO₂ injection (1–3 km depth) the stress state is in a normal-faulting regime.

2.1.3 Seismicity data currently available

The Horda Platform region of the North Sea has a moderate level of natural seismicity. Figure 12 shows the summary map of seismicity in the Horda Platform and surrounding region. The highest level of seismicity is concentrated to the north and northeast of the Horda Platform and along sections of the Øygarden fault. Also shown in Figure 12 is the station coverage for onshore western Norway and available offshore stations. The illustrated earthquake catalogue is based on the Norwegian National Seismic Network (NNSN), which has good station coverage since the 1980s (Figure 12). More recently, efforts were made to improve the instrument network in the offshore region (Oye *et al.*, 2021; Zarifi *et al.*, 2022b). In 2020, a new dedicated array of 9 broadband seismometers (HNAR; blue triangle in Figure 12) was deployed on the island of Holsnøy. The HNAR array was designed to improve coverage and detection quality for the planned offshore CO₂ storage site at Aurora as part of the Northern Lights CCS project. So far, the improvements in offshore event detection using HNAR have been substantial. In the first two years of operation (May 2020 to May 2022), about 132 additional earthquakes were detected by the HNAR array, with the majority of these events in the range of $1.0 \leq M_L \leq 1.5$ (Zarifi *et al.*, 2022b). Efforts were also made to use selected stations from offshore PRM systems at the Grane, Snorre and Oseberg oilfields (Figure 12) to improve azimuthal coverage and location accuracy (Zarifi *et al.*, 2022a).

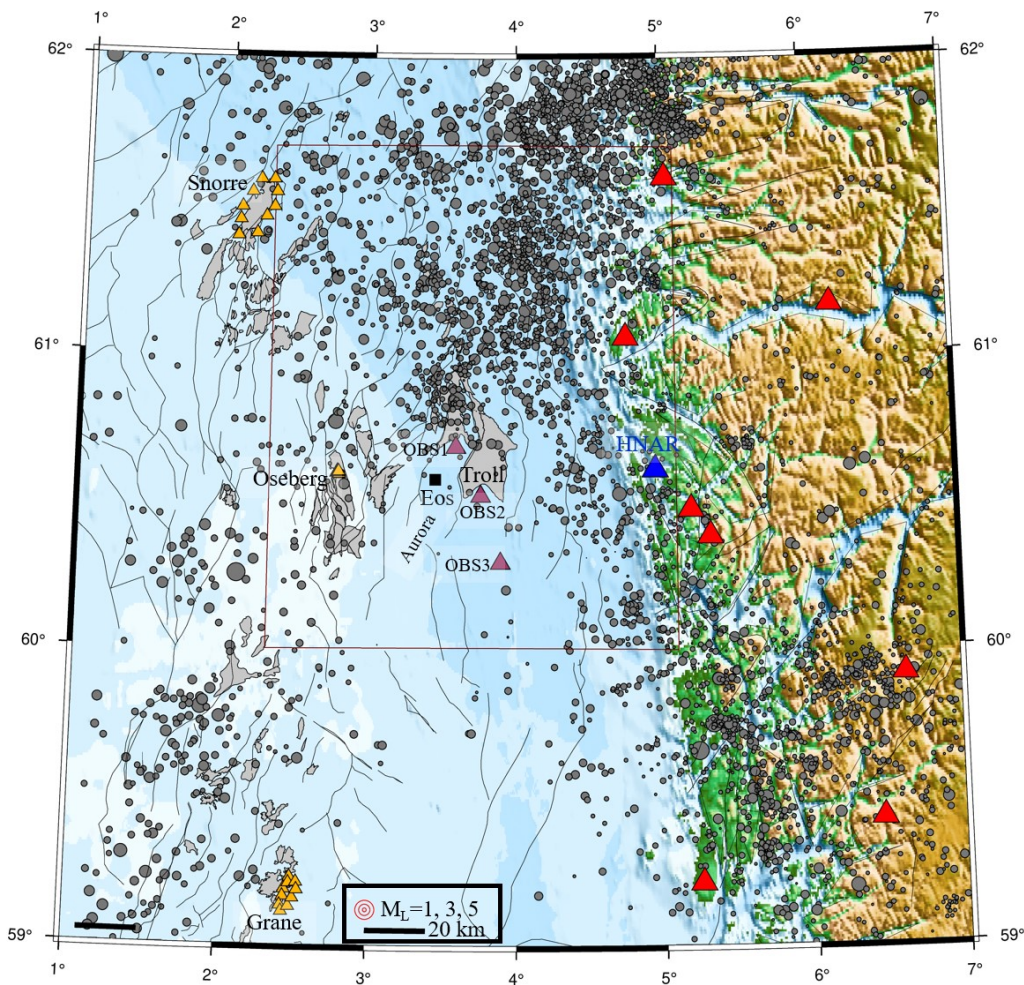


Figure 12. Seismicity on the Horda Platform based on the NNSN catalogue (2001–2021). The red triangles are selected broadband seismic stations from the NNSN, the blue triangle is the broadband HNAR array, and the purple triangles are the temporary OBS deployed (October 2021–October 2022) to focus on passive monitoring of Aurora and the Eos injection well. The yellow triangles are the selected stations from the PRM systems at the Grane, Snorre and Oseberg oilfields used for earthquake detection. The thin red rectangle shows the area of interest for passive monitoring on the Horda platform.

Although the majority of the earthquakes in the Horda Platform and surrounding area are minor ($M < 3.0$), a few earthquakes with magnitude exceeding $M_L = 4.5$ have occurred. The largest event in proximity to the planned CO_2 injection well (Eos) at the Northern Lights project is an earthquake with $M_L = 4.5$, which occurred on 8th June 1980, located approximately 50 km north of the injector. Recently, an earthquake with $M_L = 4.6$ occurred about 120 km to the west of Florø on 21st March 2022. This event was located just north of the Horda Platform and was strongly felt throughout southern Norway. These events felt by the populations on the coast are clearly important to understand as part of offshore CO_2 storage developments. Technically, the larger events also provide the opportunity to improve methods for determining location and depth accuracy (Zarifi *et al.*, 2022a).

Figure 13 shows the same regional seismicity dataset, with the addition of focal mechanisms determined for selected earthquakes based on the NNSN report (Tjaland and Ottemoller, 2018). These Fault Plane Solutions (FPS) show a general trend moving from a more strike-slip character along the Norwegian onshore to offshore transition zone, and then towards a more reverse fault regime further

offshore. These stress trends are further discussed by Zarifi *et al.* (2022b) and are a topic of ongoing research in Work Package 2.

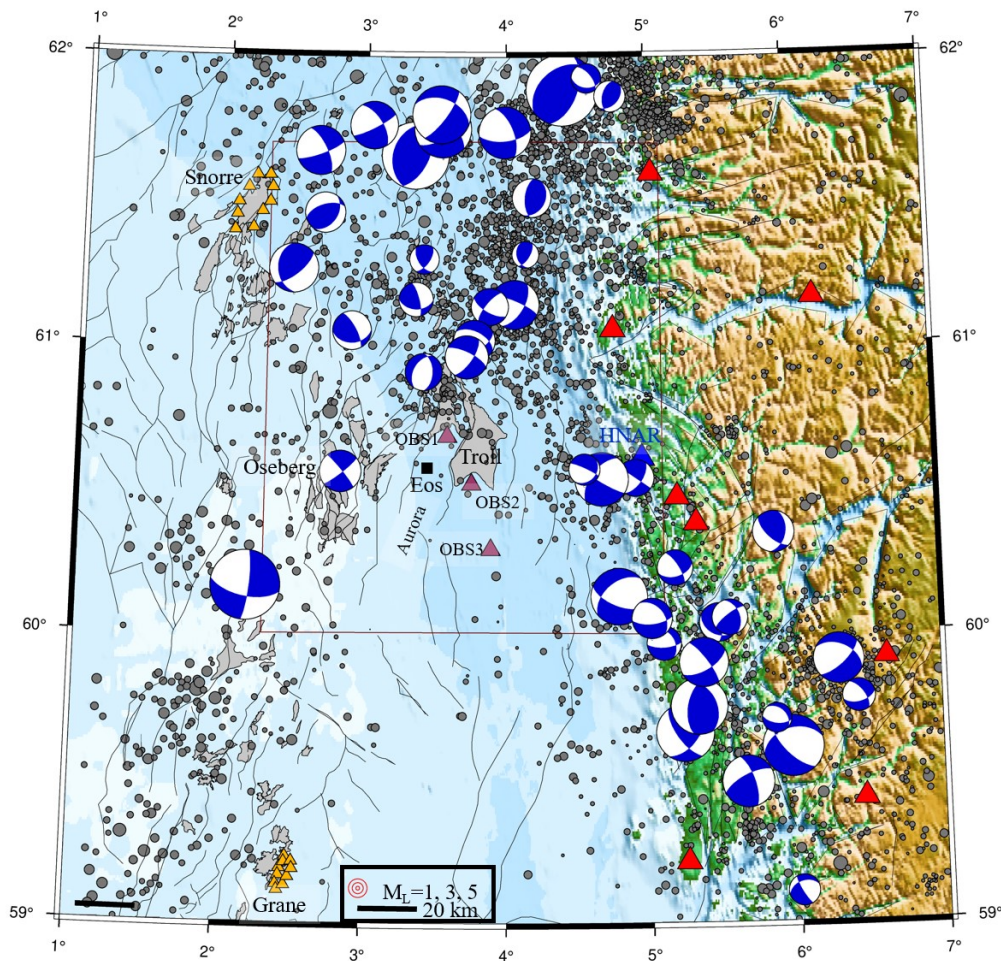


Figure 13. Seismicity in the Horda platform based on the NNSN catalogue (2001–2021), with ‘beachballs’ showing the reviewed focal mechanisms of earthquakes in and around the Horda Platform based on the NNSN report (Tjaland and Ottemoller, 2018). The triangles are seismic detection stations as described in Figure 12.

Finally, it is useful to summarize the seismicity in the region using a well-known scaling relation: the Gutenberg-Richter relation (G-R), which describes the relationship between earthquake size and frequency. Using the available catalogue of seismicity for the Horda platform area of interest (over the last 20 years), Zarifi *et al.* (2022a) derived the G-R function shown in Figure 14. The obtained b-value within the Horda Platform is very close to 1, indicating normal tectonic behaviour. The magnitude of completeness, M_{\min} , (the minimum estimated magnitude for which the catalogue is complete) is $\sim 1.5 M_L$. The largest event in this dataset has a $M_L = 3.7$. Larger events of M_L 4 to 5 have occurred in the wider region and could occur within the Horda Platform area.

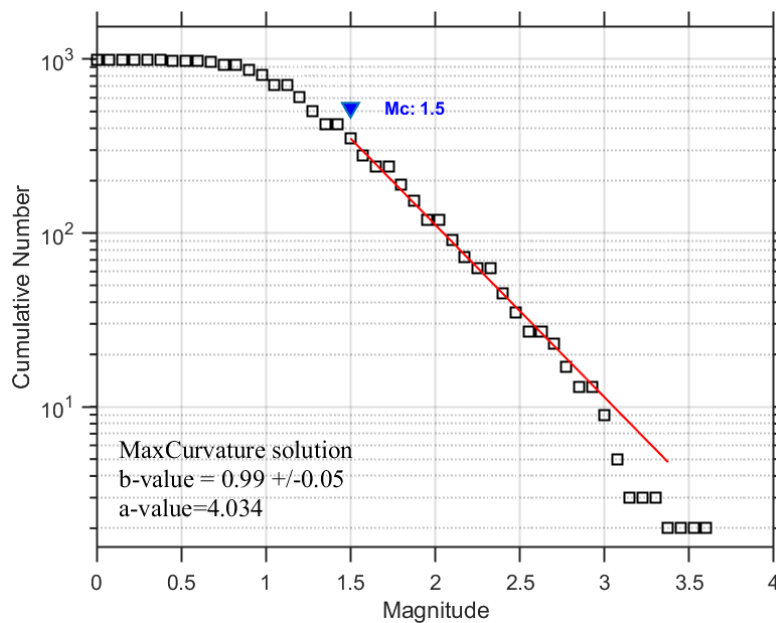


Figure 14. Frequency-magnitude relationship in the Horda platform (period 2001–2021, based on the NNSN catalogue). Magnitude of completeness (M_{min}) is 1.5 in local scale. The b -value is ~ 1 (0.99), indicating a normal tectonic setting.

2.1.4 Rock failure studies

A number of recent studies have been focused on the Northern Lights/Aurora (Thompson *et al.*, 2021; 2022a; 2022b) and Smeaheia (Skurtveit *et al.*, 2018; Wu *et al.*, 2022) areas of the Horda Platform. These studies include interpretations of both regional and local *in situ* stress magnitudes by investigation of extended leak-off test databases (Figure 15), as well as *in situ* stress orientations (again by database analysis but augmented by local well results). Limited interpretations of material properties have also been included in these studies, based on a significant amount of recent laboratory testing programs (proprietary Equinor data, though some data are shared publicly e.g., CO₂DataShare). Screening for fault failure at Smeaheia using the available rock properties from intact formations (CO₂DataShare Smeaheia dataset) highlights the need for more focus on the material properties, specifically for faults (Figure 16) (Skurtveit *et al.*, 2018). In addition, a number of related studies have been performed which interpret material properties over the wider region (Grande *et al.*, 2022; Jalali *et al.*, 2022; Mondol *et al.*, 2022a; 2022b).

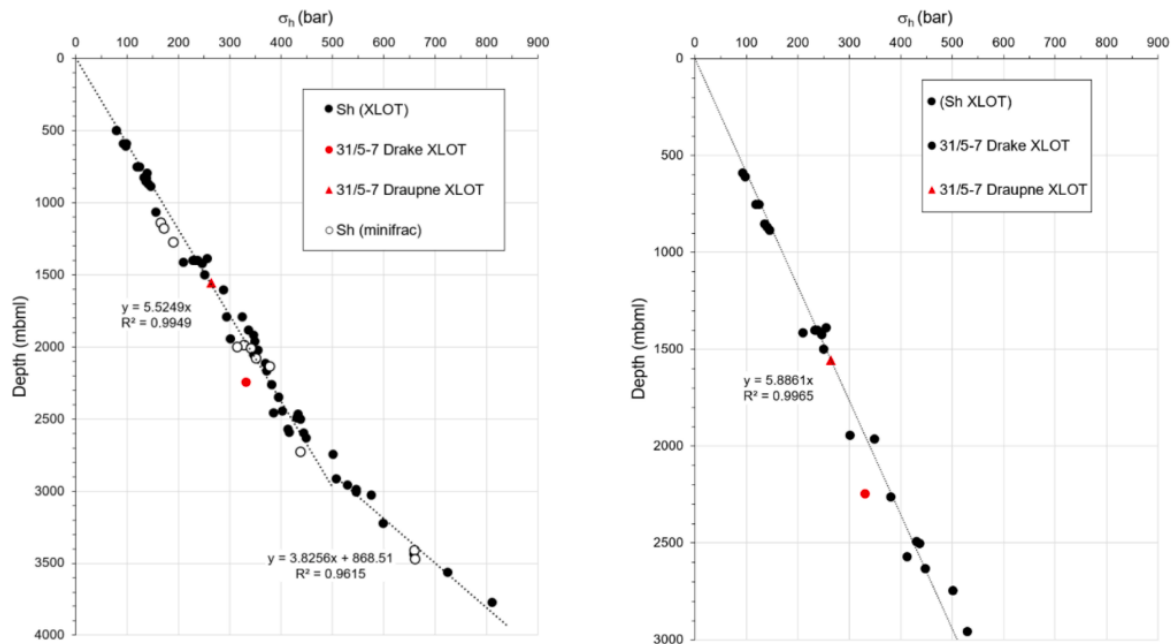


Figure 15. Left: Horizontal stress trends in Aurora based on XLOT data from well 31/5-7, compared with XLOT and minifrac data from the area (the trend below 3000 m is due to overpressure). Right: XLOT data for depths <3000 m with normal hydrostatic pore pressure $\pm 10\%$ only. Figure after Thompson et al. (2022a).

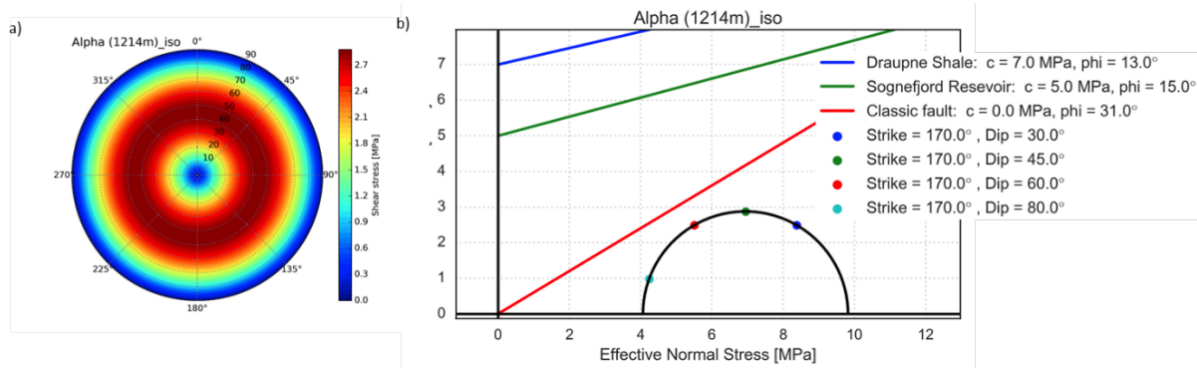


Figure 16. Using a normal faulting regime and calculating stress as a function of fault plane orientation for top Sognefjord Formation in the Alpha structure. Mohr Coulomb diagram including selected dips for the Vette Fault Zone showing the large variation in failure criteria for intact rock samples and cohesionless fault assumption (Skurtveit et al., 2018).

A common thread through these studies is that a relaxed/normal stress state is shown to be present at depths of interest for CO₂ storage over the wider Horda Platform area. This is especially true of the shallower sediments (<3500 m) though more complex stress states (e.g., strike-slip) may be present in the deeper sediments near the base of the sedimentary packages and/or nearer to the crystalline basement. Stress rotation complexities near fault structures cannot be ruled out (i.e., existence of local strike-slip conditions in shallower sediments). Recent geomechanical modelling highlights stress changes as well as stress rotation along bounding faults in the Smeaheia area (Choi et al., 2022). This work further discusses various assumptions for calculation of stress changes away from the injection well and approaching the reservoir boundaries.

The works referenced above also suggest that mineralogical variations play a key role in stress contrast development. This seems particularly true of the Dunlin Group Drake Formation (caprock/seal for Dunlin sand CO₂ injection/storage), where high clay content may lead to higher creep potential in these intervals, allowing them to retain a higher horizontal stress level. The main interval referred to here is termed the Intra Drake Formation, which is also a regional seismic reflector and thus critical to seal integrity in the wider area. Of further interest to present geomechanical studies is the ongoing pore pressure depletion over the wider Horda Platform area due to depletion of the Troll field, which affects the sands of the Viking Group. Wells drilled in the area indicate, however, hydrostatic conditions in the underlying Dunlin Group sands, proving the Drake Formation as an effective seal.

2.2 UK SNS Bunter storage play

2.2.1 Structural and basin setting

The Bunter Sandstone Formation (BSF) of the Southern North Sea (SNS) is a key target reservoir for geological storage of supercritical CO₂ in the UK. One of the principal reasons is that the formation has been affected by post-depositional halokinesis in the underlying Zechstein Group evaporites. This resulted in folding of the BSF into a series of elongate anticlinal structures which are expected to form effective structural traps, or closures for buoyant CO₂. One of these structures is known as Endurance (also known as Bunter Closure 35 and previously identified as 5/42). Endurance was proposed as the storage site for the White Rose CCS Project, and the UK's first CO₂ storage appraisal well 42/25d-3 was drilled at Endurance in 2013. Although the White Rose Project was cancelled in 2015, several structures, including Endurance, are currently being considered for CO₂ storage by various industry consortia. Three carbon storage appraisal and storage licences focussed on the BSF, encompassing Endurance and several other connected structures in the Silverpit Basin area have been granted by the UK licencing authority to date, and further acreage has been offered by the licencing authority. The extent of the BSF and location of structural closures are identified in Figure 17.

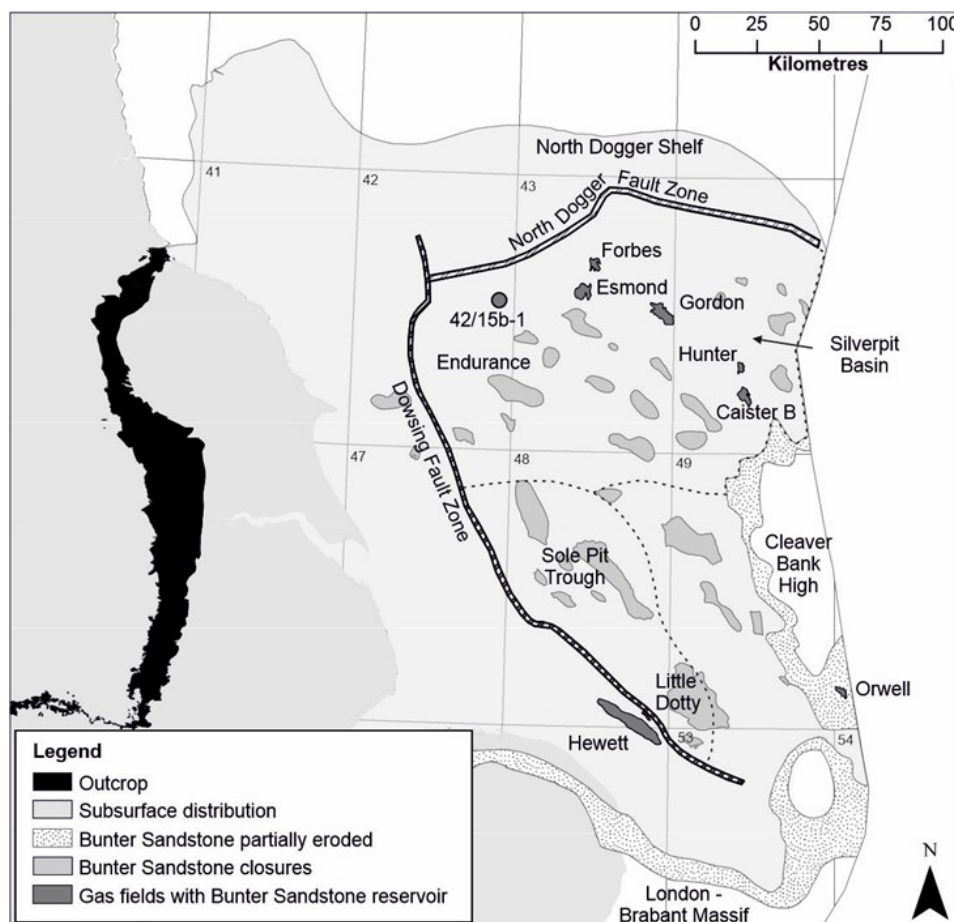


Figure 17. Location of the Bunter Sandstone Formation, gas fields, Endurance and other structural closures, and major structural elements. The locations of the Dowsing and North Dogger fault zones are approximate; they are each composed of several individual, commonly en echelon faults. Figure modified after Williams et al. (2014) and structural closures from the UK's CO₂ Storage Evaluation Database (Bentham et al., 2014). Offshore quadrant and field linework contain public sector information licenced under the Open Government Licence v3.0. BGS © UKRI (2022).

The BSF is the offshore extension of the Lower Triassic (Scythian) Sherwood Sandstone Group, which outcrops extensively in Eastern England (Figure 17). Regional dip is towards the east, from onshore to offshore. Continuity is interrupted by the Dowsing Fault Zone and overlying Dowsing Graben System, which separates the Eastern England Shelf from the deeper basin to the east (Cameron *et al.*, 1992; Stewart and Coward, 1995). Whilst the Dowsing Fault Zone displaces Permian and older strata, faults of the younger Dowsing Graben System only locally affect the pre-Triassic strata because faults are detached within Zechstein Group evaporites. At the southern end of the fault zone in the vicinity of the Hewett Gas Field, the Dowsing Graben System is directly linked to the underlying Dowsing Fault Zone by major faults that cut both the pre- and post-Zechstein successions (Cooke-Yarborough and Smith, 2003; Williams *et al.*, 2014). The generally northwest to southeast trending elongate anticlines that currently form the principal play for CO₂ storage in the BSF mostly occur in the area to the east of the Dowsing Graben System and to the south of the genetically-related North Dogger Fault Zone described by Griffiths *et al.* (1995). Halokinesis was initiated at least as early as the Late Triassic (Allen *et al.*, 1994), and continued intermittently throughout the later Mesozoic. A later major halokinetic episode occurred in the Silverpit Basin area during the Eocene, and continued progressively into the Oligocene before terminating prior to deposition of the Nordland Group during the Miocene (Underhill, 2009). Much of the tectonic shortening caused by folding of the post-Zechstein cover rocks in the area affected by halokinesis was accommodated by lateral displacement of the North Dogger and Dowsing Graben fault systems.

The depth at which the formation is encountered varies considerably as a consequence of the folding, however the crests of the closures considered for CO₂ storage are typically found at depths exceeding 1 km. The closures are affected to varying degrees by crestal faulting associated with formation of the structures (Bentham *et al.*, 2013). Although some of these faults have significant throws, in most cases there is minimal offset on these crestal faults, and Williams *et al.* (2014) show that the faults do not negatively impact on natural gas containment in the faulted BSF gas fields. At the structures considered for storage, faults observed in the overburden generally sole-out in overlying Triassic halite formations, with little to no seismically-resolvable offset of the top BSF reflector. Conversely, crestal faults are known to offset the upper BSF seismic reflector at some sites (Bentham *et al.*, 2013; Williams *et al.*, 2014). The mechanical response of these faults to injection-induced pressure perturbations is likely to be an important consideration for CO₂ storage projects (White Rose, 2016; Williams *et al.*, 2014).

The Greater Bunter Sandstone region which forms the UK case study in the SHARP project, is in the Silverpit Basin, to the east of the Dowsing Fault Zone, north of the Sole Pit Trough, and south of the North Dogger Fault Zone. The region contains the Endurance structure and several other saline aquifer closures. The CO₂ storage potential of this region was evaluated through numerical modelling by Noy *et al.* (2012). The area is bounded by a series of major fault systems, salt walls and reactive fault-salt structures which are believed to isolate the unit from the surrounding saline aquifer (Smith *et al.*, 2011). Within this area the saline aquifer is believed to be well connected with no major structural impediments to lateral fluid migration. This is supported by re-pressurisation of the aquifer following gas-production at the Esmond Gas Field, as described by Bentham *et al.* (2017). An apparent underpressure of 0.07 MPa (10 psi) was encountered in the Endurance appraisal well, which has been mooted to have resulted from gas production at the Esmond gas complex (White Rose, 2016; Gluyas and Bagadu, 2020). However, recent re-analysis of the Endurance pressure data provides an alternative and preferred explanation, whereby the difference in pressure is explained by the difference in depth between the two wells and a significant salinity gradient across the brine column (BP, 2021a).

At one particularly high-relief structure to the east of Endurance, the BSF crops beneath a thin veneer of Quaternary deposits, and there is a risk that CO₂ storage may result in the expulsion of brine (rather than CO₂, which will be trapped in the closures) to the seabed (Noy *et al.*, 2012; White Rose, 2016; BP, 2021a).

The stratigraphy relevant to CO₂ storage in the BSF is shown in Figure 18. The BSF was deposited in an arid to semi-arid terrestrial environment and comprises a series of coalescing alluvial fans dissected by braided river channels and sheetflood sandstones (Bifani, 1986; Ketter, 1991; Ritchie and Pratsides, 1993). Reservoir properties are highly variable, with core plug-derived porosity values showing significant scatter around an arithmetic mean of 19% (Noy *et al.*, 2012). Well testing at the Endurance site indicated an average reservoir permeability of 270 mD, with no barriers or baffles to fluid flow within at least 1.3 km of the well, with this radius constrained by the duration of the test, suggesting the connected aquifer volume to be somewhat larger (Furnival *et al.*, 2014). Halite and anhydrite cements are common and locally occlude porosity, with varying quantities observed at individual locations and depths (Ketter, 1991; Williams *et al.*, 2013a; 2013b; Furnival *et al.*, 2014). The Endurance site itself is in a particularly porous and permeable part of the reservoir with minimal late-stage porosity-occluding cement within the structure (White Rose, 2016; BP, 2021b). Slightly reduced permeability is expected to be encountered elsewhere (Bentham *et al.*, 2017). The top seal is provided by fine-grained strata of the Upper Triassic Haisborough Group, a thick succession dominated by red mudstones, laterally equivalent to the Mercia Mudstone Group, onshore UK. The seal capacity of the Haisborough Group is enhanced over much of the SNS by one or more of three widespread, yet not ubiquitous halite members (Heinemann *et al.*, 2012). In the study area, the immediate top seal is provided by a thin shale unit known as the Solling Claystone, which separates the BSF from the Röt Halite Member above. In some parts, a thin Intra-Solling Sandstone is also present. The seal capacity of the Solling Claystone is demonstrated at the Esmond Gas Field where it has inhibited aquifer recharge to the depleted upper gas reservoir (Intra-Solling Sandstone) following cessation of gas production (Bentham *et al.*, 2017).

The sealing properties of laterally-equivalent strata have been evaluated onshore UK (Armitage *et al.*, 2013; 2015) and in the Netherlands sector of the SNS (Spain and Conrad, 1997). Measured porosities from caprock samples in the P15-14 well in the Netherlands range from 0.7 to 5.4%, with vertical permeabilities ranging from 0.002 to 0.240 mD. A gas-water capillary pressure displacement pressure of 4.688 MPa was measured for the Solling Claystone immediately above the BSF, suggestive that the core sample would be expected to retain a gas column of 594 m (Spain and Conrad, 1997). Mercia Mudstone Group strata from onshore UK suggest CO₂ column heights of 70–540 m could be retained (Armitage *et al.*, 2013). The estimates above may provide conservative estimates of the likely seal capacity of Haisborough Group strata in the study area, as the Röt Halite Member immediately overlies the Solling Claystone. Seal integrity of approximate age-equivalent strata in the East Irish Sea Basin is excellent where Triassic hydrocarbon reservoirs are overlain by halite-dominated intervals in the Mercia Mudstone Group (Seedhouse and Racey, 1997).

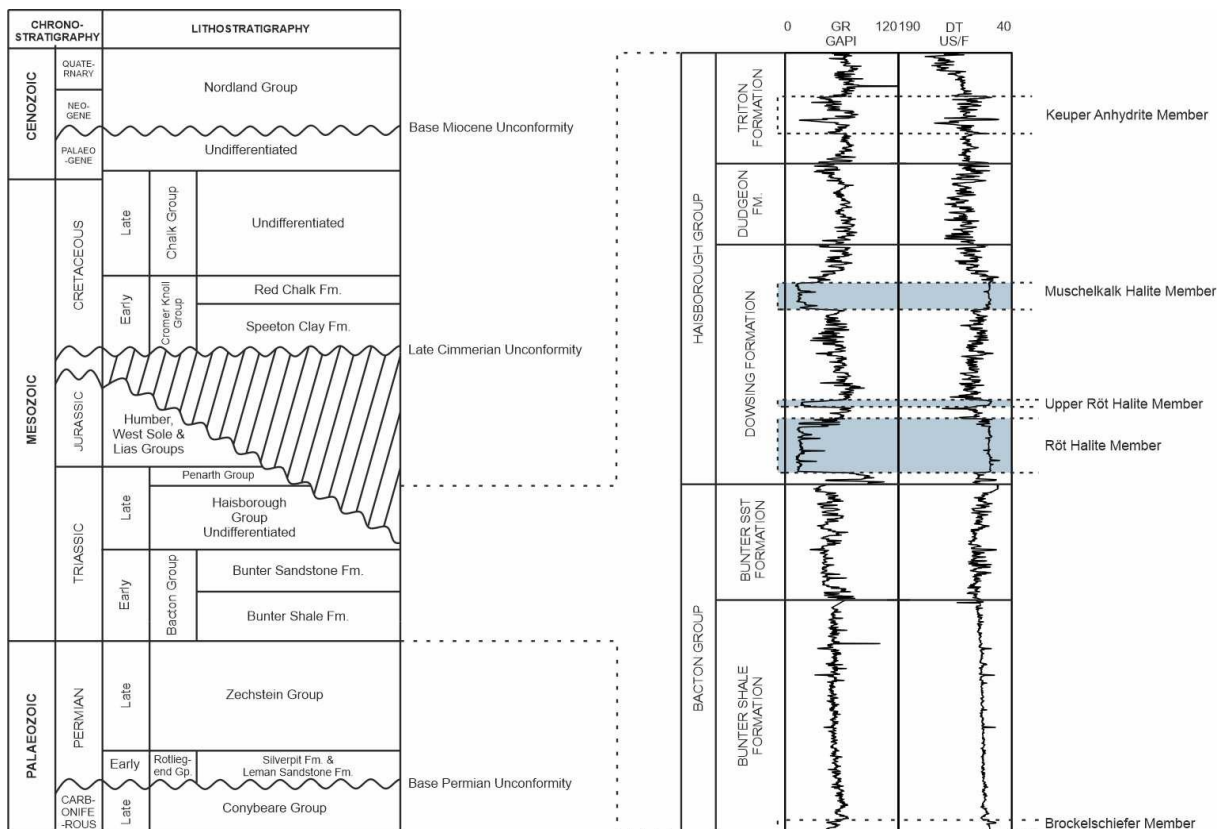


Figure 18. Generalised stratigraphy and geophysical log response through the Triassic succession in the NW part of the UK Southern North Sea. Figure reproduced after Noy *et al.* (2012) and Williams *et al.* (2014). BGS © UKRI (2022).

2.2.2 In situ stress conditions

Plate-boundary forces provide a first-order control on stress orientations across NW Europe, with strike-slip stress conditions prevailing ($S_{Hmax} > S_v > S_{Hmin}$) and S_{Hmax} oriented approximately NW–SE (Müller *et al.*, 1992; Golke and Coblenz, 1996; Heidbach *et al.*, 2008; 2010; Kingdon *et al.*, 2022). Kingdon *et al.* (2016) showed that this NW–SE ‘ridge-push’ stress direction is relatively consistent onshore UK, while Baptie (2010) identified that both strike-slip and reverse stress states persisted onshore. Williams *et al.* (2014; 2015) postulated that the Zechstein evaporites might be acting to decouple the post-Zechstein stress field affecting the Mesozoic section from the prevailing basement stresses in the SNS. Bell (1996) and Tingay *et al.* (2011) showed that detachment of stress fields can occur above mechanically weak horizons in sedimentary basins. Several authors have previously identified that superposition of local factors, including halokinesis, have resulted in variable S_{Hmax} orientations in other parts of the North Sea (Ask, 1997; Hillis and Nelson, 2005). Stress orientation anomalies have also been associated with salt bodies in many other parts of the world, including the Nile Delta (Tingay *et al.*, 2011), Gulf of Mexico (Yassir and Zerwer, 1997) and the North German Basin (Roth and Fleckenstein, 2001; Heidbach *et al.*, 2007). Although supporting evidence in the SNS is limited, borehole stress indicators suggest that the azimuth of S_{Hmax} over the BSF closures is oriented along the structural strike, whereas S_{Hmax} is oriented in the regional NW–SE orientation below the Zechstein evaporites (Figure 19).

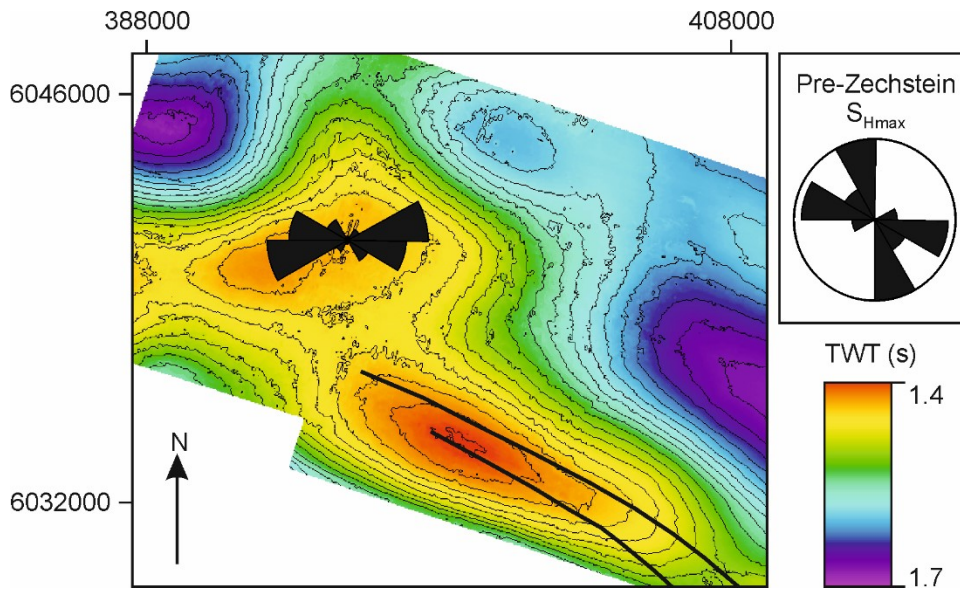


Figure 19. Orientation of S_{Hmax} from breakout analysis in a single well over a BNS structure in the UK Quadrant 43. The rose diagram is plotted at the well location on the structure, and shows only the S_{Hmax} orientations in the post-Zechstein succession, while the inset rose diagram shows the S_{Hmax} orientation in pre-Zechstein strata. Figure reproduced from Williams *et al.* (2014). BGS © UKRI (2022).

Teufel (1991) showed a similar effect at the Ekofisk Field in the Norwegian sector of the Central North Sea, with radial S_{Hmax} orientations around the closure and axial S_{Hmax} orientation along the structural crest. Williams *et al.* (2015) interpreted breakout data from the wider UK SNS to determine if this effect is widespread across the basin (Figure 20).

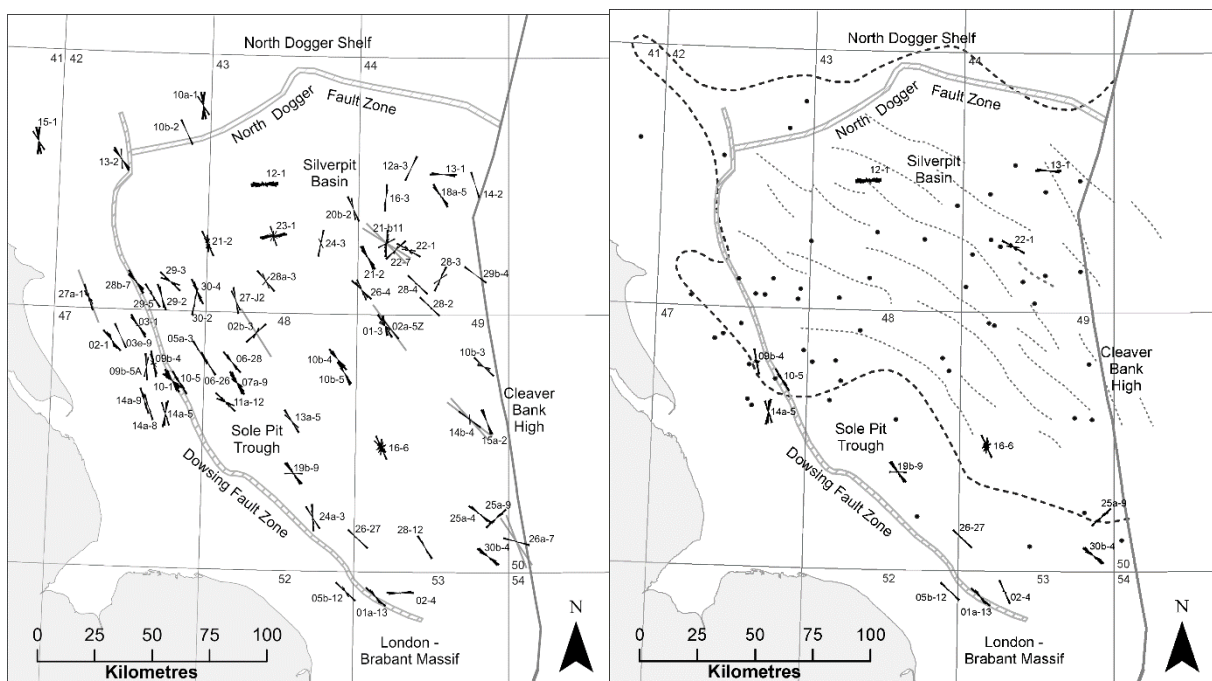


Figure 20. Left: Frequency plots showing S_{Hmax} orientations for all logged stratigraphic intervals across the UK Southern North Sea from analysis of four-arm caliper logs (roses) and borehole image logs (grey lines). Right: Post-Zechstein S_{Hmax} orientations displayed as frequency plots by well. The thick dashed line marks the area affected by halokinesis, while the faint dotted lines represent the approximate axes of major salt-induced folds in the post-Zechstein cover rocks. Figures reproduced from Williams *et al.* (2015). BGS © UKRI (2022).

The data used to derive stress orientations from borehole breakout and drilling-induced tensile fractures (4-arm calipers and borehole image logs) are generally only acquired over certain depth ranges of interest in hydrocarbon wells. In the UK SNS, there is a scarcity of such data at depths most relevant to CO₂ storage in the BSF, although the available data suggest that S_{Hmax} orientations are more variable within the area affected by halokinesis (Figure 20). This supports the stress detachment hypothesis, however it is important to recognise the limitations of the available data. High quality image logs through the BSF and its overburden would be highly beneficial in reducing the uncertainty. Further evidence is provided by the fault patterns affecting the structural closures, which mimic the axial and radial S_{Hmax} orientations observed by Teufel (1991). Whilst the fault patterns may be indicative of the stress conditions during formation of the closures, they do not necessarily provide clarification of the contemporary stress state. Recent analysis of borehole image logs from the Endurance appraisal well yielded little stress indicator information because the well was drilled close to gun barrel, with no visible borehole breakouts or drilling-induced tensile fractures (BP, 2021c). Dispersion analysis of sonic scanner logs however identified some minor slowness anisotropy in the BSF, with the fast shear azimuth, assumed to be representative of S_{Hmax} , estimated at 92–105° (BP, 2021c). This orientation differs from the regional average NW–SE orientation indicative of plate-boundary forces and is approximately perpendicular to the structural contours. This supports the notion that stresses at potential BSF storage sites result from interaction between local structural geometries and regional forces (Figure 21).

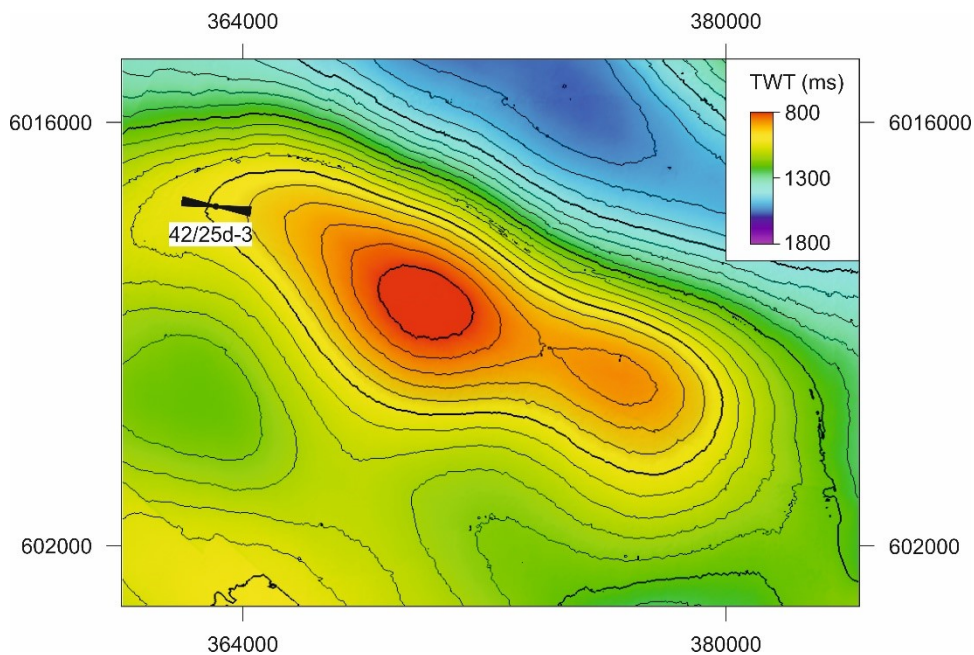


Figure 21. Two-way travel time (TWT) structure at top BSF level at the Endurance structure. Interpreted S_{Hmax} orientation derived from dispersion analysis of sonic scanner logs from well 42/25d-3, shown by black lines at well location. The data range shown is reported by BP (2021c). BGS © UKRI (2022).

It is generally assumed that the state of stress above the Zechstein is one of normal faulting where $S_v > S_{Hmax} \geq S_{Hmin}$, which differs from the expected strike-slip stress state of deeper pre-Zechstein strata. A normal stress state was assumed in a geomechanical modelling study of CO₂ injection at the Endurance site (White Rose, 2016). Williams *et al.* (2015) presented a compilation of stratigraphically-constrained leak-off test (LOT) and formation integrity test data (FIT) from the UK SNS (Figure 22). The data suggest that the magnitude of the least principal stress in the Mesozoic to Recent succession is

slightly lower than the vertical stress, indicating that S_{hmin} is the least principal stress and excluding the possibility of compressional tectonics. Lithological effects are clearly seen in the data, with the mechanical properties of halite and claystone dominated lithologies contributing to higher test values.

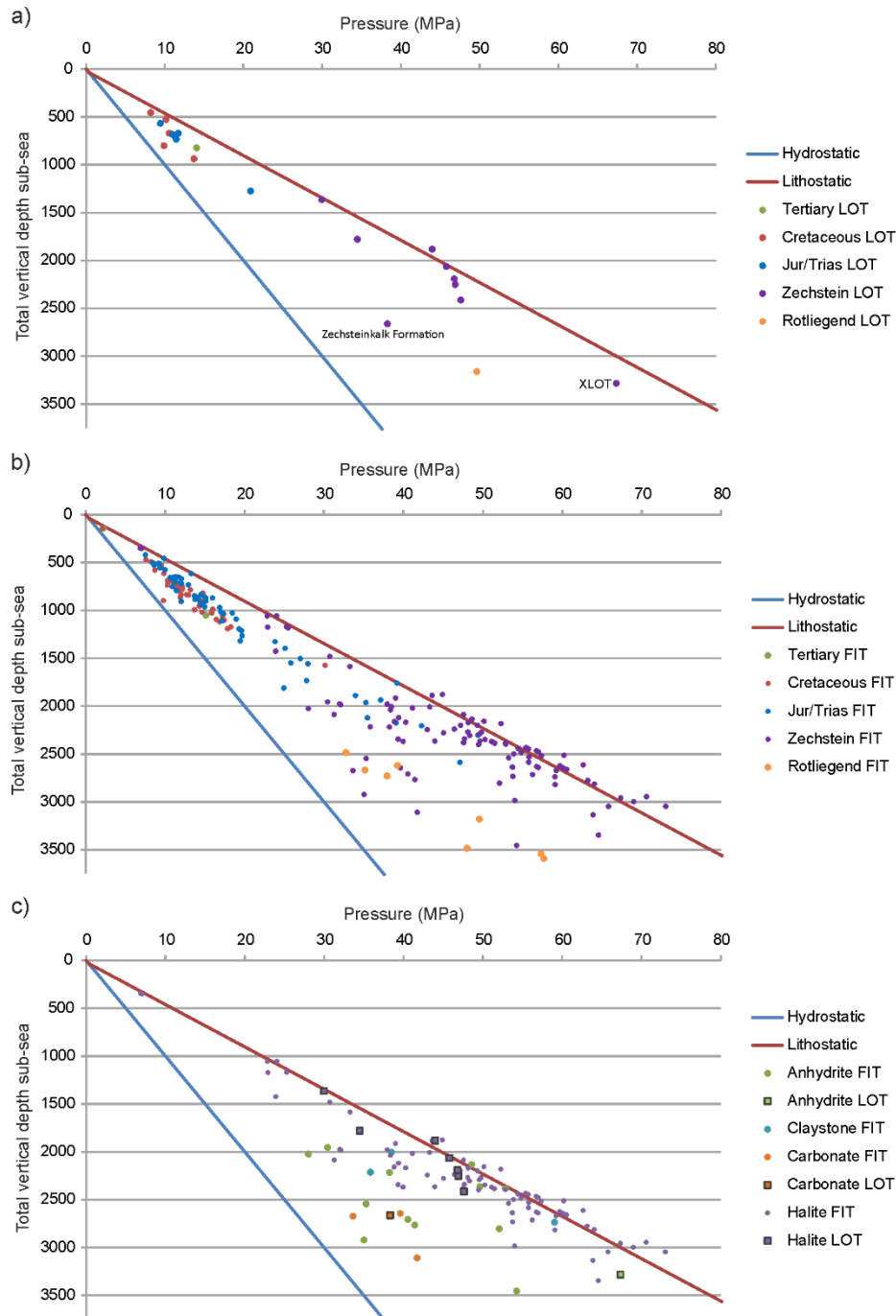


Figure 22. Compilation of a) LOT data from the UK SNS, b) FIT data, and c) LOT and FIT by dominant lithology in the Zechstein Group. A hydrostatic gradient of 10 MPa/km is shown along with a notional overburden gradient of 22.5 MPa/km. XLOT is an extended LOT, for which only a single measurement is recorded. Figure reproduced from Williams et al., 2015. BGS © UKRI (2022).

Horizontal stress information estimated from minifrac data acquired in the Endurance appraisal well were presented by White Rose (2016), and are reproduced in Table 2. The Röt Halite FIT showed no indication of leak-off or fracturing, and stresses are likely closer to lithostatic within the pure halite

layers. The acquired minifrac data from the BSF and Solling Claystone provide high quality stress measurements based on five cycles of breakdown, pump-in and shut-in. Closure stresses, taken as a proxy for the least principal stress, were calculated on the last three iterations, yielding consistent estimates, and are regarded as accurate estimates of S_{hmin} . A single XLOT was attempted in the Liassic Shales (Jurassic) in the overburden at a depth of 746 m (below rotary table) and achieved a pressure of 19.5 MPa/km, very similar to the Solling Claystone minifrac values. This implies good mechanical sealing potential in the shallow clay sections in the absence of any pre-existing weaknesses. The White Rose (2016) study estimated the magnitude of S_{Hmax} as a function of S_{hmin} for both the BSF and the Solling Claystone (Table 2).

Table 2. FIT and minifrac data acquired from the 42/25d-3 Endurance appraisal well (White Rose, 2016). Depths are given in units of m True Vertical Depth Sub-Sea (TVDSS).

Unit	Depth (m TVDSS)	S_{hmin} (MPa)	S_{hmin} gradient (MPa/km)	Regional S_{Hmax}/S_{hmin}	Type
Röt Halite	1339	21.4	16	-	FIT
Solling Claystone	1363	26.4	19.4	1.2	Minifrac
BSF	1520	26.2	17.2	1.15	Minifrac

2.2.3 Seismicity data currently available

Seismic detection capability in the Endurance region is moderate, as shown in Figure 23. There is presently a sparse distribution of seismometers on the east coast of Britain, which is reflective of the lower levels of seismic activity relative to the west coast. The smallest routinely detectable event in the Endurance licence area is around M_L 2.2. This means smaller events with $M < 2$ are likely to be missed, which could result in an incomplete picture of activity in the area. There have been several hundred recorded earthquakes in the region, however, as shown in Figure 24.

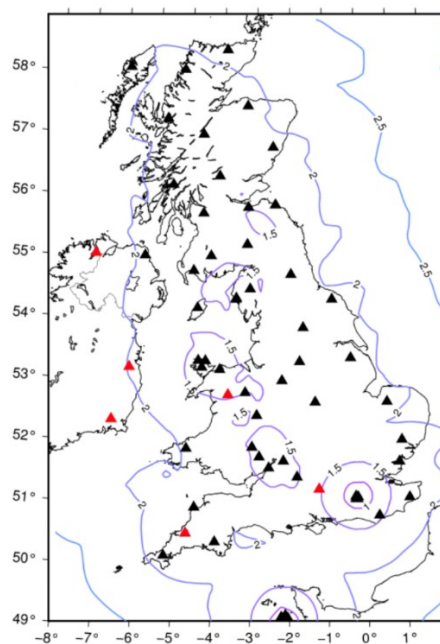


Figure 23. Detection capability of the UK national seismic network mostly operated by the British Geological Survey (BGS). Triangles show the station locations, with black showing those operated by the BGS, and red denoting stations operated by other agencies. Contours show the detection capability in local magnitude M_L . In the Endurance region, the smallest routinely detectable event is around M_L 2.2. Figure reproduced from Baptie (2020). BGS © UKRI (2022).

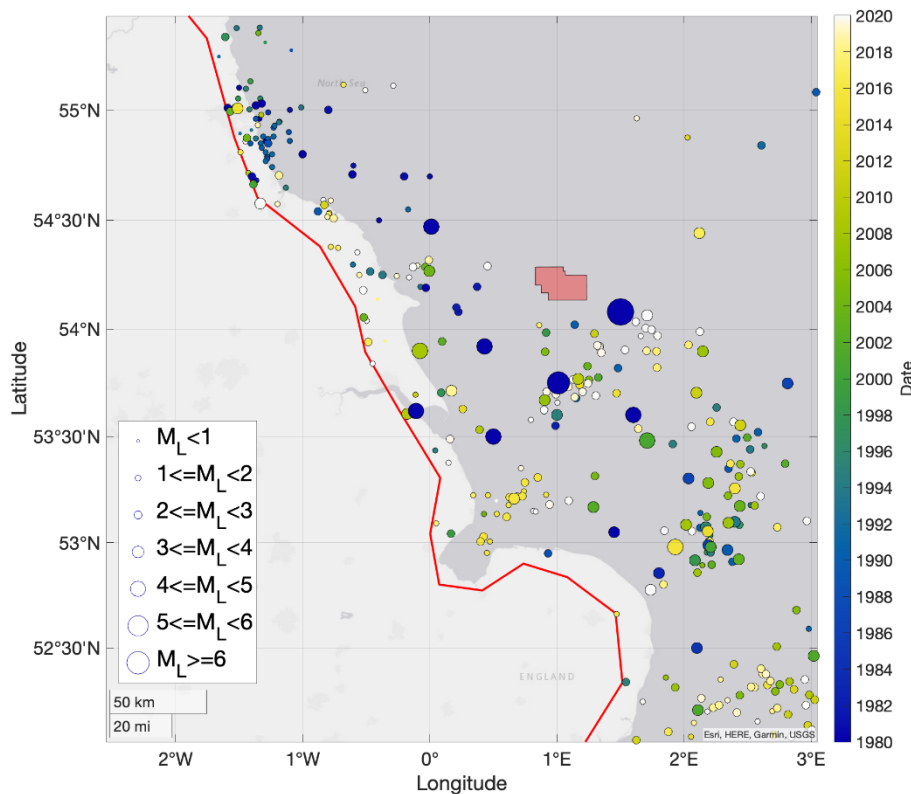


Figure 24. Earthquake hypocentres from the latest Work Package 2 seismicity catalogue. The red line shows the boundary of the study area, while the red box shows the extent of the Endurance carbon storage licence. Earthquake locations are sized by magnitude and coloured by time, limited to between 1980 and 2020 (see Figure 4).

While no events were reported directly inside the Endurance licence block, several large magnitude events have occurred in the general vicinity (Figure 24). The largest events in the storage complex are comparatively historical, being the February 09th 1958 M_L 5.1, around 50 km to the south, and the June 07th 1931 M_L 6.1 around 35 km to the southeast. It should be noted that this M_L 6.1 earthquake is the largest event recorded near the British Isles, and the largest in the BGS earthquake catalogue. Since 1985, with the advent of widely distributed seismic stations and a meaningful reduction in the magnitude of completeness, 5 events above a $M_L > 2$ were detected within 50 km of the Endurance storage licence. The largest of these was the June 21st 1998 M_L 2.8 event, 22 km to the south of the storage licence.

Focal mechanism data are sparse in the region (Figure 25), and offshore focal mechanisms are particularly uncommon due to the limited azimuthal coverage of seismic stations in the region. This should be improved through the data amalgamation and reanalysis ongoing in SHARP Work Package 2. In general, strike-slip mechanisms are prevalent across Britain, and this trend continues with the few events with focal mechanisms on the east coast of England. Mechanisms with a much greater component of reverse faulting are found further towards the south, with correspondingly larger magnitudes.

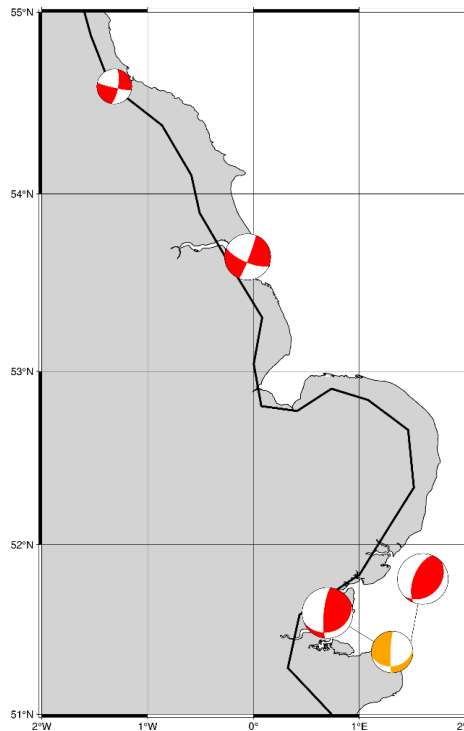


Figure 25. Focal mechanisms in the Endurance region. Very little data are available in the area, but those that are present exhibit strike-slip mechanisms, consistent with nearby stress measurements both onshore and offshore. Figure reproduced from Weemstra et al. (2022).

Figure 26 shows the distribution of event magnitudes shown in Figure 24. The b-value of 0.72 ± 0.21 is lower than expected for typical tectonic seismicity, however, there are few events (less than 100) above the stable M_{\min} to define the G–R b-value. Being based on so few events means this is not a statistically robust b-value. However, as they come from data collected and processed from a single agency (the BGS), it would be expected that magnitude homogenisation would not be an issue. An increase in the detection capability would increase the number of detected events and allow for a statistically significant gauge on earthquake activity in the region.

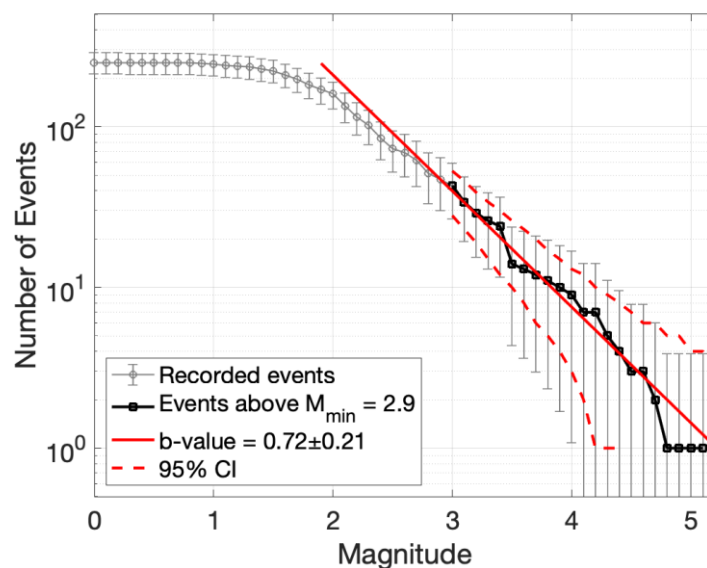


Figure 26. Magnitude-frequency distribution for the events shown in Figure 24.

2.2.4 Mechanical properties

A comprehensive programme of laboratory investigations, petrophysical log analyses and literature review was conducted for the Endurance site to inform a geomechanical modelling study for the intended storage project (White Rose, 2016). Key parameters derived are detailed in Table 3. Although they were examined experimentally, salt creep responses were not considered in the modelling study, and the Biot's Elastic Coefficient (α) was assumed to be 1 in all units.

As shown in Table 3, the Young's Modulus measured in the halite samples was extremely low (~0.1 Mpsi), however the halite plugs were noted to be heterogenous, with anhydrite crystals, stringers and small anastomising microfractures. It was unclear as to whether such samples resulted from coring and handling processes, so both Young's Modulus and Poisson's Ratio are highly uncertain. While the parameters detailed in Table 3 are representative of the Endurance site, it is unclear as to how variable these parameters may be across the region.

Table 3. Published, measured and modelled geomechanical property ranges for the Röt Halite, Solling Claystone and BSF. The VISAGE cases refer to the geomechanical model parameterisation for the Endurance model. The weak-case halite parameters with low Young’s Modulus are designed to compensate in linear elastic failure modes for the creep deformation behaviour of halite over months to years when responding to changes in load. Data summarised after White Rose (2016).

Unit	Source	Young’s Modulus (GPa)	Poisson’s ratio	Unconfined compressive strength (MPa)	Friction angle	Linear thermal expansion coefficient (1E-5/°C)
Röt Halite Member	Senergy Report (source unknown)	31.2 (P50)	0.22 (P50)	3.2	22	4 (highly temperature dependent)
	Core tests (static)	0.689 (samples disaggregating?)	0.27	12.9	44	4 (average from 3.85 at 20°C and 4.24 at 40°C to 80°C)
	Linear elastic log analysis (dynamic)	34.5	0.28 or 0.36	59.5	-	-
	Liang et al. (2007)	5.2 (zero confining stress)	0.31	18.5 (range 15-32)	31	-
	VISAGE weak Röt Halite case	6 (constant)	0.28 or 0.36	11-14 (average 12.9). Not used	39 (not used)	4
	VISAGE reference case	31-34 (average 33)	0.28 (constant)	11-14 (average 12.9). Not used	39 (not used)	4
Solling Claystone	Senergy (source unknown)	11.1 (P50)	0.29 (P50)	28.3	34 (P50)	0.33
	Core tests (static)	13.8	0.17 (average)	53.1	30	1.4
	Linear elastic log analysis (dynamic)	29.4	0.28 or 0.36	37	-	-
	VISAGE reference case average	11-20 (average 14)	0.22-0.26 (average 0.24)	25.6-116.5 (average 50.2)	34-39 (average 36)	1.4
Bunter Sandstone Formation	Senergy (source unknown)	13 (P50)	0.26 (P50)	19.5 (P50)	35 (P50)	0.9
	Core tests (static)	14.5	0.19 (average)	46.2	41	1.2
	Linear elastic log analysis (dynamic)	29.5	0.27 or 0.36	39.7	-	-
	VISAGE reference case average	7.5-32.4 (average 12.5)	0.19-0.37 (average 0.25)	0.83-411.5 (average 39)	24-46 (average 36)	1.2

2.2.5 Rock failure studies

Williams *et al.* (2014) conducted a conservative analysis of rock-failure in the BSF, including an assessment of the reactivation potential of pre-existing, cohesionless and optimally-oriented faults. Using pressure and stress gradient data first presented by Noy *et al.* (2012), a Mohr analysis was used to calculate the pressure required to reactivate such a fault. In practice, existing faults will not necessarily lack cohesion, and may in fact possess higher strength than the surrounding rock in the event of strain-hardening behaviour during deformation. Albeit conservative, the results provide a lower-bound estimate for potential rock-failure limits. Figure 27 illustrates the rock failure estimates of Williams *et al.* (2014).

While the regional data compilations presented by Noy *et al.* (2012) and Williams *et al.* (2014; 2015) provide a useful regional context, data acquired from the Endurance site indicate that use of a single fracture pressure gradient neglects the important impact of stratigraphically-constrained lithological variations in fracture pressure (Table 2). Site specific geomechanical characterisation is therefore recommended to accurately determine rock failure constraints for individual sites during 'round 2' rock failure assessments.

A detailed 3D geomechanical analysis was conducted for the Endurance CO₂ storage site by White Rose (2016), based on a first-load case of 2.68 Mt/year CO₂ injection over 20 years. Key results are summarised in Table 4 and provide an indication of the impact of various uncertain parameters. The reference case found that only minor failure would be expected in the upper BSF layers at the crest of the structure with some minor stress changes around overburden faults. Potential issues generally related to cooling due to temperature contrasts between the injected CO₂ stream and the surrounding rock, which results in failure of the uppermost BSF and lower parts of the Röt Halite above the injection wells in pessimistic (limit case) model iterations. Some failure may be expected based on a limit case where a weak overburden fault is elongated such that it penetrates through the Röt Halite and into the BSF. Excessive cooling in the upper part of the BSF is an important consideration as the modelling shows that thermal stresses may lead to tensile failure of the upper reservoir and of the Röt Halite. The halite is particularly prone to tensile failure during cooling as a result of its high Linear Thermal Expansion Coefficient (LTEC), and may require consideration in well completion design and injection strategies.

Thermally induced fracture modelling undertaken for the Endurance site indicates that the risk of vertical fracture growth is both low and manageable (BP, 2021d). None of the scenarios considered in the modelling resulted in fractures reaching the top of BSF by the end of the injection period. The most important parameters identified in this work were the Young's modulus and the LTEC, which control the thermo-elastic stress reduction during injection. The study also indicates that there is low risk of CO₂ migrating vertically to the top of the BSF via induced fractures.

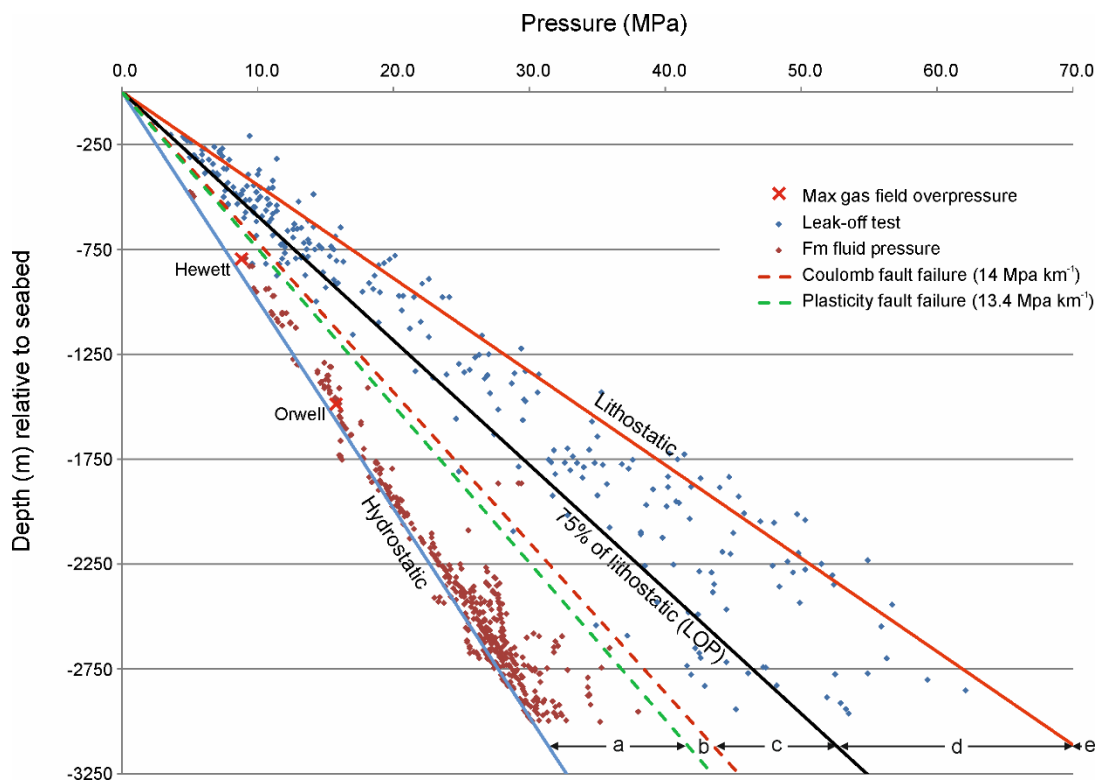


Figure 27. Pressure measurements and LOP data from the UK SNS overwritten by hydrostatic pressure gradient, overburden (lithostatic) gradient and conservative fracture pressure gradient after Noy et al. (2012), and fault reactivation gradients (Coulomb and Coulomb Plasticity) calculated by Williams et al. (2014). Leak-off pressure measurements can be loosely divided into the following rock failure categories: a) tests not being fully taken to leak-off, b) reactivation of optimally-oriented faults, c) reactivation of non-optimally oriented faults, d) failure of intact rock, e) local variations or high tensile strength lithologies. Coefficient of friction of 0.56 used after short-term laboratory experiments using simulated fault-gouge analogous to BSF, after Samuelson and Spiers (2012). Pressure data shown courtesy of IHS, reproduced from Noy et al. (2012). Figure reproduced from Williams et al. (2014). BGS © UKRI (2022).

Table 4. Key results of geomechanical modelling cases for the Endurance CO₂ storage site (White Rose, 2016).

Geomechanical model case	Conditions	Results
Initial case	No faults, weak halite	Simple cooling at perforations, tensile failure in Röt Halite from cooling
Pessimistic limit case (linear)	Very weak faults, one overburden fault extending to upper BSF	Plume cooling above one well affecting Röt Halite. Some failure seen in BSF fault and in cooled Röt
Pessimistic lines case (non-linear)	Non-linear run of above	Increased elastic strains around faults
Limit case (weak halite)	Weak faults, one overburden fault extending to upper BSF, weak halite	Plume cooling above one well, some failure in upper BSF, and in halite above plume
Limit case (strong halite)	Weak faults, one overburden fault extending to upper BSF, strong halite	Plume cooling above one well, some failure in upper BSF, and in halite above plume. Greater likelihood of cooling related tensile failure in halite with higher Young's Modulus and lower Poisson's Ratio compared to weak halite case
Optimistic limit case	Strong faults, one overburden fault extending to upper BSF, weak halite	Plume cooling above one well, some minor failure in upper layers at crest, tensile failure in halite above the plume, no obvious stress changes around faults
Reference case (linear)	Weak faults, no fault extension, weak halite	Plume cooling above one well, some minor failure in upper layers at crest, some minor stress changes and strain around overburden faults but no thermal or fault-related yielding. No significant failure
Reference case (non-linear)	Non-linear run of above	Results very similar to linear case

2.3 Aramis site

The Aramis project is a cooperation between Shell, TotalEnergies (TE or TEPNL), EBN and Gasunie to establish a large-scale open access offshore CCS infrastructure consisting of a cluster of depleted gas fields (and possibly aquifers) targeted for storage, and a dense-phase CO₂ pipeline connecting that cluster to an onshore CO₂ hub (Figure 28). Storage of CO₂ is planned to commence with two depleted gas fields, the K14-FA field that is currently operated by NAM, and the K06/L04 and L07 fields operated by TotalEnergies (Figure 29 and Figure 30). Injection of CO₂ is planned to start in 2026 (Figure 31).



Figure 28. Illustration of the Aramis pipeline and the approximate location of the offshore CCS locations (<https://www.aramis-ccs.com/project>).



Figure 29. Map of the Netherlands onshore and offshore, with existing gas (green) and oil (red) fields and the area of interest for the Aramis CCS project (red circle). (<https://www.nlog.nl/kaart-boringen>).

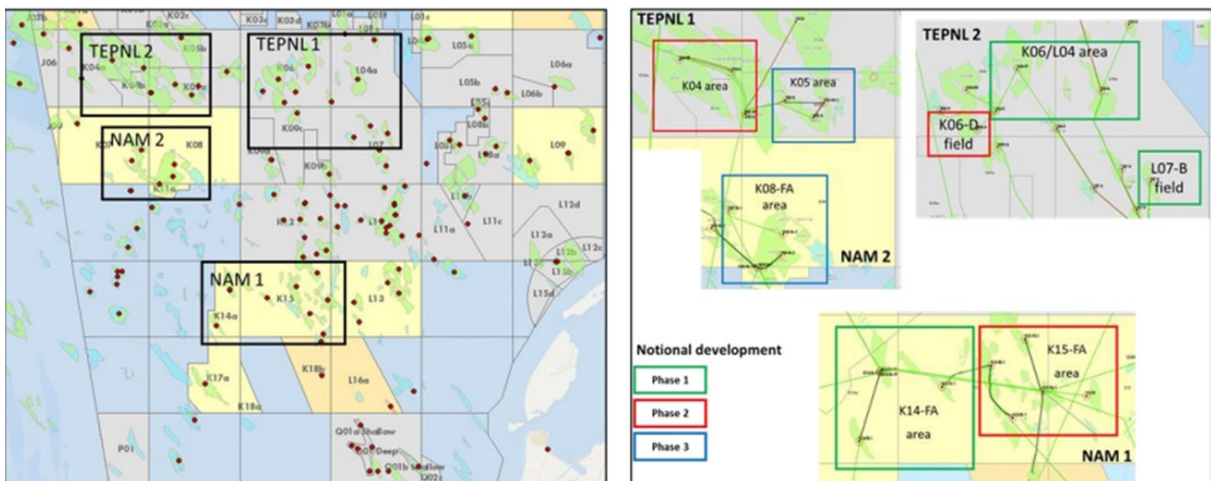


Figure 30. Areas of interest for the Aramis CCS storage sites, using depleted gas fields of NAM and TotalEnergies (TEPNL). Left shows the license areas within which storage candidates are being identified, while right shows the individual fields that are identified for notional phased development (<https://www.rvo.nl/sites/default/files/2021/12/Rapport-Ruimtelijke-Verkenning-15-november-2021-Ruimtelijke-verkenning-CO2-transport-en-opslag.pdf>).

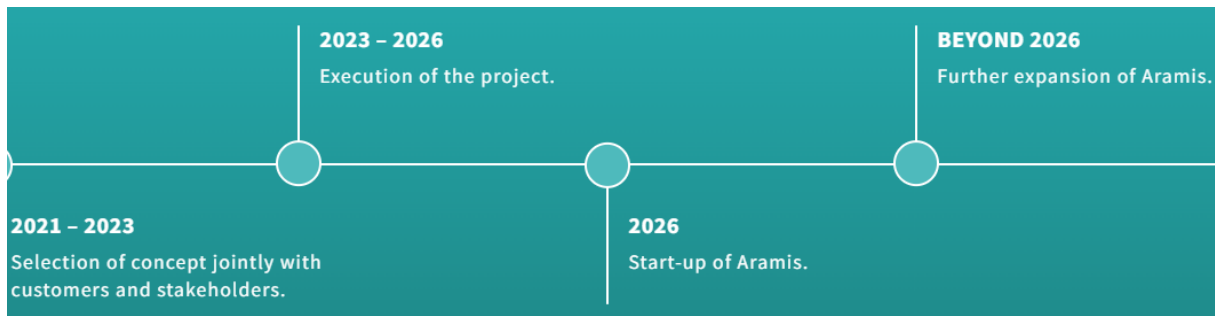


Figure 31. Current timeline for Aramis CCS (<https://www.aramis-ccs.com/project>).

2.3.1 Structural and basin setting

The Aramis Area of Interest (AOI) lies at junction of four tectonic areas (Figure 32), resulting in both locally varying structural trends and stress settings, as well as overprinting of multiple faulting styles within the area. The main target formation for storage is the Rotliegend sandstone, which is the reservoir rock for the majority of hydrocarbon fields in the Netherlands. Additional potential storage formations are found in the Upper Triassic and Lower Cretaceous (Figure 33). The primary seal for Rotliegend reservoirs is the Zechstein Formation, which includes halite layers and forms an excellent seal.

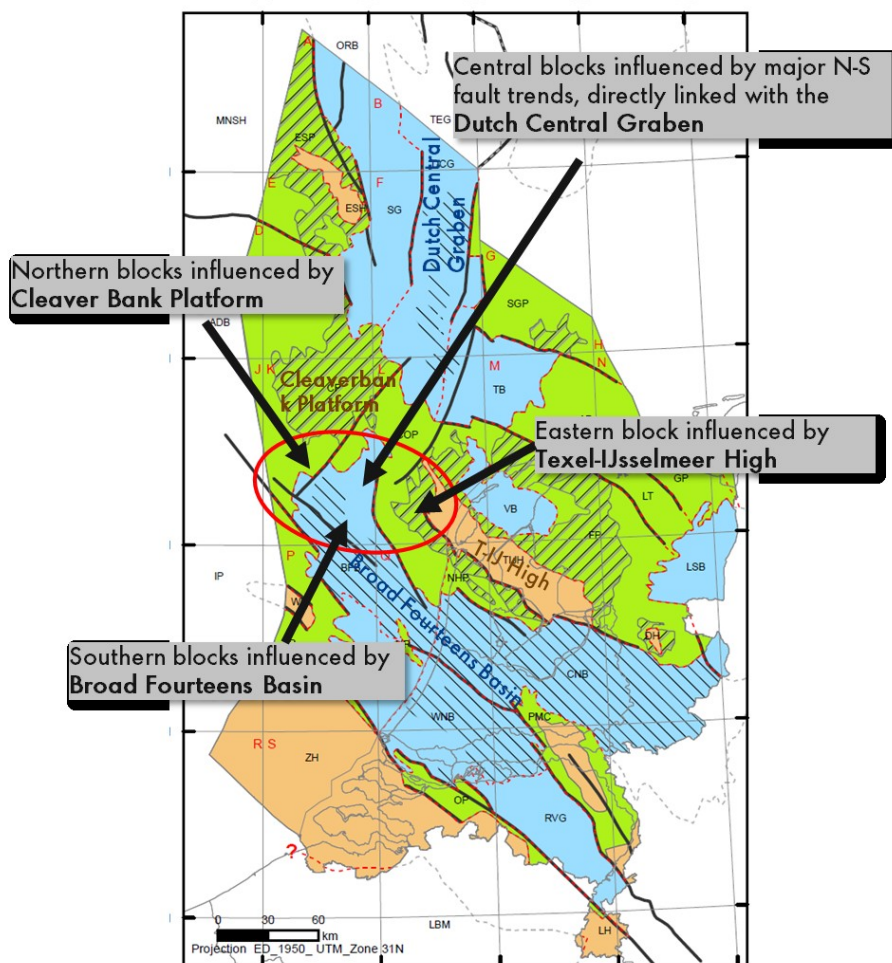


Figure 32. Aramis AOI overlapping four different tectonic areas (Kombrink et al., 2012).

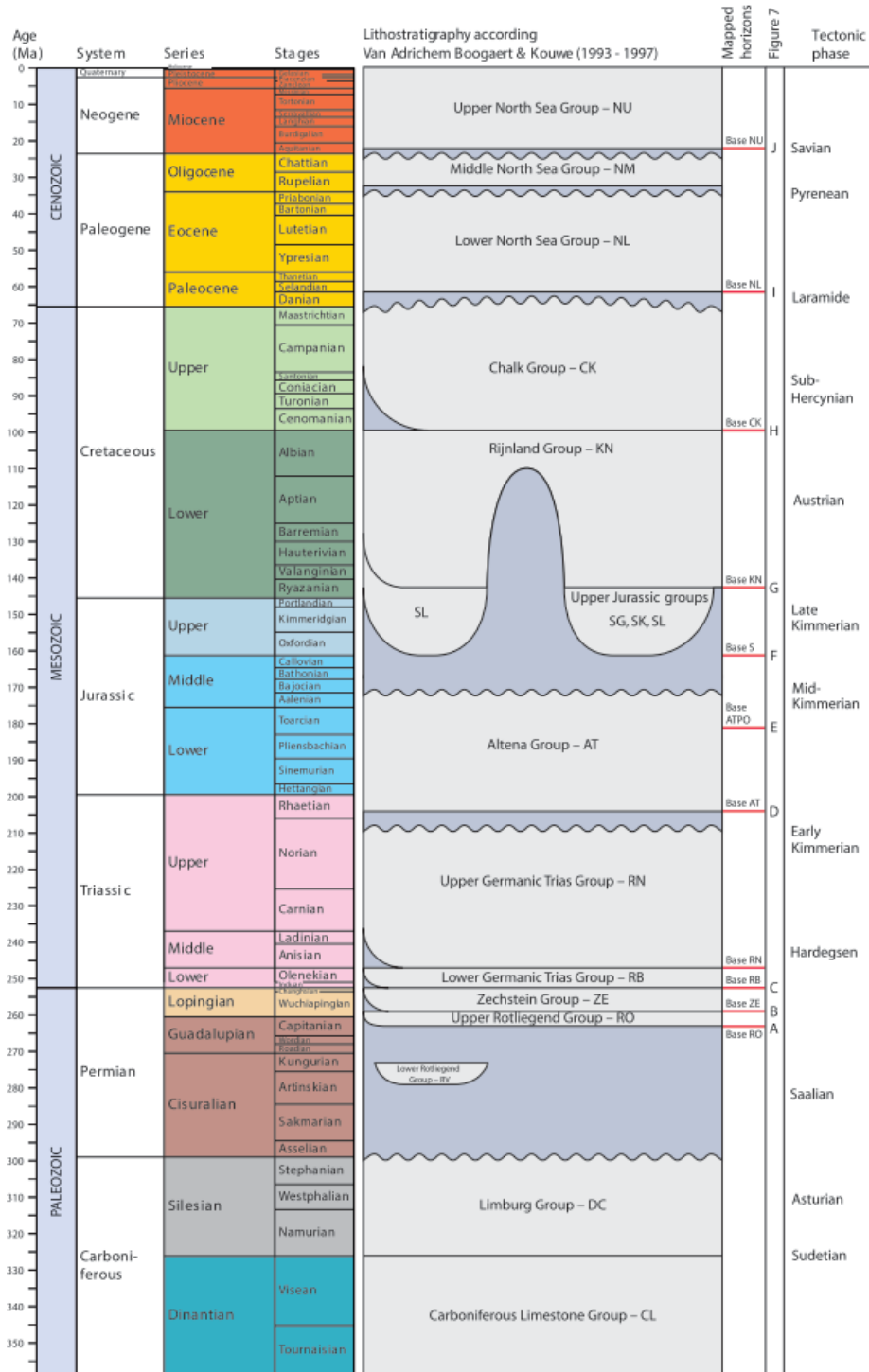


Figure 33. Simplified stratigraphic diagram of the Netherlands (Kombrink et al., 2012). The Permian Rotliegend Group is the primary target for CCS with Zechstein salt as the primary seal. Alternative potential storage formations include sands in the Upper Triassic and Lower Cretaceous.

The Dutch subsurface is generally characterised by a first-order classification of structural highs (horsts) and lows (grabens), which are all found within the Aramis AOI. A High is defined as an area with significant non-deposition and erosion down to the Carboniferous or Permian (Kombrink et al., 2012), such as the Texel-IJsselmeer High east of the Aramis AOI. The northern part of the AOI is part of

the Cleaver Bank Platform, characterised by erosion of the Lower and Upper Jurassic (Kombrink *et al.*, 2012). The key feature of the Aramis AOI is that it borders the edge of both the Dutch Central Graben and the Broad Fourteens Basin, resulting in two partly overlapping structural styles.

These structural features were mainly formed during Late Jurassic and Early Cretaceous rifting, where domains close to highs underwent major uplift in the Jurassic, and mostly mild uplift during Late Cretaceous inversion, except in the grabens where inversion has been more intense. The Broad Fourteens Basin experienced the deepest burial (Figure 34). In general, the graben areas experienced the most intense deformation and faulting.

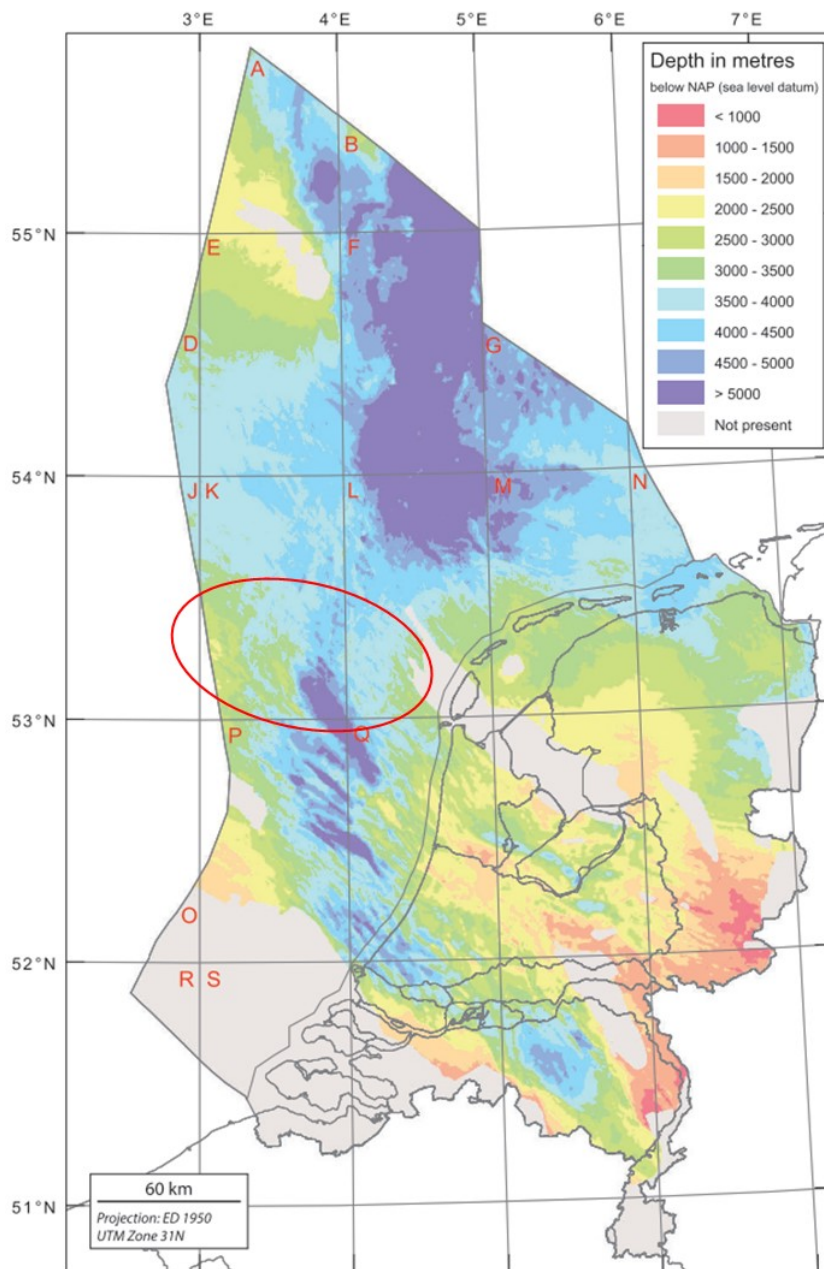


Figure 34. Depth of the base of the Upper Rotliegend Group with the circle highlighting the area within which the Aramis AOI is located. The Broad Fourteens Basin is clearly recognisable as the deep NW-SE graben, which towards the north extends into the Dutch Central Graben. On either side to the west and the east are the Cleaver Bank Platform and Texel-IJsselmeer High respectively.

Within the Broad Fourteens Basin, which covers the largest part of the AOI, multiple phases of faulting and fault reactivation have been identified, commencing with the formation of NW–SE trending horst-grabens in the Carboniferous during the Variscan Orogeny (Ligtenberg *et al.*, 2011). During the Early Kimmerian tectonic phase, E–W to NE–SW extensional tectonics caused rapid subsidence of the grabens. The North Sea became subjected to regional tensional stresses associated with increased rifting in the Norwegian Greenland Sea and Tethys Ocean. The NE–SW extensional activity increased during the Late Jurassic to Early Cretaceous, related to opening of the Atlantic. NW–SE trending faults were reactivated and locally strongly developed N–S fault trends developed in combination with rapid subsidence of the Broad Fourteens Graben. The convergence of Africa and Europe from the Late Cretaceous to Paleocene resulted in northward compression induced basin inversion, reactivating pre-existing faults with reversed oblique strike-slip movements (Ligtenberg *et al.*, 2011).

2.3.2 In situ stress conditions

The orientation of the maximum horizontal stress offshore Netherlands is relatively consistently NNW–SSE to NW–SE (Figure 35) exhibiting a present-day normal faulting regime. The Dutch Geological Survey (TNO) has published an extensive dataset of LOT pressures compiled from wells in the Netherlands (Figure 36 and Figure 37). The aquifers in the Aramis AOI are hydrostatically pressured (Figure 38). The gas fields considered for CO₂ storage are in some cases depleted to about 10% of their initial pressure.

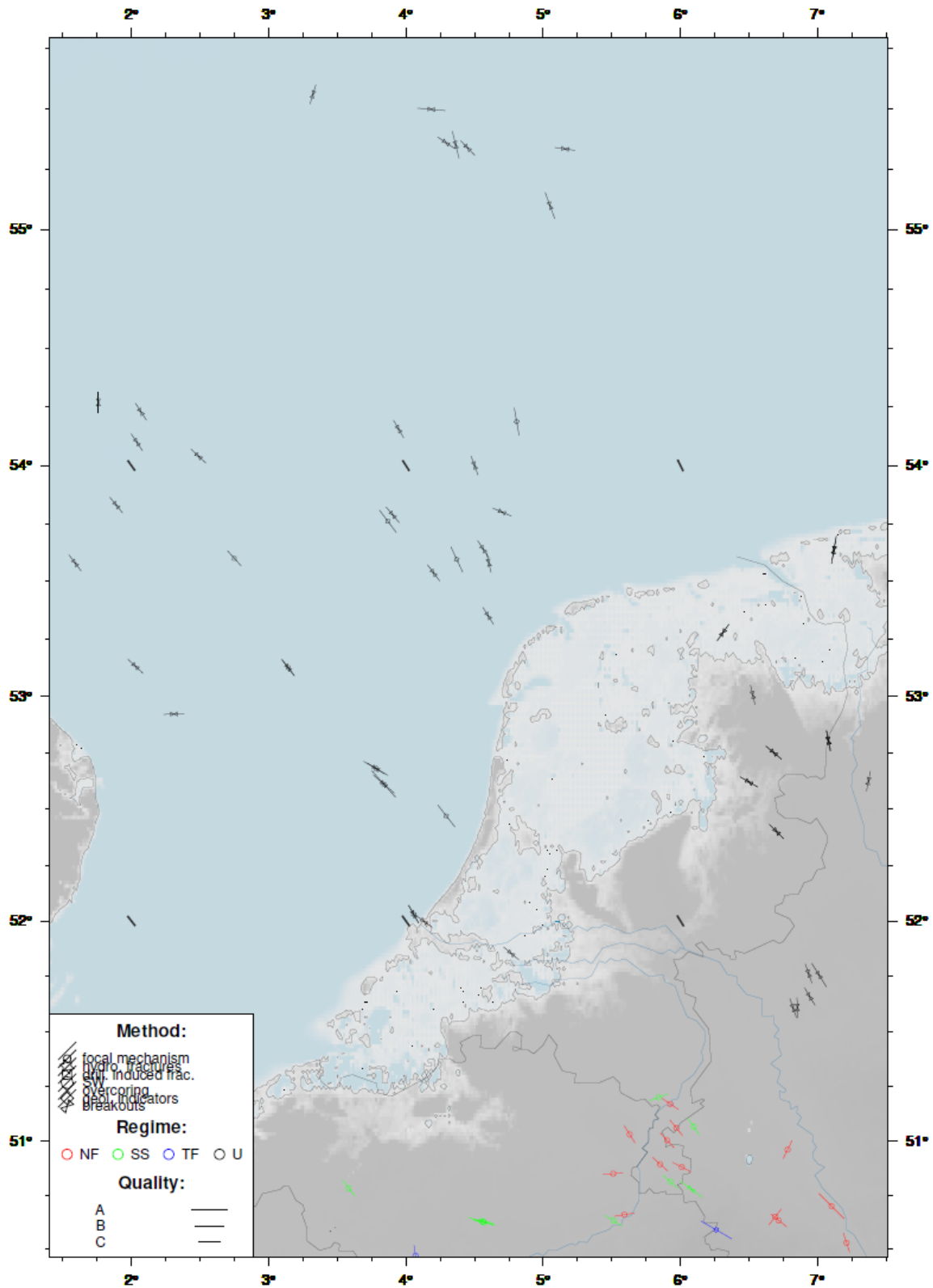


Figure 35. Stress map generated using <https://www.world-stress-map.org/casmo> (Heidbach et al., 2018).

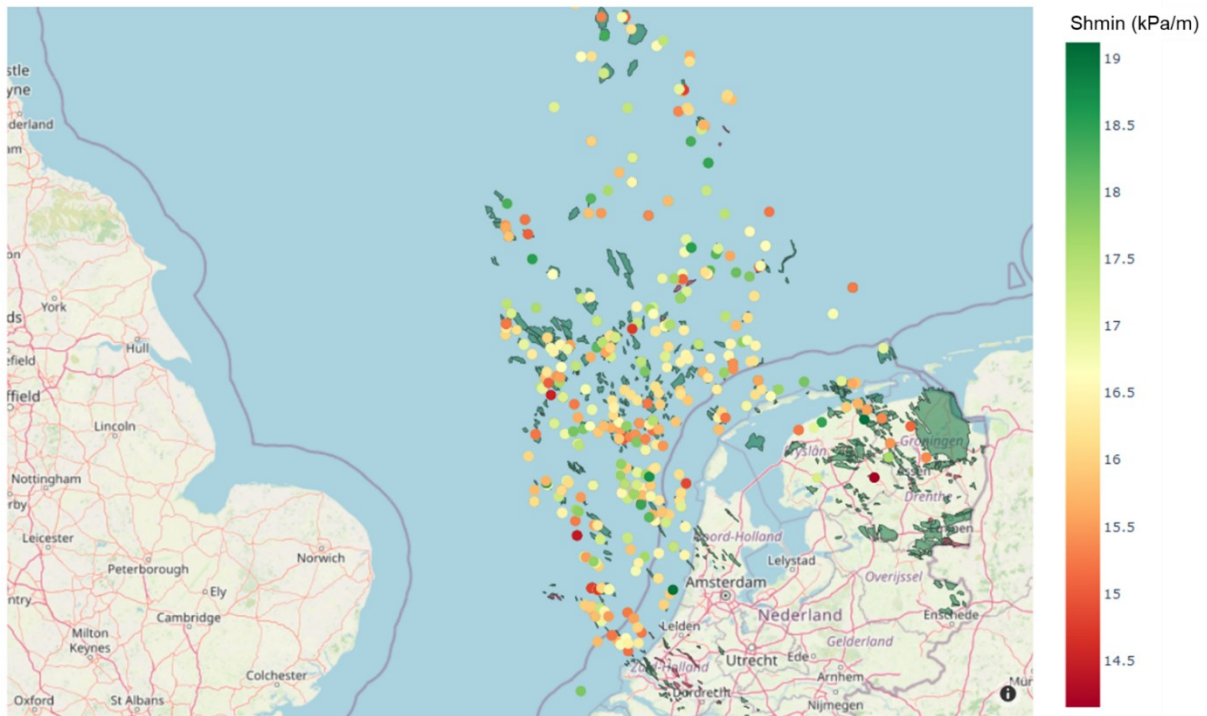


Figure 36. Spatial distribution of Leak-off Pressure tests shown as dots, coloured by the corresponding S_{hmin} gradient calculated from the test data. Data obtained from <https://www.nlog.nl/pressure-southern-north-sea-psns-database>.

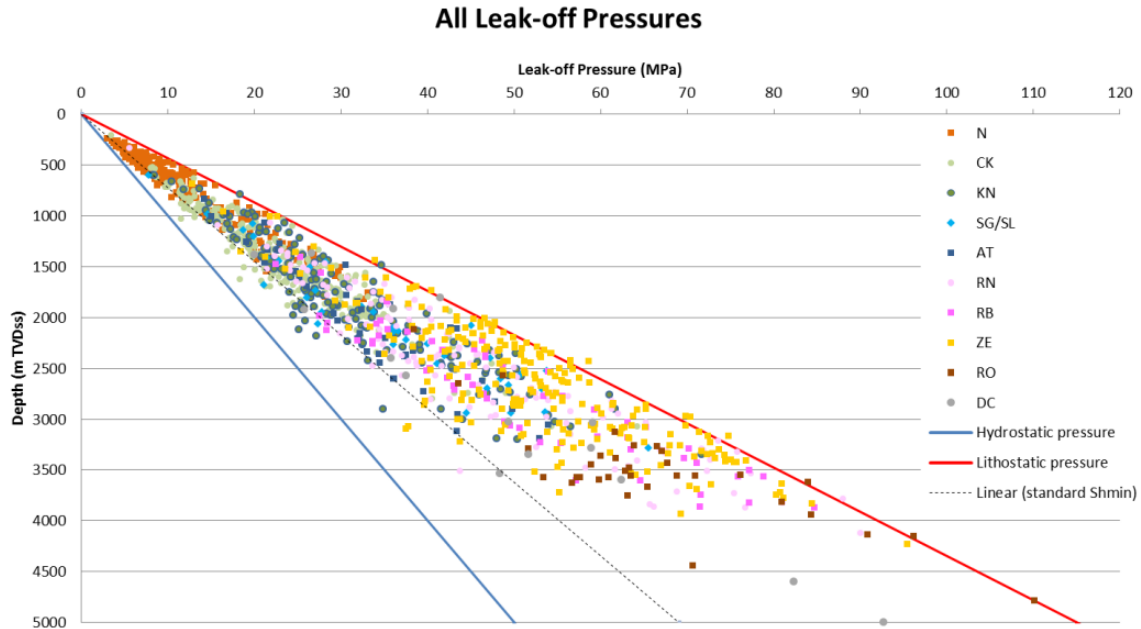


Figure 37. Pressure-depth plot for all leak-off pressure points that are publicly available in The Netherlands, coloured by lithology. For a legend of the abbreviations see labels in Figure 33 (<https://www.nlog.nl/sites/default/files/2020-05/TNO-Report-2015-R10065-final-public2020.pdf>).

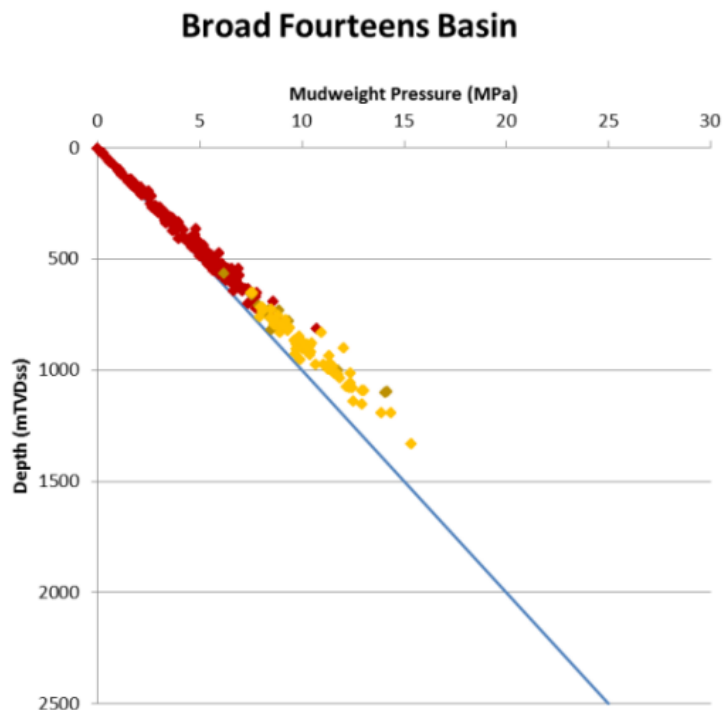


Figure 38. Pressure-depth plot based on mud-weight pressure measurements from the Broad Fourteens Basin (<https://www.nloq.nl/sites/default/files/2020-05/TNO-Report-2015-R10065-final-public2020.pdf>).

2.3.3 Seismicity data currently available

Seismicity is monitored through a network of downhole and surface geophones operated by the Royal Netherlands Meteorological Institute (KNMI) (Figure 39). Up-to-date catalogues of (micro)seismic events for the Netherlands are available for download through the KNMI. Event-related as well as continuous waveform data (since approximately 2010) can also be obtained through KNMI. As indicated in Figure 39, the detection threshold and corresponding M_{\min} vary spatially, with a M_{\min} of 2 offshore, including in the vicinity of the Aramis AOI. The detection threshold also varies temporally, as the network was upgraded over time, with most significant improvements since 1995.

Natural seismicity occurs mostly in the southeast of The Netherlands (Figure 40). Induced microseismic events are mostly observed around the Groningen Gas Field (area in red circle in Figure 40) and other smaller gas and oil fields, both onshore and offshore. There are two events along the eastern edge of the Aramis AOI (Table 5). Most of the induced events are associated with gas depletion (Muntendam-Bos *et al.*, 2022). A small subset of the events can be attributed to underground gas storage operations.

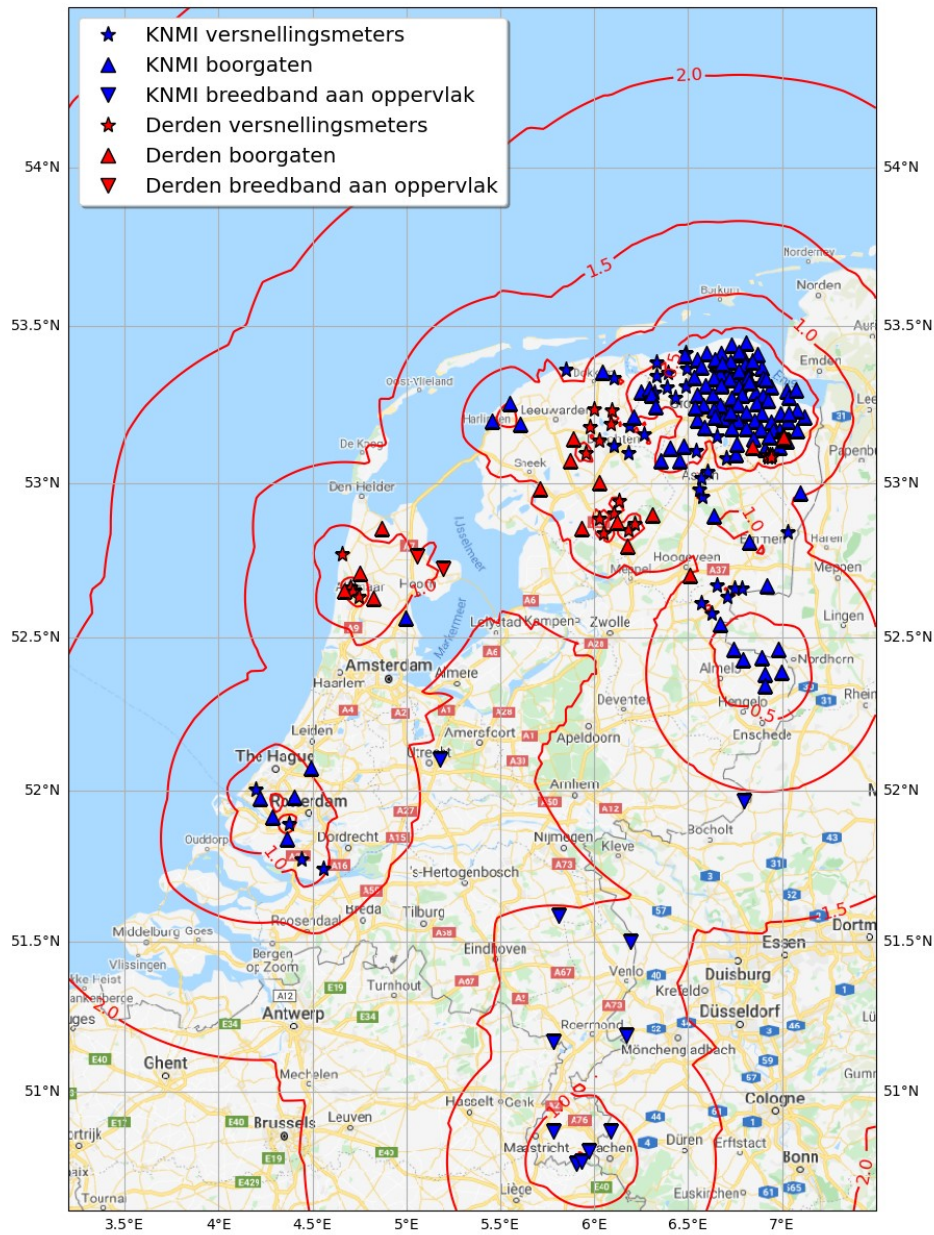


Figure 39. Overview of seismic stations in The Netherlands and the corresponding magnitude of completeness contours (red) (<https://dataplatform.knmi.nl/dataset/netherlands-earthquake-magnitude-completeness-map-1>).

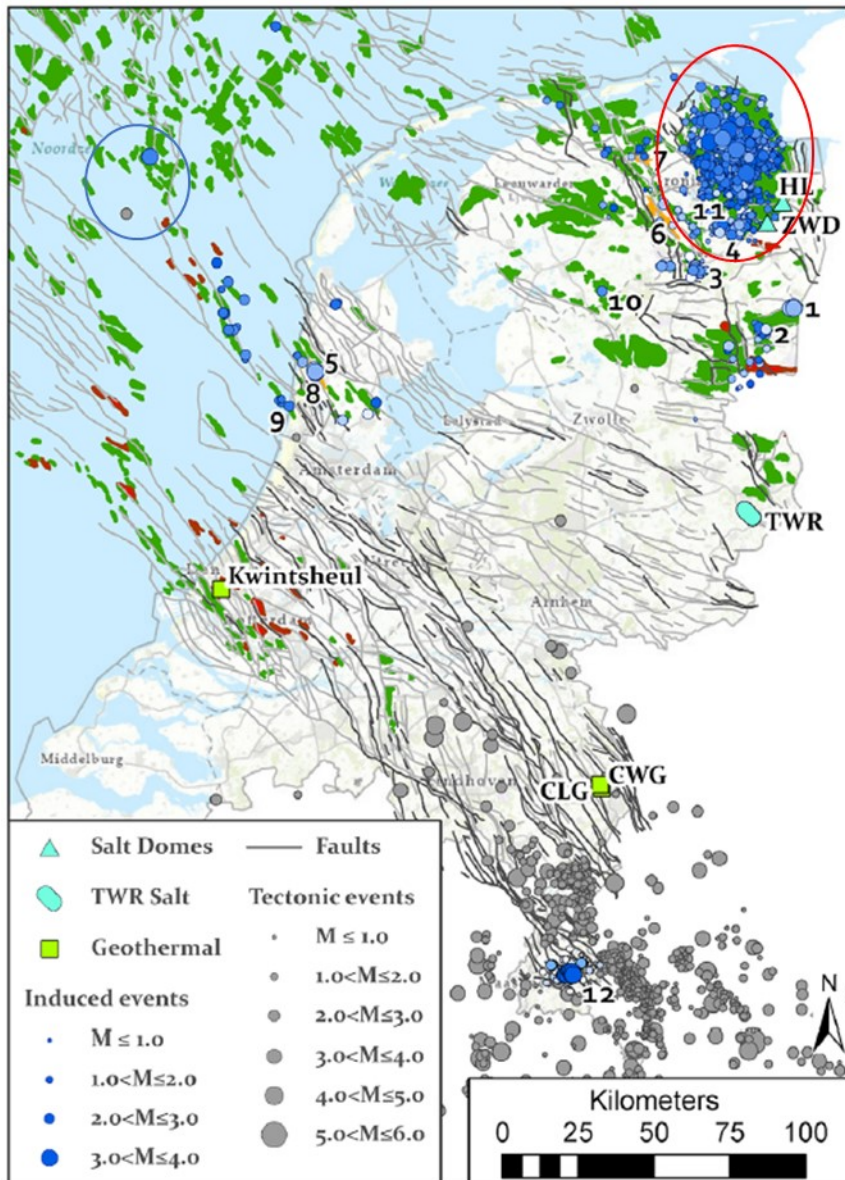


Figure 40. Overview of seismicity in The Netherlands (Muntendam-Bos et al., 2022). Two events, one tectonic and one induced, have been observed on the eastern edge of the Aramis AOI (events in blue circle).

Table 5. Events within the Aramis AOI.

Origin time	Magnitude	Type	Latitude	Longitude	Depth
2020-03-27T03:25:29	2.7	Tectonic	53.1122	3.7748	18.8
2011-10-09T04:33:42	3.1	Induced	53.2807	3.8850	3.0

2.3.4 Mechanical properties

Mechanical rock property data from wells within the Aramis AOI are not available in the public domain. However, the reservoir rocks of the Rotliegend sandstone, which is the primary target for CO₂ storage,

as well as the overlying and underlying sandstones and shales, have been studied extensively in the onshore Groningen Gas Field. Core material retrieved from a recent well was used to characterise the Poisson’s ratio and Young’s modulus of Carboniferous, Permian and Lower Triassic rocks as a function of porosity, using triaxial tests at reservoir pressure and temperature conditions (Figure 41).

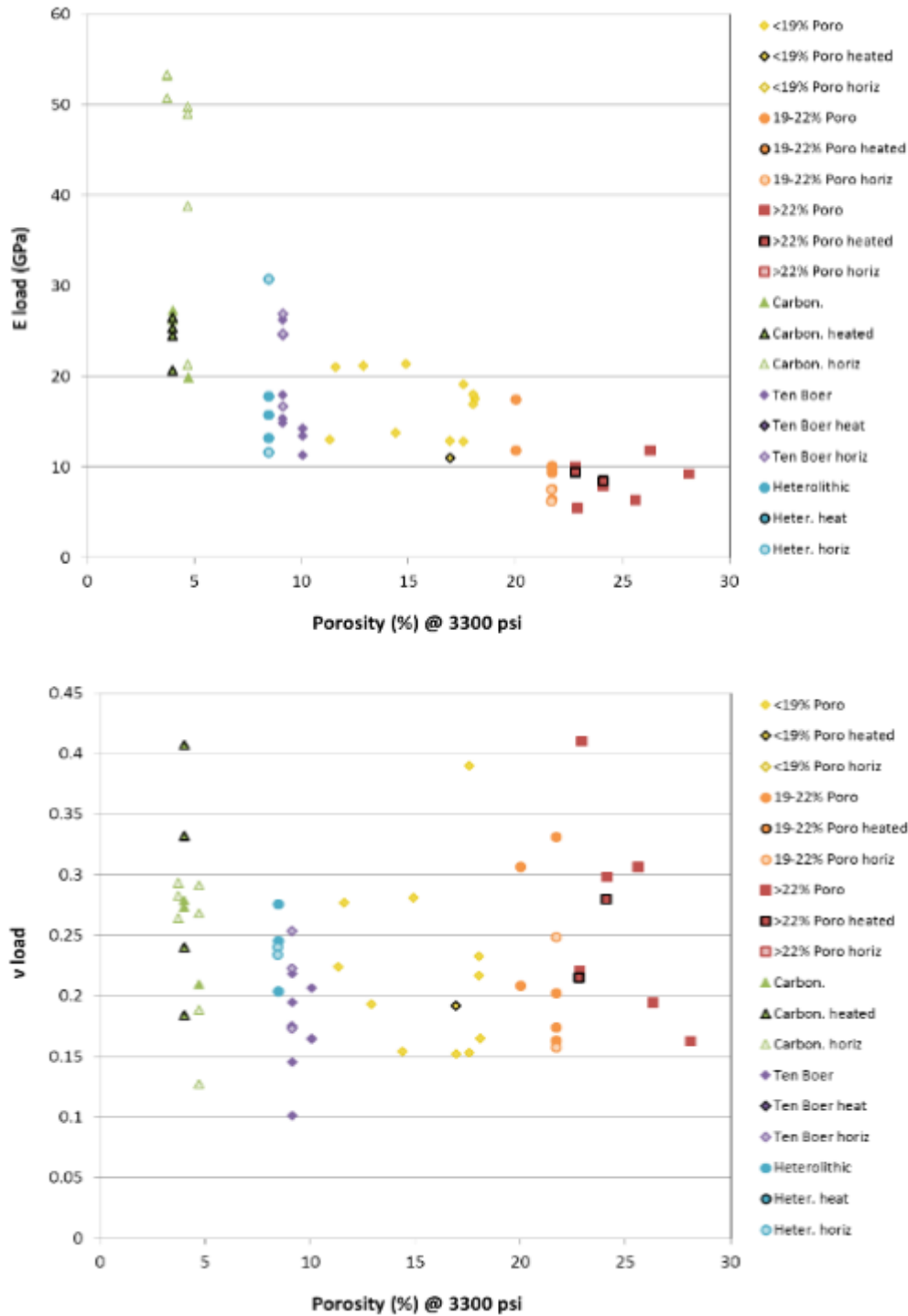


Figure 41. Young’s modulus (top) and Poisson’s ratio (bottom) as a function of porosity under varying confining pressures for Rotliegend samples with different porosity ranges (legend items with ‘poro’) and Carboniferous and Ten Boer claystone samples (Kole et al., 2020).

2.3.5 Rock failure studies

Although there is extensive well and core data in the Dutch offshore, there are no published geomechanical studies for the Aramis region specifically aimed at derisking CO₂ storage. The mechanical integrity of the Rotliegend and overlying formations has been studied onshore for the Groningen gas field. From that work, it has been found that the strength of fault surfaces in the Rotliegend sandstone and surrounding formations has been investigated using friction experiments with simulated fault gouge material under *in situ* conditions (Figure 42). An important finding is the observed velocity-strengthening behaviour in most formations except the Basal Zechstein. The friction coefficient for the Rotliegend sandstone is close to 0.6, but can be as low as 0.4 for the overlying Ten Boer Claystone formation.

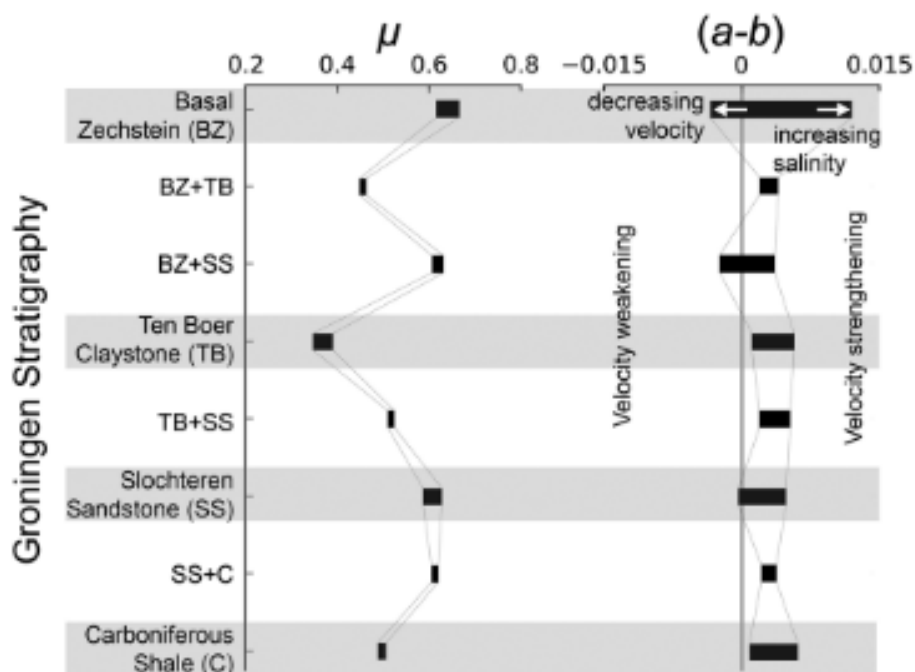


Figure 42. Friction coefficient μ and rate sensitivity parameter $(a-b)$ for the Rotliegend (Slochteren Sandstone) and surrounding formations (Hunfeld et al., 2017).

To facilitate safe injection and storage of CO₂ in the Aramis area of interest, further rock mechanical studies are required. The gas fields in the region have experienced significant depletion, which is generally accompanied by a strongly altered stress state, which impacts future drilling activities and has implications for wellbore stability. Injection of supercritical CO₂ into these depleted fields can lead to Joule-Thompson cooling resulting in thermal stress changes. For injection into saline aquifers in the region, the fracture gradients and caprock pressure limits need to be established to avoid fracturing of top seals. Although the Aramis area is a mature hydrocarbon region with extensive well log and core data availability, the amount of recent geomechanical data is limited. A combination of rock mechanical tests and numerical models are required to gain a further understanding of:

- The reduction of the fracture gradient within the reservoir during the depletion phase;
- The reduction of the fracture gradient in the reservoir due to cooling effects resulting from cold CO₂ injection;
- The failure behavior of the rock material in relation to changes in stress states.

Rock mechanical tests will need to include triaxial tests on reservoir and caprock core material to both verify the validity of and to expand on understanding based on legacy data compilations. Quantifying the relationship between static and dynamic (log-derived) elastic rock properties will also be required. Performing these tests under variable temperature conditions will enable insights into potential thermal stress effects. Uniaxial Pore Volume Compressibility tests could be used to gain further insights into the stress paths during depletion and injection. These data can be further used in numerical models to help assess operational limits during injection. Field-scale 3D finite element models can aid in understanding stress changes in the reservoir and overburden associated with proposed injection scenarios, as well as changes in fault stability. Near-wellbore or sector models can provide an understanding of induced fracture growth during injection and will be required to support completion design. Direct stress measurements in the field such as extended leak-off tests, are important sources of model calibration and provide further insights into the in-situ stress paths.

2.4 Lisa Structure

2.4.1 Structural and basin setting

The Lisa Structure is located in the Danish part of the northeastern North Sea in the Fjerritslev Trough (Figure 43). The structure is in an early stage of maturation in terms of characterisation for CCS. The western half of the structure is covered by a dense grid of vintage 2D seismic data, while the eastern part is covered by a more open seismic grid. The structure was drilled by the hydrocarbon exploration well J-1 in 1970, to a depth of 1952 m. No conventional cores were acquired, but 28 plucks were retrieved from the deeper part of the well between 1380–1950 m measured depth. No data on mechanical properties or *in situ* stress have been acquired, and no specific rock failure studies on the J-1 well or well material have been conducted. The variable depth and thickness of the chalk interval over the Lisa Structure, and the limited geophysical data and well coverage in the area renders the existing velocity model uncertain.

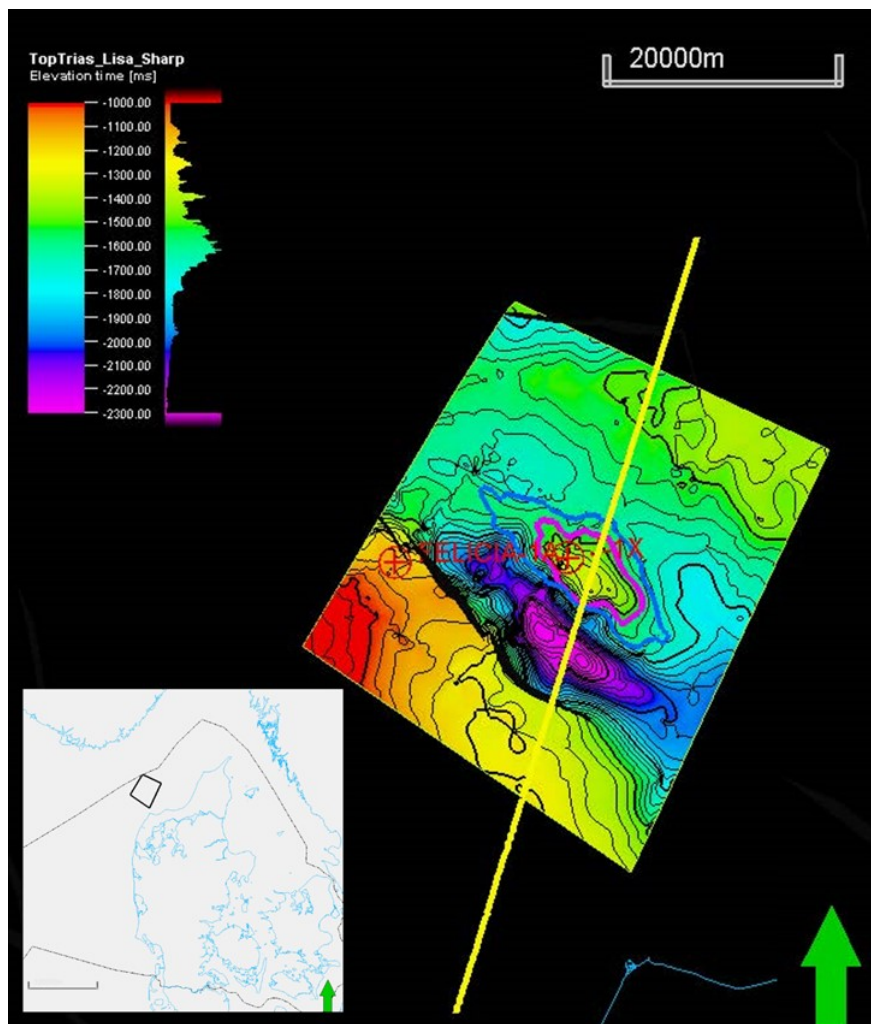


Figure 43. Time structure map of the Top-Gassum Formation at the Lisa Structure. Blue and purple polygons delineate the Lisa closures at the top of the Gassum Formation (purple) and Haldager sandstone Formation – the two primary reservoirs.

The Fjerritslev Trough extends from the Norwegian–Danish Shelf and continues onshore Jutland to the southeast. The trough forms part of the Sorgenfrei-Tornquist Zone that physically borders the

Norwegian–Danish Basin. The Fjerritslev Trough in the Lisa area defines a half-graben confined by a NW–SE striking fault zone located around 10 km southwest of the Lisa Structure (Figure 43). The fault zone, as in the rest of the Sorgenfrei-Tornquist Zone, has experienced various phases of deformation since the Late Palaeozoic. In the Middle Triassic to Early Jurassic, down-faulting and flexing across the confining fault zone resulted in considerable lateral thickness variations across the trough, particularly within the Carnian to Norian interval that may record a climax to the extensional period (Figure 44).

Following Cimmerian uplift and erosion during the Middle Jurassic, post-rift sagging together with mild extension dominated until the Middle Cretaceous. Subsequently, during the Late Cretaceous and Cenozoic, the Fjerritslev Trough was mildly inverted, resulting in doming and erosion over the basin centre.

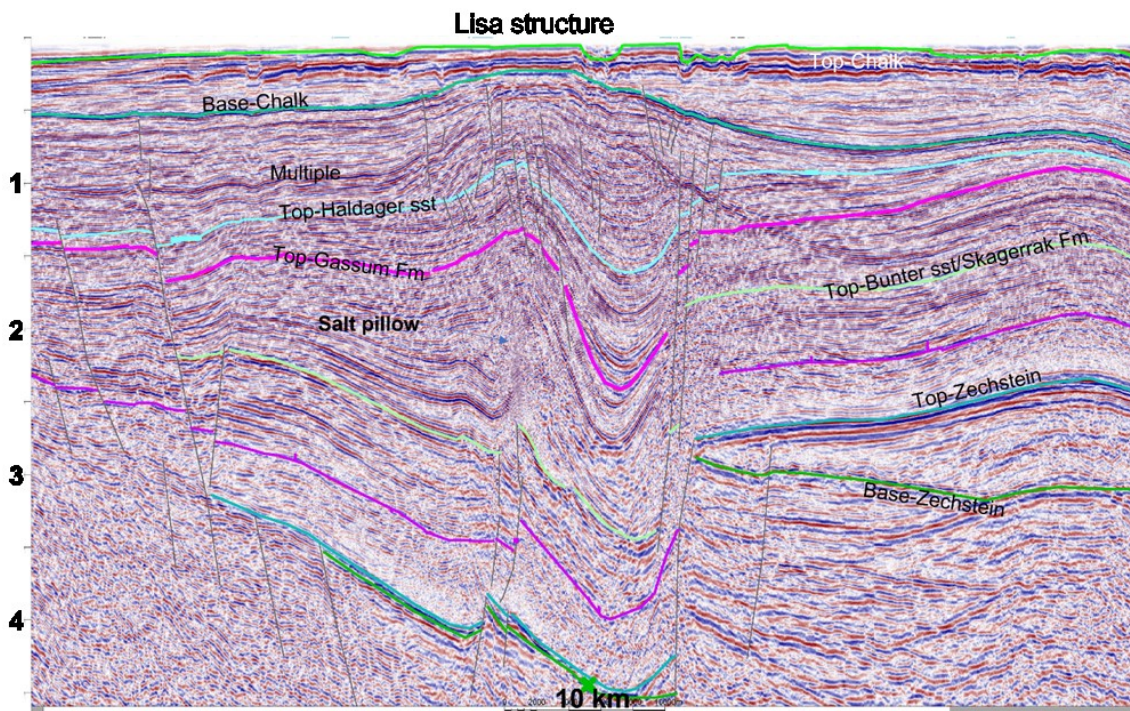


Figure 44. Seismic transect across the Lisa Structure. The tops of the two reservoir levels are picked with the light blue and pink horizons. Vertical scale in seconds TWT. Location of section is shown in Figure 43.

The Lisa area is underlain by Triassic through Upper Cretaceous rocks that rest on a thin veneer of Zechstein sediments and Rotliegend and older undifferentiated strata. The oldest Triassic strata consist of Bunter mudstone and sandstone formations and directly overlie the sand-dominated Skagerrak Formation intersected in the nearby Felicia well (Figure 43). In the Felicia well, the Skagerrak Formation is capped by evaporite-bearing Oddesund Formation and Vinding Formation corresponding stratigraphically to the Keuper Formation. In Felicia, three salt-bearing intervals up to ~50 m thick were intersected within the Oddesund Formation. Seismic data document thickness increases of Oddesund and Vinding formations towards Lisa; and at Lisa, Oddesund Formation salt has mobilised into a salt pillow (Figure 44), supporting an increase in salt thickness. The stratigraphy of the J-1x well is indicated in Figure 45. The J-1x well is typically considered to terminate in 183 m of sandy Skagerrak Formation (Bertelsen, 1980; Nielsen and Japsen, 1991). However, the basal ~70 m consist of gypsum/anhydrite-bearing, arcose sandstones and purple-brown shales which were originally considered as Keuper Formation, a notion that is supported here. The overlying 111 m sandy succession is presumably of

Rhaetian age. It is characterised by an upward drop in feldspar content and by calcareous shales of lighter red to yellowish-brown colours above the Keuper Formation, and thus distinguishes from the ~70 m thick basal Keuper Formation. This 111 m thick unit instead resembles the overlying 72 m thick, marginal marine Rhaetian-Hetangian Gassum Formation both litho- and biostratigraphically. We therefore attribute the 111 m to the Gassum Formation. The Gassum Formation comprises the primary reservoir in the Danish area outside the Central Graben, and attains a thickness of 183 m in J-1x well at Lisa.

The Gassum Formation is overlain by 623 m of shale-dominated Fjerritslev Formation that is capped by the Cimmerian Unconformity. The unconformity is overlain by 19 m of Middle Jurassic Haldager Sandstone Formation, which is highly porous and permeable. The overlying 283 m Børglum and Frederikshavn formations and the 558 m thick Lower Cretaceous unit predominantly comprises shale and silty shale units. The fine-grained Upper Jurassic to Lower Cretaceous is buried beneath 134 m chalk which is erosionally overlain by 36 m of Pleistocene-Holocene deposits.

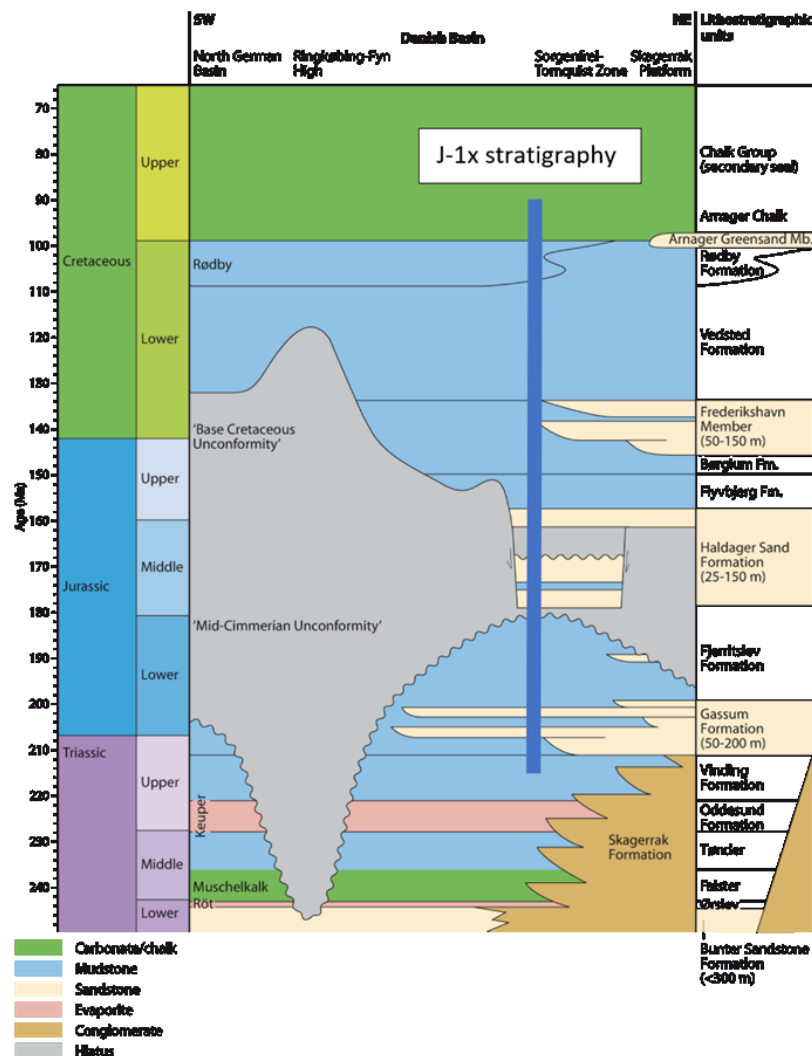


Figure 45. Simplified stratigraphic chart over the Danish area outside the Central Graben with the stratigraphy intersected by the J-1x well at Lisa indicated.

The Lisa Structure is a faulted anticline formed over a slightly elongated salt pillow (Figure 43 and Figure 44). The pillow formed by mobilisation of Middle–Late Triassic salt. Stratigraphic thickness

variations across the salt pillow suggest the primary salt movement to have occurred between the Early Jurassic and Middle Cretaceous. Structural relief of the Lisa Structure was enhanced by latest Cretaceous to Paleogene inversion that resulted in sub-regional doming across the Fjerritslev Trough (Figure 44).

Both the Haldager Sandstone and the Gassum Formation reservoirs have been offset by faults with heaves of up to a few hundred metres but usually less. Most faults die out within the Lower Cretaceous, but some continue into, and possibly through, the Upper Cretaceous Chalk. It is not clear if certain faults penetrate the Pleistocene, but some sinkholes and fluvial incisions in the top Chalk surface are controlled by underlying structures.

2.4.2 *In situ stress and seismicity data*

No earthquakes are known to have occurred on top of or within the Lisa Structure (Figure 46). The nearest known earthquakes are related to an earthquake swarm centred around 50 km west of the Lisa Structure. Sørensen *et al.* (2011) modelled fault plane solutions from well-defined Skagerrak earthquakes and derived a regional stress pattern with maximum compression in the northwest by north to southeast by south direction (Figure 46). They concluded that earthquakes originated from depths of 11–25 km and relate to N–S striking faults south of the Sorgenfrei-Tornquist Zone. The seismicity is therefore attributed to activity over the Sorgenfrei-Tornquist Zone. Recent reanalysis focussing on the most reliable earthquake data suggests a less systematic stress sense signal in the Skagerrak region (Figure 47).

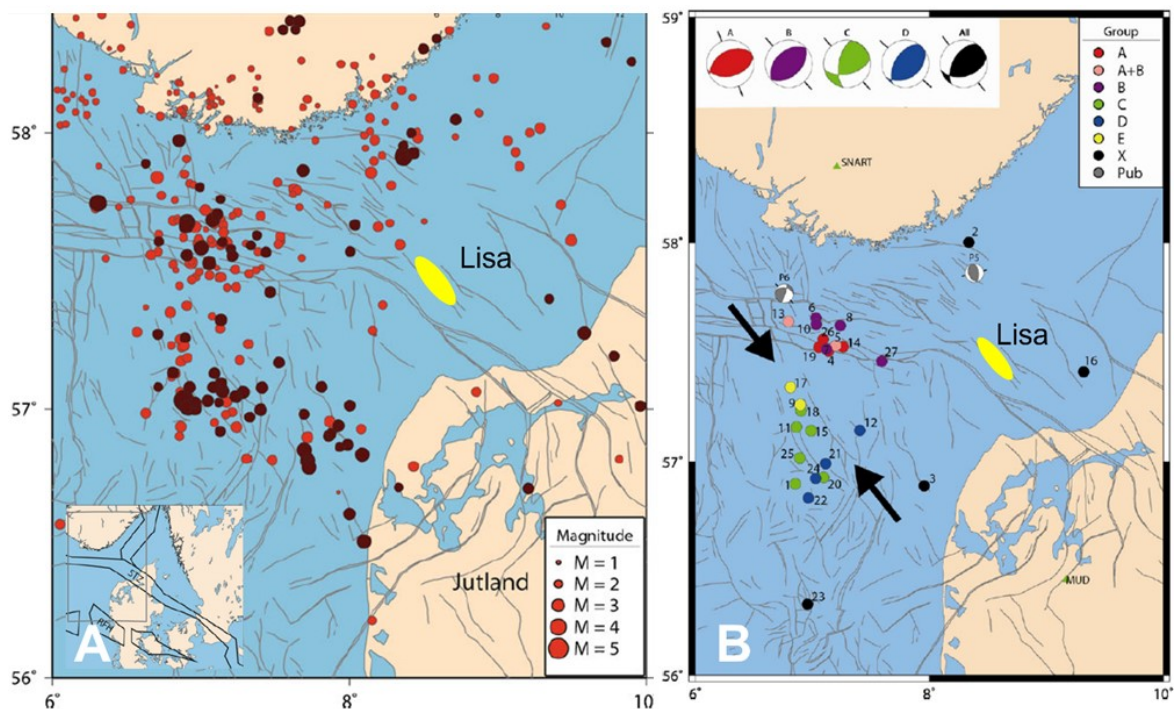


Figure 46. Left: Instrumental earthquakes recorded between 1980 and 2011 in the northern Skagerrak. Dark dots indicate events recorded with the highest confidence. Right: Earthquakes grouped to determined focal mechanisms. Earthquakes are plotted on top of known faults in the region. After Sørensen *et al.* (2011).

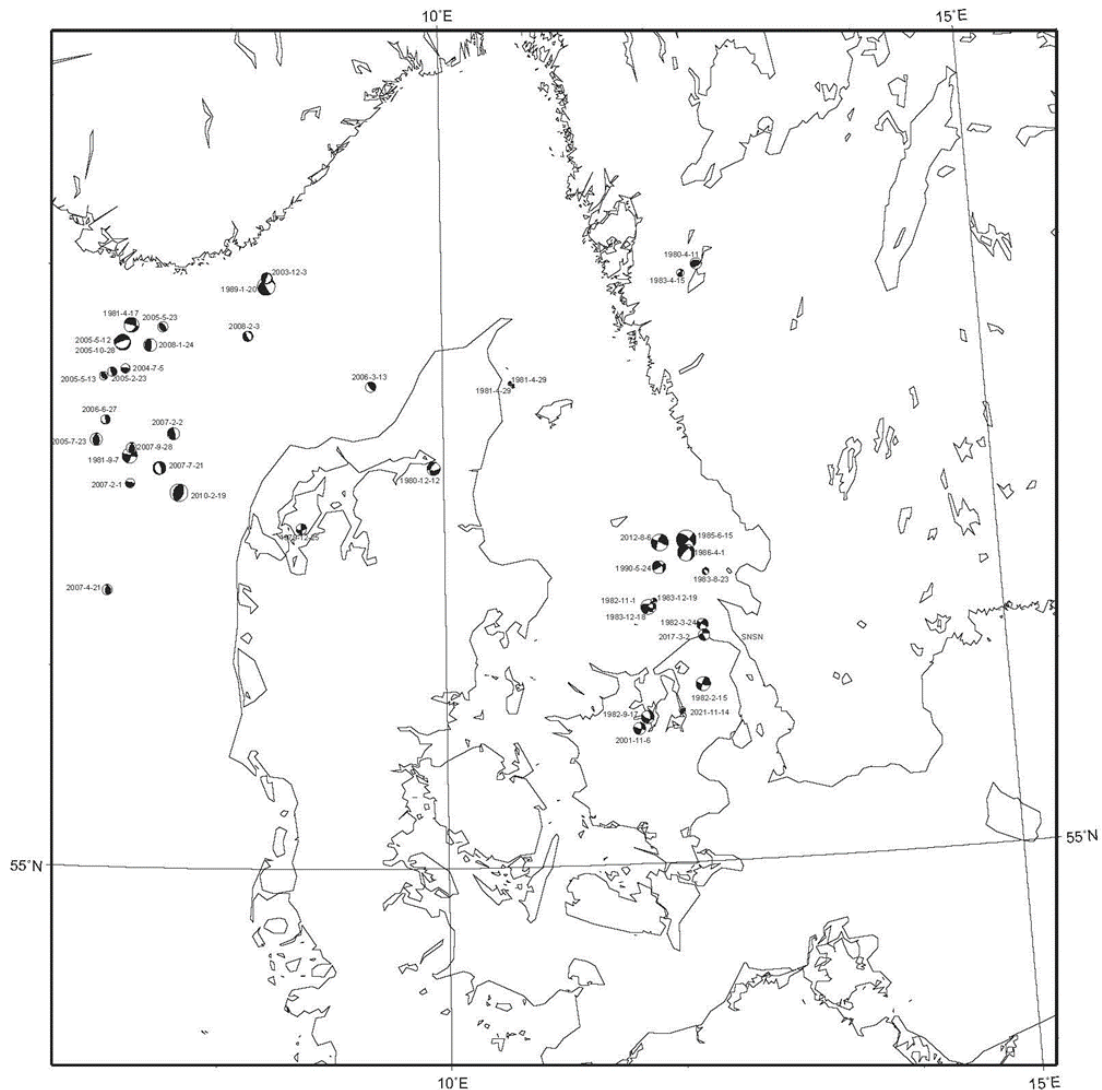


Figure 47. Focal mechanisms filtered and extracted from GEUS' database with the most reliably recorded earthquakes plotted for the SHARP Project.

2.4.3 Rock mechanics and rock failure

The current knowledge of the mechanical state of the rocks present in the area is limited. Samples from the Gassum formation have been provided to TU Delft as part of Work Package 3 to measure key properties, including permeability, porosity, density, V_p/V_s , and bulk moduli. In addition, there is information on leak-off pressures from wells in the area. A recent compilation of leak-off pressures from the nearby Felicia-1 well and from onshore wells around Denmark is available in internal GEUS documents and is shown in Figure 48.

Borehole breakout observations in the Danish area have been compiled by Ask *et al.* (1996) and Ask (1997). Work Package 2 has compiled a complete overview of borehole stress observations based on breakouts and drilling induced tensile fractures from the SHARP region of interest.

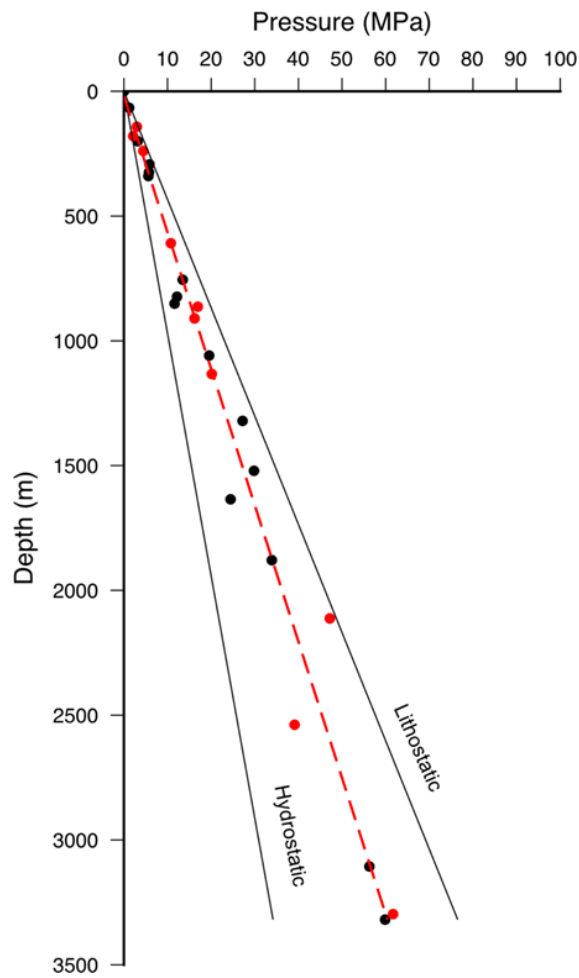


Figure 48. Leak-off test data from Danish wells. The red dots show wells within 120 km of the Lisa Structure. Lithostatic pressure assumes an average rock density of 2.4 gm/cc and hydrostatic pressure assumes an average fluid density of 1.05 g/cc. Red dashed line is best fit to the leak-off pressures. Data were compiled by N. Springer, L. Kristensen, T. Laier, and P. Frykman at GEUS.

2.5 Rajasthan region

2.5.1 Structural and basin setting

The proposed site, Bhagewala Heavy Oil Field, Rajasthan, India, is a suitable candidate to implement the experience and learnings from other international CO₂ storage projects to accelerate new CCS initiatives in India. It will also provide an opportunity to fast-track implementation of the next generation monitoring systems for CO₂ storage and CO₂ Enhanced Oil Recovery (EOR) projects. The Bhagewala Oil field, situated in the pericratonic Bikaner-Nagaur Basin in Rajasthan, covers 77,500 km² of the northwestern part of the Indian shield, as depicted in Figure 49. The paleogeographic reconstructions suggest that the Bikaner-Nagaur Basin was formed by extension along the Najd Fault System of the Arabian Plate during the Late Proterozoic to Early Cambrian, and is related to the latest phase of the Pan-African Orogenic event (Pollastro, 1999; Al-Husseini, 2000; Dmitry *et al.*, 2007). The Bikaner-Nagaur basin is relatively shallow, with maximum depth to basement estimated to be 1.5–2 km (Dasgupta *et al.*, 1988). This basin contains a 1000 to 1500 m thick Infracambrian to Cambrian mixed evaporite, carbonate, and siliciclastic sequence overlain by a thin sequence of Permian to Holocene rocks (Pareek, 1981; 1984; Dutta, 1983; Dasgupta *et al.*, 1988).

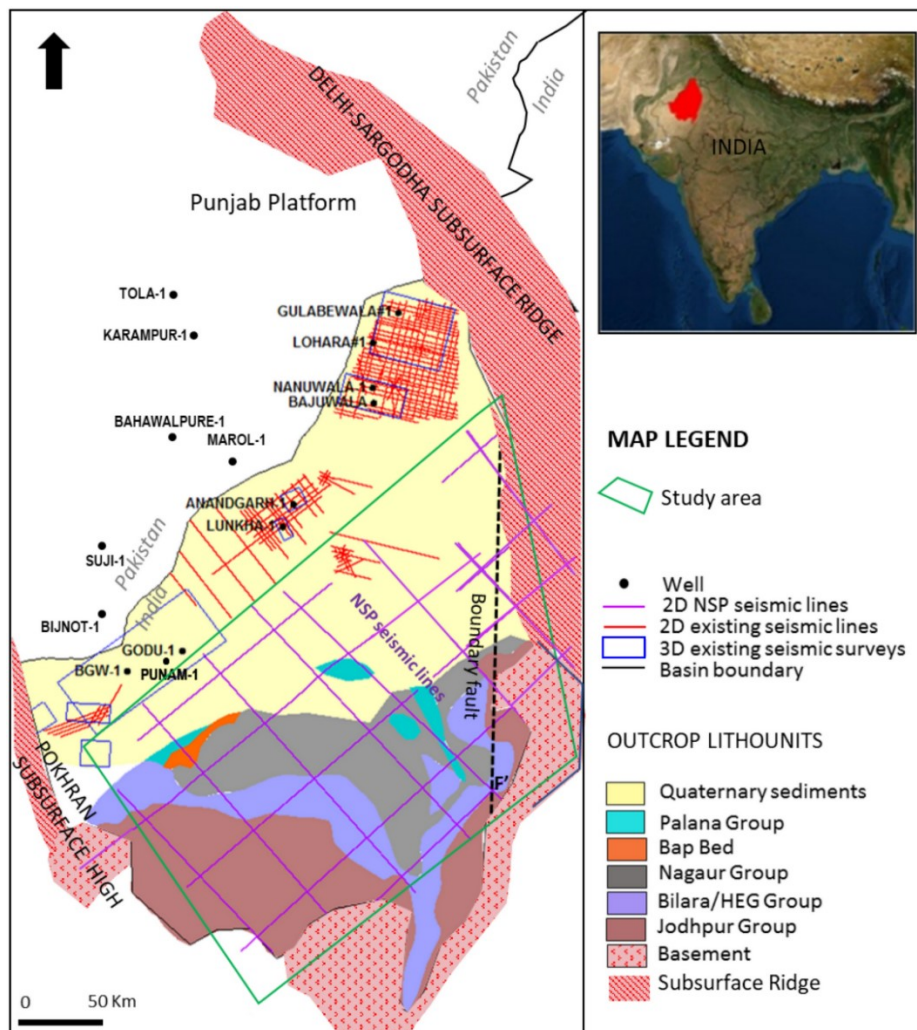


Figure 49. Location of Bhagewala Oil field (Mandal *et al.*, 2022).

In 1991, Oil India Limited (OIL) discovered heavy oil in the Baghewala-1 well (BGW-1, Figure 49) and about 7 bbl of viscous, 17.6°API gravity oil was recovered during a production test at the basal Jodhpur Formation sandstone at a depth interval of 1103–1117 m, as depicted in Figure 50. The heavy oil is a dark, viscous fluid (267 cp at 90°C, 1700 cp at 60°C, 6667 cp at 30°C). This clastic depth interval underlies laminated, organic-rich Infracambrian dolomites of the Bilara Formation. Crude oil similar to that encountered in the Jodhpur Formation occurs at Bilara, Hanseran Evaporite, and Upper Carbonate formations as well (Figure 51). The BGW-1 well was drilled on a N–NE trending basement high northeast of the Pokaran High (Figure 49). As depicted in Figure 51, the stratigraphic sequence in the well includes nearly 1400 m of non-fossiliferous sedimentary rocks unconformably overlying Malani Suite volcanic rocks dated at about 745 ± 10 Ma (Crawford and Compston, 1970). Dasgupta and Bulgauda (1994) have tentatively assigned these non-fossiliferous rocks to the Cambrian and Infracambrian based on stratigraphic correlations with the Infracambrian Salt Range Series of Pakistan and the Infracambrian Marwar Supergroup of India. The Cambrian and Infracambrian rocks are overlain by a thick Permian to Triassic sequence of about 60 m, and nearly 400 m of Jurassic and younger rocks.

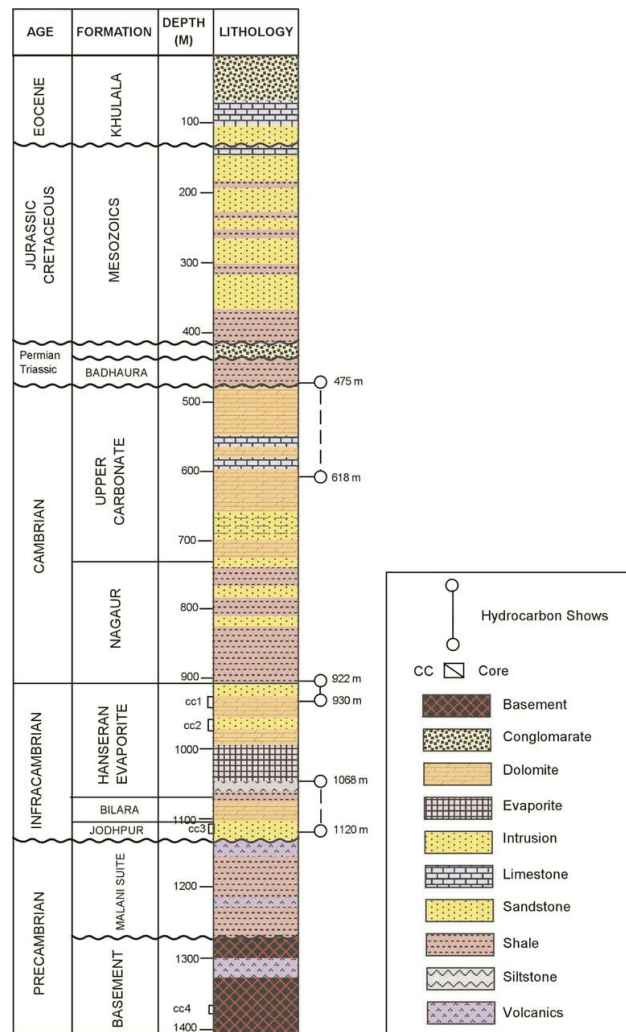


Figure 50. Stratigraphic column for the Baghewala-1 well (Peters et al., 1995; Cozzi et al., 2012).

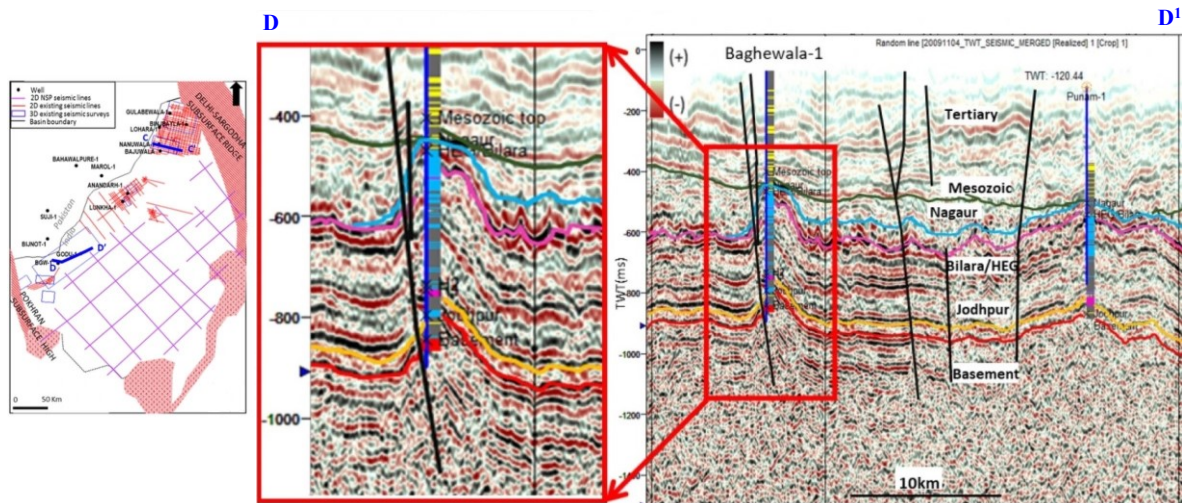


Figure 51. DD' seismic section transecting the Baghewala-1 well shows compressional structures bounded by steeply dipping faults (Mandal et al., 2021).

Since the discovery of the oil field in 1991, 20 wells have been completed in the field to date, with average well depth around 1200 m vertical depth. Sustained production of heavy oil (14–17°API and viscosity of 10,000 cp) commenced from two wells since 2017 using cold production techniques, chemical stimulation and artificial lift. The thermal EOR method using Cyclic Steam Stimulation (CSS) was tested in one pilot well in 2019. The following data are available in the Bhagewala Oil field:

- Basic well log suites for 20 wells;
- 2D and 3D seismic data, including 210 km² of 3D seismic data;
- Around 275 m of total core length from 10 wells;
- Geomechanical test data available from a few wells;
- A geological model.

In this context, discussions have been initiated by the IITB research group to collect data and core samples from the field operator (OIL) for use in the SHARP Project.

As depicted in Figure 51, the thickness of the Nagaur Group gradually thins towards the southwest and pinches out near the Baghewala structure, whereas the Mesozoic section thins toward the northeast. Further, it has been observed that the southwestern part of the basin is dominated by deep-seated NNE–SSW trending sub-parallel faults. Anticlinal structures have been identified in patches and are primarily bounded by the major fault systems. These anticlines are genetically correlated with Cambrian compression and were confined to the Neoproterozoic–Cambrian level only. These fault-bounded anticlinal structures are proven hydrocarbon traps with dimensions ranging between 10–50 km², such as the Baghewala structures. Incidentally, the shallow depth sections are mostly undeformed with only a limited number of minor faults.

2.5.2 *In situ stress conditions*

A stress map for northwestern India and bordering Pakistan is shown in Figure 52. The dominance of compressional stresses in the Himalayan region and strong variations in stress directions across different areas of the Indian Subcontinent are consequences of the unique dynamic tectonic situation (Cloetingh and Wortel, 1985). While the World Stress Map contains an abundance of focal mechanism

data in the Himalayan region, there are very few stress indicators available from borehole breakout data, and very little information from which to determine the stress orientation in India's pericratonic and intracratonic basins. No data is available from the Baghewala field area. Limited data along the N–S striking Cambay and Barmer basins (along the western edge of Figure 52) suggest that S_{Hmax} may be oriented parallel or sub-parallel to major basin-bounding faults.

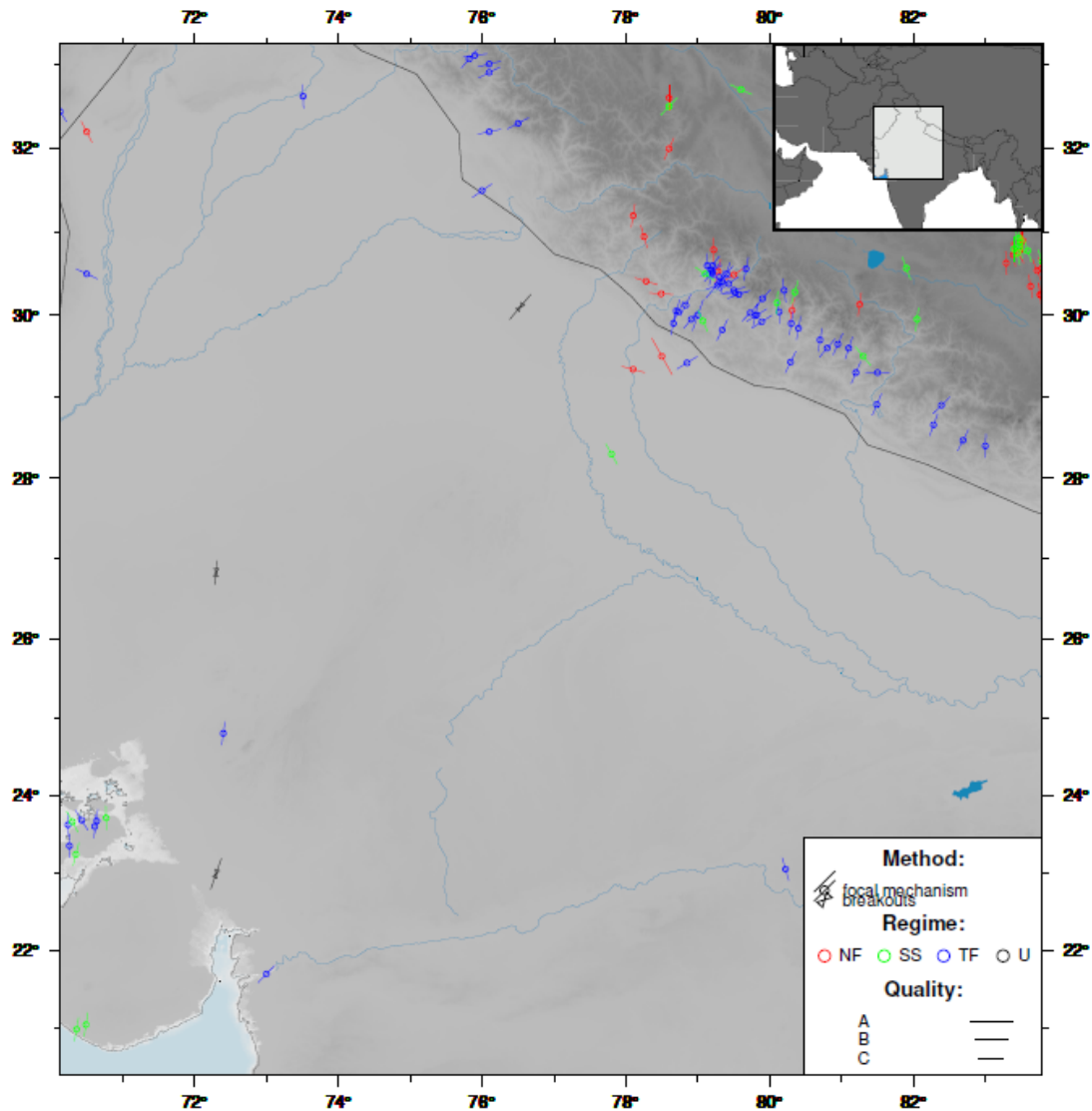


Figure 52. Stress map for northwest India and part of Pakistan, generated using the World Stress Map CASMO service (Heidbach et al., 2016; 2018).

Ganguli and Sen (2020) show that in the Ankleshwar region of the Cambay Basin, relative stress magnitudes suggest that a normal faulting regime is prevalent in post-rift strata, while a transition from normal to strike-slip faulting occurs within syn-rift strata. It is unclear at present if similar conditions prevail in the older Bikaner-Nagaour Basin.

2.5.3 Seismicity data currently available

Seismicity data for India are available from the National Center for Seismology (NCS), the nodal agency of the Government of India for monitoring earthquake activity. NCS maintains a national seismic

network of more than 150 stations distributed across the country. The online data portal provides access to the earthquake catalogue. Data from northwestern India are shown in Figure 53. To date, few events have been recorded from the Bikaner-Nagaur region of interest.

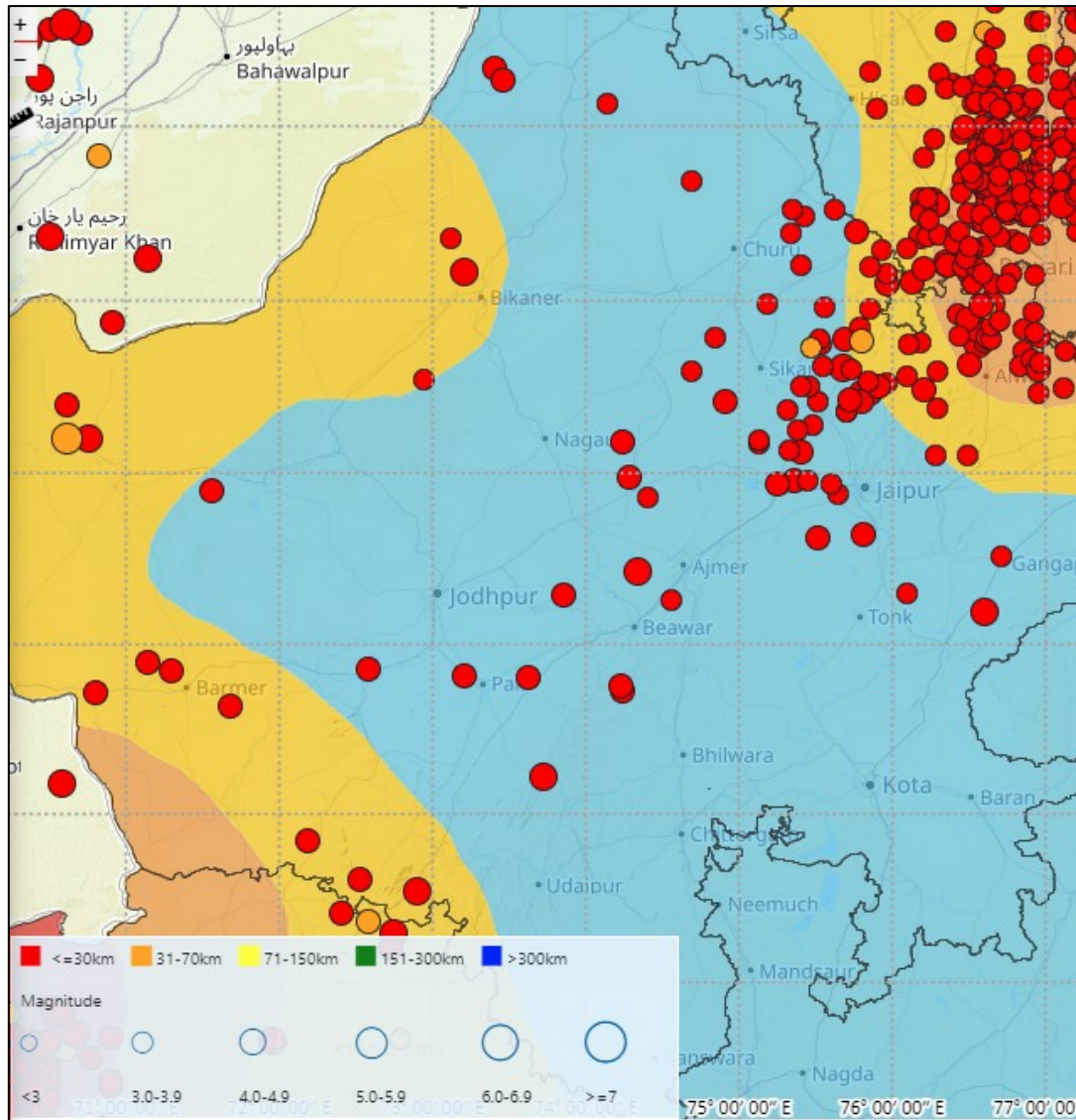


Figure 53. Local magnitude (M_l) data courtesy of the National Center for Seismology website (<https://riseq.seismo.gov.in/riseq/Earthquake/archive>). The shaded background colours refer to the earthquake zones of India. The blue colour refers to zone 2, classified as a low damage risk zone; yellow represents zone 3 and moderate damage risk; orange refers to zone 4 which is classified as high damage risk. Events shown have been recorded since 1997.

3 Important issues for further work

The primary technical objectives of the SHARP Project will provide the main framework for further work, including:

- Development of state-of-the-art basin and site-scale geomechanical models for prospective case study sites in the North Sea;
- Production of a new integrated earthquake catalogue and stress map for the North Sea, to be used for seismic hazard assessment in offshore areas;
- Characterisation of deformation, failure, flow and seismic properties of caprock and reservoir rocks from North Sea sites and for a previously unstudied site in India;
- Reduction of containment risk and costs through targeted monitoring of critical rock deformation and fluid pressure;
- Development of cost-effective strategies for monitoring induced seismicity;
- Improve subsurface risk management by implementing uncertainty quantification, probabilistic methods and effective workflows for quantitative evaluation of containment risks.

Work Package 4 is focused on developing targeted strategies for monitoring rock deformation and fluid pressure impacts resulting from CO₂ storage operations. Updated stress and failure models are a key part of improving, or 'sharpening' these monitoring designs. The current report is intended to summarise 'round 1' descriptions of the existing knowledge of the structure, seismicity and *in situ* stress states of the SHARP case study sites. Existing assessments of rock failure at the sites have also been summarised. The intention is to build-upon and improve on these estimates through collation of updated understanding developed across the breadth of the SHARP Project. Table 6 outlines the prevailing knowledge gaps and uncertainties in understanding identified in the 'round 1' assessment.

It is clear from Table 6 that the portfolio of case studies includes a range of potential storage sites with a wide variation in the degree of maturity in terms of storage development phase. While detailed site characterisation and rock failure studies have been conducted for the Horda/Smeaheia and UK SNS Bunter storage play, rock failure characterisation studies at the Aramis site are limited to regional studies. Site specific data are also lacking for the Lisa Structure, where no specific rock failure assessments have been undertaken. The Bhagewala Heavy Oil Field in India is the least mature of the case studies considered in the SHARP project. While the field operator has developed extensive understanding of the field throughout its productive history, detailed studies of its CO₂ storage potential are not available in the public domain. Developing a workflow and scientific basis for rock failure risk assessments for projects at difference levels of maturity is a key objective for the SHARP project.

Table 6. Current knowledge gaps and uncertainties identified in SHARP Work Package 4.

Case Study name	<i>In situ</i> stress conditions	Seismicity data	Rock failure understanding
Horda/Smeaheia (Norway)	Second-order stress effects and the transition from strike-slip to normal stress conditions. Not possible to rule-out stress rotations near faults	Fault plane solutions indicate a transitional trend from onshore (more strike-slip) to offshore (transition to reverse faulting). Low to moderate seismic activity.	Limited amount of focussed laboratory testing undertaken. Improved understanding of material properties required.
UK SNS Bunter storage play (UK)	Potential impact of Zechstein evaporites on contemporary stress state in the supra-salt section	Moderate seismic detection capability in the offshore region due to sparse distribution of seismometers along the coast (M2 and below likely to be missed). Sparse focal mechanism data, and very few offshore, where azimuthal coverage is limited	Potential issues related to excessive cooling of upper reservoir and caprock, with halite caprock particularly prone to tensile failure due to high linear thermal expansion coefficient. Worst case failure scenario involves weak overburden fault penetrating through the halite into the reservoir
Aramis site (Netherlands)		Limited data from the Aramis site	Mechanical properties from wells within the site not available in the public domain – existing studies are based on data from Groningen
Lisa Structure (Denmark)	No data on <i>in situ</i> stress specifically acquired at the site, and only limited data available regionally	No earthquakes known over the structure, but good data is available from the Skagerrak	Few data on mechanical properties available, and no rock failure studies conducted for the site to date beyond estimate of fracture pressure from regional LOT compilation
Bhagewala Heavy Oil Field (India)	Minimal data available in the public domain – limited to data presented by the World Stress Map	Limited data is available (no fault plane solutions); however, data were not evaluated in detail at present	No specific rock failure studies conducted to date

In the next stage of SHARP Work Package 4, we plan to make more focused assessments of rock failure risks, considering the following themes:

1. Where precisely measurements of geomechanical properties are required (i.e., which specific rock units, and when can we rely on analogue data);
2. What information is ideally needed prior to injection start-up, and conversely which data could be acquired during field operations to reduce uncertainties;
3. How can pre-injection seismicity surveillance be used to improve and quantify risk assessments, especially regarding state of stress estimations;
4. How could smart monitoring schemes (e.g., downhole pressure gauges, strain measurement using DAS fibre systems, or strategically placed broadband seismometers) be used to most effectively monitor rock strain during site operations.

Some more general themes that also need to be developed include gaining an improved understanding of deep basement/crustal stresses and associated seismicity as compared with stress and strain distribution in the sedimentary cover. This issue generally requires a higher quality location and depth

determination for seismic events than is normally achieved using regional seismic station networks. Uncertainties in stress orientation data from borehole measurements are also typically caused by a mix of poor data quality (or sparse sampling) and true natural stress variations. Integration of datasets (e.g., seismicity data together with downhole core measurements and dynamic pressure tests) is a key part of reducing these uncertainties and thereby making rock failure estimates ‘sharper.’

The maturity of rock failure studies can also be placed within the context of the Storage Readiness Levels (SRL) developed in the ACT-funded ALIGN-CCUS project (Akhurst *et al.*, 2021). The SRL framework can be used to communicate the entirety of technical appraisal, permitting and planning activities achieved at a potential CO₂ storage site, while highlighting activities that remain to be completed. As illustrated in Figure 54, the framework complements and expands on the Storage Resource Management System (SRMS) developed by the Society of Petroleum Engineers (SPE, 2017).

Storage Readiness Level (SRL)	Storage Resources Management System Storage project maturity classes and subclasses (SPE-SRMS, 2017)		
SRL 9 – Storage site on injection	Discovered storage resources	Commercial (capacity)	On injection
SRL 8 – Commissioning of the storage site and test injection in an operational environment			Approved for development
SRL 7 – Storage site is permit ready or permitted			Justified for development
SRL 6 – Storage site integrated into a feasible CCS project concept or a portfolio of sites (contingent storage resource)		Sub-commercial (contingent storage resources)	Development pending – Project activities ongoing
			Development on hold or unclarified
			Development not viable
SRL 5 – Storage site validated by detailed analyses, then a relevant ‘real world’ setting	Undiscovered storage resources	Prospect – Project sufficiently well-defined to be viable drilling target	
SRL 4 – Storage site validated by desktop studies and storage project concept updated		Lead – Project poorly defined and needs data and/or evaluation	
SRL 3 – Screening study to identify an individual storage site and an initial project concept		Play – Requires more data and/or evaluation	
SRL 2 – Site identified as theoretical capacity in a storage atlas			
SRL 1 – First-pass assessment of storage capacity at country-wide or basin scales			

Figure 54. Complementary equivalence of the SRL framework with the SPE’s SRMS project maturity classes (after Akhurst *et al.*, 2021).

From a rock failure (or storage integrity) perspective, it is possible to identify the characterisation activities that would be required to progress through the SRL framework (Table 7). These may serve as

a generic guide to the iterative studies generally required to progress from regional-scale understanding to more detailed site-specific geomechanical characterisation studies. This will include identification of the uncertainties at each stage of the rock failure assessment to inform further technical studies (e.g., data mining, analogue studies, laboratory programmes, new data acquisition programmes, baseline surveys, MMV planning etc.). Rock failure and geomechanical studies provide vital inputs to risk assessment and management processes, and should be continually reviewed as projects develop. Following commissioning of a CO₂ storage site, rock failure models should be verified and updated based on operational data such as flow rates, pressure measurements, microseismic observations and other information from the MMV methods deployed.

Table 7. Geomechanical requirements for progression through the Storage Readiness Level Framework of Akhurst et al. (2021).

SRL	Descriptive title	Rock failure/geomechanical activities likely to be required to meet SRL	SHARP case studies
SRL 1	First pass assessment of storage capacity at country-wide or basin scales		
SRL 2	Site identified as theoretical capacity	Initial collation of existing information and identification of activities required to progress the site	Bhagewala Heavy Oil Field
SRL 3	Screening study to identify an individual storage site and initial storage concept updated	Collation of regional data related to structure (major fault/fracture systems), <i>in situ</i> stress, earthquake focal mechanisms and rock mechanical property data	Aramis site & Lisa Structure
SRL 4	Storage site validated by desktop studies and storage project concept updated	Interpretation of site-specific data and development of a detailed 1D geomechanical model	UK SNS Bunter Sandstone storage play, and Horda Platform storage play
SRL 5a	Storage site validated, firstly by detailed analysis, then in a relevant 'real world' setting	Detailed risk assessment-led rock failure investigations and risk reduction activities to inform a storage permit application - including 3D geomechanical modelling	
SRL 5b		New data is acquired where needed, including acquisition of <i>in situ</i> stress measurements and/or laboratory measurements from downhole samples if appropriate	
SRL 5c		All storage site data will have been acquired, analysed and technical appraisal completed - updated 3D geomechanical modelling	
SRL 6	Storage site integrated into a feasible CCS project concept or portfolio of sites (contingent storage resource)	Any remaining concerns addressed and residual risks effectively managed	Aurora site (part of Horda Platform storage play) and Endurance (part of the UK SNS Bunter Sandstone storage play)
SRL 7	Storage site is permit ready or permitted		
SRL 8	Commissioning of the storage site and test injection		
SRL 9	Storage site on injection	Updated understanding from operational data	e.g. Snøhvit CCS project

4 References

- Akhurst, M., Kirk, K., Neele, F., Grimstad, A-A., Bentham, M. and Bergmo, P. 2021. Storage Readiness Levels: communicating the maturity of site technical understanding, permitting and planning needed for storage operations using CO₂. *International Journal of greenhouse Gas Control*, 110, 103402.
- Al-Husseini, M.I. 2000. Origin of the Arabian plate structures: Amar collision and Najd Rift. *Geo Arabia*, 5, 527–542.
- Allen, M.R., Griffiths, P.A., Craig, J., Fitches, W.R. and Whittington, R.J. 1994. Halokinetic initiation of Mesozoic tectonics in the southern North Sea: a regional model. *Geological Magazine*, 131 (94), 559–561.
- Alnes, H., Eiken, O., Nooner, S., Sasagawa, G., Stenvold, T. and Zumberge, M. 2011. Results from Sleipner gravity monitoring: Updated density and temperature distribution of the CO₂ plume. *Energy Procedia*, 4, 5504–5511.
- Armitage, P.J., Worden, R.H., Faulkner, D.H., Aplin, A.C., Butcher, A.R. and Espie, A.A. 2013. Mercia Mudstone Formation caprock to carbon capture and storage sites: petrology and petrophysical characteristics. *Journal of the Geological Society, London*, 170, 119–132.
- Armitage, P.J., Worden, R.H., Faulkner, D.R., Butcher, A.R. and Espie, A.A. 2015. Permeability of the Mercia Mudstone: suitability as caprock to carbon capture and storage sites. *Geofluids*, 16 (1), 26–42.
- Ask, M.V.S., Muller, B., and Stephansson, O. 1996. In situ stress determination from breakouts in the Tornquist Fan, Denmark. *Terra Nova*, 8, 575–584.
- Ask, M.V.S. 1997. In situ stress from breakouts in the Danish Sector of the North Sea. *Marine and Petroleum Geology*, 14, 231–243.
- Bacci, V.O., O'Brien, S., Frank, J. and Anderson, M. 2017. Using a walk-away DAS time-lapse VSP for CO₂ plume monitoring at the Quest CCS Project. *CSEG Recorder*, 42 (3), 18–21.
- Baig, I., Faleide, J.I., Mondol, N.H. and Jahren, J. 2019. Burial and exhumation history controls on shale compaction and thermal maturity along the Norwegian North Sea basin margin areas. *Marine and Petroleum Geology*, 104, 61–85.
- Baptie, B. 2010. Seismogenesis and state of stress in the UK. *Tectonophysics*, 482, 150–159.
- Baptie, B. 2020. Earthquake Seismology 2019/2020. British Geological Survey Open Report, OR/20/039.
- Bell, J.S. 1996. In situ stress in sedimentary rocks (part 2): applications of stress measurements. *Geoscience Canada*, 23 (3), 135–153.
- Bell, R.E., Jackson, C.A.-L., Whipp, P.S. and Clements, B. 2014. Strain migration during multiphase extension: observations from the northern North Sea. *Tectonics*, 33, 1936–1963.
- Bentham, M.S., Green, A. and Gammer, D. 2013. The occurrence of faults in the Bunter Sandstone Formation of the UK sector of the Southern North Sea and the potential impact on storage capacity. *Energy Procedia*, 37, 5101–5109.
- Bentham, M., Mallows, T., Lowndes, J. and Green, A. 2014. CO₂ STORage Evaluation Database (CO₂Stored). The UK's online storage atlas. *Energy Procedia*, 63, 5103–5113.
- Bentham, M., Williams, G., Vosper, H., Chadwick, A., Williams, J. and Kirk, K. 2017. Using pressure recovery at a depleted gas field to understand saline aquifer connectivity. *Energy Procedia*, 114, 2906–2920.
- Bertelsen, F. 1980. Lithostratigraphy and depositional history of the Danish Triassic. *Danmarks Geologiske Undersøgelse Serie B*, Volume 4. DGU, Denmark.
- Bifani, R. 1986. Esmond gas complex. In: Brooks, J., Goff, J.C. and van Hoorn, B. (Eds.). *Habitat of Palaeozoic Gas in N.W. Europe*. Geological Society, London, Special Publications, 23, 209–221.
- BP, 2021a. Primary Store Dynamic Model and Report. Key Knowledge Document, NS051-SS-REP-000-00015.
- BP, 2021b. Primary Store Geological Model and Report. Key Knowledge Document, NS051-SS-REP-000-00014.
- BP, 2021c. Primary Store Geomechanical Model & Report. Key Knowledge Document, NS051-SS-REP-000-00012.
- BP, 2021d. Endurance Well Injectivity Fracturing Study with REVEAL™. Key Knowledge Document, NS051-SS-REP-000-00017.
- Brown, K.M., Bekins, B., Clennell, B., Dewhurst, D., and Westbrook, G.K. 1994. Heterogenous hydrofracture development and accretionary fault dynamics. *Geology*, 22, 259–262.
- Cameron, T.D.J., Crosby, A., Balson, P.S., Jeffery, D.H., Lott, G.K., Bulat, J. and Harrison, D.J. 1992. *The Geology of the Southern North Sea*. United Kingdom Offshore Regional Report. British Geological Survey and HMSO, London.

- Chadwick, A., Williams, G., Delepine, N., Clochard, V., Labat, K., Sturton, S., Buddensiek, M.L., Dillen, M., Nickel, M., Lima, A.L. and Arts, R. 2010. Quantitative analysis of time-lapse seismic monitoring data at the Sleipner CO₂ storage operation. *The Leading Edge*, 29 (2), 170–177.
- Chiaromonte, L., White, J.A., Hao, Y. and Ringrose, P. 2013. Probabilistic risk assessment of mechanical deformation due to CO₂ injection in a compartmentalized reservoir. In 47th US Rock Mechanics/Geomechanics Symposium. OnePetro, ARMA-2013-577.
- Chiaromonte, L., White, J.A. and Trainor-Guitton, W. 2015. Probabilistic geomechanical analysis of compartmentalization at the Snøhvit CO₂ sequestration project. *Journal of Geophysical Research: Solid Earth*, 120 (2), 1195–1209.
- Choi, J.C. and Skurtveit, E. 2021. Tools and Workflows for Fault Stability Assessment used in NCCS. NCCS T9 workshop, Oslo, Norway.
- Choi, J.C., Skurtveit, E., Huynh, K.D.V. and Grande, L. 2022. Uncertainty of Stress Path in Fault Stability Assessment During CO₂ Injection: Comparing Smeaheia 3D Geomechanics Model with Analytical Approaches. *International Journal of Greenhouse Gas Control*, Submitted.
- Cloetingh, S. and Wortel, R. 1985. Regional stress field of the India Plate. *Geophysical Research Letters*, 12 (2), 77–80.
- Cooke-Yarborough, P. and Smith, E. 2003. The Hewett fields: Blocks 48/28a, 48/29, 48/30, 52/5a, UK North Sea: Hewitt, Big Dotty, Little Dotty, Della, Dawn and Delilah fields. In: Glyuas, J.G. and Hichens, H.M. (Eds.). *United Kingdom Oil and Gas fields, Commemorative Millennium Volume*. Geological Society, London, Memoir, 20, 731–740.
- Cozzi, A., Rea, G. and Craig, J. 2012. From global geology to hydrocarbon exploration: Ediacaran-Early Cambrian petroleum plays of India, Pakistan and Oman. In: Bhat, G.M., Craig, J., Thurow, J.W., Thusu, B. and Cozzi, A. (Eds.). *Geology and Hydrocarbon Potential of Neoproterozoic–Cambrian Basins in Asia*. Geological Society, London, Special Publications, 366, 131–162.
- Crawford, A.R. and Compston, W. 1970. The age of the Vindhyan system of peninsular India. *Geological Society of London Quarterly Journal*, 125, 351–371.
- Dasgupta, S.P., Kumar, V., Chandra, R. and Jairam, M.S. 1988. A framework of the Nagaur-Ganganagar evaporite basin, Rajasthan. *Indian Minerals*, 42, 57–64.
- Dasgupta, U. and Bulgauda, S.S. 1994. An overview of the geology and hydrocarbon occurrences in the western part of Bikaner–Nagaur basin. *Indian Journal of Petroleum Geology*, 3 (1), 1–17.
- De Lesquen, C., Andrews, J. and Rasheva, S. 2020. Good quality LWD Images in horizontal wells invalidate the strike-slip theory in the Northern North Sea. ISRM International Symposium-EUROCK 2020, OnePetro, 2020.
- Dixon, T. and Romanak, K.D. 2015. Improving monitoring protocols for CO₂ geological storage with technical advances in CO₂ attribution monitoring. *International Journal of Greenhouse Gas Control*, 41, 29–40.
- Dixon, T., McCoy, S.T. and Havercroft, I. 2015. Legal and regulatory developments on CCS. *International Journal of Greenhouse Gas Control*, 40, 431–448.
- Dmitry, A., Al-Husseini, M.I. and Yumiko, I. 2007. Review of middle east paleozoic plate tectonics. *Geo Arabia*, 12, 5–56.
- Duffy, O.B., Bell, R.E., Jackson, C.A.L., Gawthorpe, R.L. and Whipp, P.S. 2015. Fault growth and interactions in a multiphase rift fault network: Horda Platform, Norwegian North Sea. *Journal of Structural Geology*, 80, 99–119.
- Dutta, A.K. 1983. Geological evolution and hydrocarbon prospects of Rajasthan basins. *Petroleum Asia Journal*, 4, 93–100.
- EC, 2009. Directive 2009/31/EC of the European Parliament and of the Council of 23 April 2009 on the geological storage of carbon dioxide and amending Council Directive 85/337/EEC, European Parliament and Council Directives 2000/60/EC, 2001/80/EC, 2004/35/EC, 2006/12/EC, 2008/1/EC and Regulation (EC) No 1013/2006.
- Færseth, R.B. and Ravnas, R. 1998. Evolution of the Oseberg fault-block in context of the northern North Sea structural framework. *Marine and Petroleum Geology*, 15, 46790.
- Fellgett, M., Hopper, J.R., Grande, L., Kingdon, A., Williams, J., Dichiarante, A.M. and Filomena, C. 2022. Borehole Stress Observations. SHARP Project Deliverable 2.2.
- Fjær, E. 2008. Petroleum related rock mechanics. 2nd edition. Elsevier, Amsterdam.
- Folstad, P.G., Morgan, P., Bertrand, A., Rossing, M. and Lyngnes, B. 2015. Ekofisk Permanent Seismic Monitoring - Results After first 4 years. Keynote Speech at the Third EAGE Workshop, Conference Proceedings, Volume 2015, 1–4.

- Fossen, H., Khani, H.F., Faleide, J.I., Ksienzyk, A.K. and Dunlap, W.J. 2017. Post-Caledonian extension in the West Norway–northern North Sea region: the role of structural inheritance. Geological Society, London, Special Publications, 439, 465–486.
- Furnival, S., Wright, S., Dingwall, S., Bailey, P., Brown, A., Morrison, D. and De Silva, R. 2014. Subsurface Characterisation of a Saline Aquifer Cited for Commercial Scale CO₂ Disposal. *Energy Procedia*, 63, 4926–4936.
- Furre, A.K., Eiken, O., Alnes, H., Vevatne, J.N. and Kiær, A.F. 2017. 20 years of monitoring CO₂-injection at Sleipner. *Energy Procedia*, 114, 3916–3926.
- Ganguli, S.S. and Sen, S. 2020. Investigation of present-day in-situ stresses and pore pressure in the south Cambay Basin, western India: Implications for drilling, reservoir development and fault reactivation. *Marine and Petroleum Geology*, 118, 104422.
- Gluyas, J.G. and Bagudu, U. 2020. The Endurance CO₂ storage site, Blocks 42/25 and 43/21, UK North Sea. In: Goffey, G. and Gluyas, J.G. (Eds.). *United Kingdom Oil and Gas Fields: 50th Anniversary Commemorative Volume*. Geological Society, London, Memoir, 52, 163–171.
- Gölke, M. and Coblenz, D. 1996. Origins of the European regional stress field. *Tectonophysics*, 266, 11–24.
- Goertz-Allmann, B.P., Langet, N., Kühn, D., Baird, A., Oates, S., Rowe, C., Harvey, S., Oye, V. and Nakstad, H. 2022. Effective microseismic monitoring of the Quest CCS site, Alberta, Canada. 16th International Conference on Greenhouse Gas Control Technologies, GHGT-16, 23rd–27th October 2022, Lyon, France.
- Grande, L., Mondol, N.H., Skurtveit, E. and Thompson, N. 2022. Stress estimation from clay content and mineralogy-EoS well in the Aurora CO₂ storage site, offshore Norway. 16th International Conference on Greenhouse Gas Control Technologies GHGT-16, 23-27th October 2022, Lyon, France.
- Griffiths, P.A., Allen, M.R., Craig, J., Fitches, W.R. and Whittington, R.J. 1995. Distinction between fault and salt control of Mesozoic sedimentation on the southern margin of the Mid-North Sea High. In: Boldy, S.A.R. (Ed.). *Permian and Triassic Rifting in Northwest Europe*. Geological Society, London, Special Publications, 91, 145–159.
- Harris, K., White, D., Melanson, D., Samson, C. and Daley, T.M. 2016. Feasibility of time-lapse VSP monitoring at the Aquistore CO₂ storage site using a distributed acoustic sensing system. *International Journal of Greenhouse Gas Control*, 50, 248–260.
- Harvey, S., Hopkins, J., Kuehl, H., O'Brien, S. and Mateeva, A. 2022. Quest CCS facility: Time-lapse seismic campaigns. *International Journal of Greenhouse Gas Control*, 117, 103665.
- Heidbach, O., Reinecker, J., Tingay, M., Müller, B., Sperner, B., Fuchs, K. and Wenzel, F. 2007. Plate boundary forces are not enough: Second- and third-order stress patterns highlighted in the World Stress Map database. *Tectonics*, 26, TC6014.
- Heidbach, O., Tingay, M., Barth, A., Reinecker, J., Kurfeß, D. and Müller, B. 2008. World Stress Map Database Release 2008.
- Heidbach, O., Tingay, M., Barth, A., Reinecker, J., Kurfeß, D. and Müller, B. 2010. Global crustal stress pattern based on the World Stress Map database release 2008. *Tectonophysics*, 482 (1-4), 3–15.
- Heidbach, O., Rajabi, M., Reiter, K., Ziegler, M. and WSM Team. 2016. World Stress Map Database Release 2016. GFZ Data Services.
- Heidbach, O., Rajabi, M., Cui, X., Fuchs, K., Müller, B., Reinecker, J., Reiter, K., Tingay, M., Wenzel, F., Xie, F., Ziegler, O., Zoback, M-L. and Zoback, M. 2018. The World Stress Map database release 2016: Crustal stress pattern across scales. *Tectonophysics*, 744, 484–498.
- Heinemann, N., Wilkinson, M., Pickup, G.E., Haszeldine, R.S. and Cutler, N.A. 2012. CO₂ storage in the offshore UK Bunter Sandstone Formation. *International Journal of Greenhouse Gas Control*, 6, 210–219.
- Hillis, R.R. and Nelson, E.J. 2005. *In situ* stresses in the North Sea and their applications: petroleum geomechanics from exploration to development. In: Dóre, A.G. and Vining, B.A. (Eds.). *Petroleum Geology: North-West Europe and Global Perspectives – Proceedings of the 6th Petroleum Geology Conference*. Geological Society, London, 551–564.
- Holden, N., Osmond, J.L., Mulrooney, M.J., Braathen, A., Skurtveit, E. and Sundal, A. 2022. Structural characterization and across-fault seal assessment of the Aurora CO₂ storage site, northern North Sea. *Petroleum Geoscience*, 28 (4), petgeo2022-2036.
- Hudson, T.S., Baird, A.F., Kendall, J.M., Kufner, S., Brisbourne, A., Smith, A., Butcher, A.C., Chalari, A. and Clarke, A. 2021. Distributed Acoustic Sensing (DAS) for natural microseismicity studies: A case study from Antarctica. *Journal of Geophysical Research: Solid Earth*, 126 (7), e2020JB021493.

- Hunfeld, L.B., Niemeijer, A.R. and Spiers, C.J. 2017. Frictional properties of simulated fault gouges from the seismogenic groningen gas field under in situ P–T–chemical conditions. *Journal of Geophysical Research: Solid Earth*, 122 (11), 8969–8989.
- Jalali, R., Forsberg, C.F., Ghoreishian, S.A., Grande, L., Singh, R.M. and Thompson, N. 2022. Evaluation of consolidation and stress history in the Quaternary sediments for purpose of CCS developments in the Horda Platform area, the Northern North Sea. 16th International Conference on Greenhouse Gas Control Technologies, GHGT-16, 23-27th October 2022, Lyon, France.
- Jenkins, C., Chadwick, A. and Hovorka, S.D. 2015. The state of the art in monitoring and verification—ten years on. *International Journal of Greenhouse Gas Control*, 40, 312–349.
- Liang, W., Yang, C., Zhao, Y., Dusseault, M.B. and Liu, J. 2007. Experimental investigation of mechanical properties of bedded salt rock. *International Journal of Rock Mechanics & Mining Sciences*, 44, 400–411.
- Ligtenberg, H., Okkerman, J. and De Keijzer, M. 2011. Fractures in the Dutch Rotliegend—An Overview. In: Grötsch, J. and Gaupp, R. (Eds.). *The Permian Rotliegend of the Netherlands*. SEPM Special Publication, 98.
- Ketter, F.J. 1991. The Esmond, Forbes and Gordon Fields, Block 43/8a, 43/13a, 43/15a, 43/20a, UK North Sea. In: Abbotts, I.L. (Ed.). *United Kingdom Oil and Gas Fields, 25 Years Commemorative Volume*. Geological Society, London, Memoir, 14, 425–432.
- Kingdon, A., Fellgett, M.W. and Williams, J.D.O. 2016. Use of borehole imaging to improve understanding of the in-situ stress orientation of Central and Northern England and its implications for unconventional hydrocarbon resources. *Marine and Petroleum Geology*, 73, 1–20.
- Kingdon, A., Williams, J., Fellgett, M., Rettelbach, N. and Heidbach, O. 2022. Stress Map of Great Britain and Ireland 2022. GFZ Data Services.
- Kole, P., Cannon, M., Tomic, J. and Bierman, S. 2020. Analysis of and learnings from the first four years on in-situ strain data in Zeerijp-3A. Shell and NAM BV report, February 2020.
- Kombrink, H., Doornenbal, J.C., Duin, E.J.T., den Dulk, M., ten Veen, J.H. and Witmans, N. 2012. New insights into the geological structure of the Netherlands; results of a detailed mapping project. *Netherlands Journal of Geosciences*, 91 (4), 419–446.
- Mandal, A., Saha, D. and Kumar, A. 2022. Structural analysis and seismic stratigraphy for delineation of Neoproterozoic-Cambrian petroleum system in central and eastern part of Bikaner–Nagaur basin, India. *Journal of Petroleum Exploration and Production Technology*, 12, 1709–1725.
- Müller, B., Zoback, M.L., Fuchs, K., Mastin, L., Gregersen, S., Pavoni, N., Stephansson, O. and Ljunggren, C. 1992. Regional patterns of tectonic stress in Europe. *Journal of Geophysical Research*, 97 (B8), 11783–11803.
- Mondol, N.H., Bjørnarå, T.I., Grande, L. and Thompson, N. 2022a. Rock physics analysis of Eos caprock shale for the Northern Lights CCS project, offshore Norway. 83rd EAGE Annual Conference & Exhibition, Madrid, Spain, 6–9 June.
- Mondol, N.H., Bjørnarå, T.I., Grande, L. and Thompson, N. 2022b. Caprock characterization of the Northern Lights CO₂ storage project, offshore Norway. EAGE GeoTech, 6th EAGE workshop on CO₂ geological storage, London, United Kingdom, 4–6 April.
- Mulrooney, M.J., Osmond, J.L., Skurtveit, E., Faleide, J.I. and Braathen, A. 2020. Structural analysis of the Smeaheia fault block, a potential CO₂ storage site, northern Horda Platform, North Sea. *Marine and Petroleum Geology*, 121, 104598.
- Muntendam-Bos, A.G. and Grobbe, N. 2022. Data-driven spatiotemporal assessment of the event-size distribution of the Groningen extraction-induced seismicity catalogue. *Scientific Reports*, 12 (1), 1–11.
- Nielsen, L.H. and Japsen, P. 1991. Deep wells in Denmark 1935-1990. Lithostratigraphic subdivision. *Danmarks Geologiske Undersøgelse Serie A*, DGU, 31, 177pp.
- Nguyen, B.N., Hou, Z., Bacon, D.H., Murray, C.J. and White, M.D. 2016. Three-dimensional modeling of the reactive transport of CO₂ and its impact on geomechanical properties of reservoir rocks and seals. *International Journal of Greenhouse Gas Control*, 46, 100–115.
- Noy, D.J., Holloway, S., Chadwick, R.A., Williams, J.D.O., Hannis, S.A. and Lahann, R.W. 2012. Modelling large-scale carbon dioxide injection into the Bunter Sandstone in the UK Southern North Sea. *International Journal of Greenhouse Gas Control*, 9, 220–233.
- Orlic, B. 2016. Geomechanical effects of CO₂ storage in depleted gas reservoirs in the Netherlands: Inferences from feasibility studies and comparison with aquifer storage. *Journal of Rock Mechanics and Geotechnical Engineering*, 8 (6), 846–859.

- Osmond, J.L., Mulrooney, M.J., Holden, N., Skurtveit, E., Faleide, J.I. and Braathen, A. 2022. Structural traps and seals for expanding CO₂ storage in the northern Horda platform, North Sea. *AAPG Bulletin*, 106 (9), 1711–1752.
- Oye, V., Dando, B., Wüstefeld, A., Jerkins, A. and Koehler, A. 2021. Cost-effective Baseline Studies for Induced Seismicity Monitoring Related to CO₂ Storage Site Preparation. Proceedings of the 15th Greenhouse Gas Control Technologies Conference, GHGT-15, 15–18 March 2021.
- Pareek, H.S. 1981. Basin configuration and sedimentary stratigraphy of western Rajasthan. *Journal of the Geological Society of India*, 22, 517–527.
- Pareek, H.S. 1984. Pre-Quaternary geology and mineral resources 1492 Biomarker Recognition of Source Rock, India of northwestern Rajasthan. *Geological Survey of India, Memoir*, 115, 99 pp.
- Pedersen, Å.S., Westerdahl, H., Thompson, M., Sagary, C. and Brenne, J.K. 2022. A North Sea case study: Does DAS have potential for Permanent Reservoir Monitoring? EAGE 2022, 83rd conference, Madrid, Spain. Paper number 170.
- Peters, K.E., Clark, M.E., Gupta, U.D., McCaffrey, M.A. and Lee, C.Y. 1995. Recognition of an Infracambrian source rock based on biomarkers in the Baghewala-1 Oil, India. *AAPG Bulletin*, 79, 1481–1494.
- Phillips, T.B., Fazlikhani, H., Gawthorpe, R.L., Fossen, H., Jackson, C.A.L., Bell, R.E., Faleide, J.I. and Rotevaten, A. 2019. The influence of structural inheritance and multiphase extension on rift development, the northern North Sea. *Tectonics*, 38, 4099–4126.
- Pollastro, R.M. 1999. Ghaba Salt Basin province and Fahud Salt Basin province—Oman: geological overview and total petroleum systems. *United States Geological Survey Bulletin*, 2167, 1–41.
- Ridder, S.A.L., Biondi, B.L. and Nichols, D. 2015. Elliptical-anisotropic eikonal phase velocity tomography, *Geophysical Research Letters*. 42, 758764.
- Ringrose, P.S., Mathieson, A.S., Wright, I.W., Selama, F., Hansen, O., Bissell, R., Saoula, N. and Midgley, J. 2013. The In Salah CO₂ storage project: lessons learned and knowledge transfer. *Energy Procedia*, 37, 6226–6236.
- Ringrose, P., Furre, A.K., Bakke, R., Dehghan Niri, R., Thompson, N., Paasch, B., Mispel, J., Sollid, A., Bussat, S., Vinge, T. and Vold, L. 2018. Developing optimised and cost-effective solutions for monitoring CO₂ injection from subsea wells. In 14th greenhouse gas control technologies conference, GHGT-14, Melbourne, October 2018, 21–26.
- Ringrose, P. 2020. CO₂ Storage Project Design. In: Ringrose, P. (Ed.). *How to Store CO₂ Underground: Insights from early-mover CCS Projects*. Springer Briefs in Earth Sciences, Springer Cham, 85–126.
- Ritchie, J.S. and Pratsides, P. 1993. The Caister fields, Block 44/23a, UK North Sea. In: Parker, J.R. (Ed.). *Petroleum Geology of Northwest Europe: Proceedings of the Fourth Conference*. Geological Society, London. 759–769.
- Roth, F. and Fleckenstein, P., 2001. Stress orientations found in north-east Germany differ from the Western European trend. *Terra Nova*, 13, 289–296.
- Rønnekleiv, E., Brenne, J.K., Waagaard, O.H. and Moussakhani, B. 2019. Distributed Acoustic Sensing For Submarine Cable Protection. SubOptic 2019 Conference, New Orleans, Louisiana, USA. Paper OP4-1.
- Rørstadbotnen, R.A., Dong, H., Landrø, M., Duffaut, K., Growe, K., Kakhkhorov, U., Wienecke, S. and Jacobsen, J. 2022. Quick-clay monitoring using DAS. *Geophysics*, paper accepted.
- Samuelson, J. and Spiers, C.J. 2012. Fault friction and slip stability not affected by CO₂ storage: Evidence from short-term laboratory experiments on North Sea reservoir sandstones and caprocks. *International Journal of Greenhouse Gas Control*, 11S, S78–S90.
- Seedhouse, J.K. and Racey, A. 1997. Sealing capacity of the Mercia Mudstone Group in the East Irish Sea Basin: Implications for petroleum exploration. *Journal of Petroleum Geology*, 20, 261–286.
- Smith, D.J., Noy, D.J., Chadwick, R.A. and Holloway, S. 2011. The impact of boundary conditions on CO₂ storage capacity estimation in aquifers. *Energy Procedia*, 4, 4828–4834.
- Skurtveit, E., Choi, J.C., Mulrooney, M., Osmond, J.L. and Braathen, A. 2018. 3D fault integrity screening for Smeaheia CO₂ injection site. 14th Greenhouse Gas Control Technologies Conference, GHGT-14. Melbourne, 21–26 October 2018.
- Spain, J.D. and Conrad, C.P. 1997. Quantitative analysis of top-seal capacity: Offshore Netherlands, Southern North Sea. *Geologie en Mijnbouw*, 76, 217–226.
- SPE, 2017. CO₂ Storage Resources Management System, SRMS. 50pp.
- Stewart, S.A. and Coward, M.P. 1995. Synthesis of salt tectonics in the southern North Sea, UK. *Marine and Petroleum Geology*, 12 (5), 457–475.
- Sørensen, M.B., Voss, P.H., Havskov, J., Gregersen, S. and Atakan, K. 2011. The seismotectonics of western Skagerrak. *Journal of Seismology*, 15, 599–611.

- Streit, J.E. and Hillis, R.R. 2004. Estimating fault stability and sustainable fluid pressures for underground storage of CO₂ in porous rock. *Energy*, 29, 1445–1456.
- Teufel, L.W. 1991. Influence of lithology and geologic structure on in situ stress: examples of stress heterogeneity in reservoirs. In: Lake, L.W., Carroll, H.N. and Wesson, T.C. (Eds.). *Reservoir Characterization II*. Academic Press, San Diego, 565–579.
- Thompson, N., Andrews, J.S. and Bjørnarå, T.I. 2021. Assessing potential thermo-mechanical impacts on caprock due to CO₂ injection – A case study from Northern Lights CCS. *Energies*, 14 (16), 5054.
- Thompson, N., Andrews, J.S., Meneguolo, R. and Wu, L. 2022a. Characterization of the in-situ stress on the Horda platform – A study from the Northern Lights Eos well. *International Journal of Greenhouse Gas Control*, 114, 103580.
- Thompson, N., Andrews, J.S., Teixeira Rodrigues, N.E. and Reitan, H. 2022b. Data mining of in-situ stress database towards development of regional and global stress trends and pore pressure relationships. SPE Norway Subsurface Conference, 27th April, Bergen. SPE Paper 209525.
- Tingay, M., Benthams, P., De Feyter, A. and Kellner, A. 2011. Present-day stress-field rotations associated with evaporites in the offshore Nile Delta. *GSA Bulletin*, 123 (5/6), 1171–1180.
- Tjaland, N. and Ottemoller, L. 2018. Evaluation of Seismicity in the Northern North Sea. Technical report, NNSN, University of Bergen, 10–14.
- Underhill, J.R. 2009. Role of intrusion-induced salt mobility in controlling the formation of the enigmatic ‘Silverpit Crater’, UK Southern North Sea. *Petroleum Geoscience*, 15, 197–216.
- Vasco, D.W., Rucci, A., Ferretti, A., Novali, F., Bissell, R.C., Ringrose, P.S., Mathieson, A.S. and Wright, I.W. 2010. Satellite-based measurements of surface deformation reveal fluid flow associated with the geological storage of carbon dioxide. *Geophysical Research Letters*, 37, L03303.
- Walter, F., Gräff, D., Lindner, F., Paitz, P., Köpfli, M., Chmiel, M. and Fichtner, A. 2020. Distributed acoustic sensing of microseismic sources and wave propagation in glaciated terrain. *Nature Communications*, 11, 2436.
- Weemstra, C., Kettlety, T., Kühn, D., Martuganova, E., Schweitzer, J., Baptie, B. and Dahl-Jensen, T. 2022. Integrated earthquake locations and magnitudes plus focal mechanisms for the North Sea & construction of a velocity model. *SHARP Project Deliverable 2.1*.
- Whipp, P.S., Jackson, C.L., Gawthorpe, R.L., Dreyer, T. and Quinn, D. 2014. Normal fault array evolution above a reactivated rift fabric; a subsurface example from the northern Horda Platform, Norwegian North Sea. *Basin Research*, 26, 523–549.
- Wienecke, S., Jacobsen, J., Brenne, J.-K., Landrø, M., Dong, H., Rørstadbotnen, R. A., Kakhkhorov, U. and Growe, K. 2022. Distributed acoustic sensing for quick clay monitoring. EGU General Assembly 2022, Vienna, Austria, 23–27 May 2022, EGU22-6538.
- Williams, J.D.O., Benthams, M., Jin, M., Pickup, G., Mackay, E., Gammer, D. and Green, A. 2013a. The effect of geological structure and heterogeneity on CO₂ storage in simple 4-way dip structures; a modelling study from the UK Southern North Sea. *Energy Procedia*, 37, 3980–3988.
- Williams, J.D.O., Jin, M., Pickup, G.E., Hannis, S.D. and Mackay, E.J. 2013b. Modelling carbon dioxide storage within closed structures in the UK Bunter Sandstone Formation. *International Journal of Greenhouse Gas Control*, 18, 38–50.
- Williams, J.D.O., Holloway, S. and Williams, G.A. 2014. Pressure constraints on the CO₂ storage capacity of the saline water-bearing parts of the Bunter Sandstone Formation in the UK Southern North Sea. *Petroleum Geoscience*, 20, 155–167.
- Williams, J.D.O., Fellgett, M.W., Kingdon, A. and Williamson, J.P. 2015. *In-situ* stress orientations in the UK Southern North Sea: Regional trends, deviations and detachment of the post-Zechstein stress field. *Marine and Petroleum Geology*, 67, 769–784.
- White Rose, 2016. K43: Field Development Report, Technical: Storage. Capture Power and National Grid. 234pp.
- Wu, L., Thorsen, R., Ottesen, S., Meneguolo, R., Hartvedt, K., Ringrose, P. and Nazarian, B. 2021. *Petroleum Geoscience*, 27 (3), 2020-102.
- Wu, L., Skurtveit, E., Thompson, N., Michie, E., Fossen, H., Braathen, A., Fisher, Q., Lidstone, A. and Bostrøm, B. 2022. Containment Risk Assessment and Management of CO₂ Storage on the Horda Platform. 16th International Conference on Greenhouse Gas Control Technologies, GHGT-16, 23-27th October 2022, Lyon, France.
- Yassir, N.A. and Zerwer, A. 1997. Stress regimes in the Gulf Coast, offshore Louisiana: data from well-bore breakout analysis. *AAPG Bulletin*, 81 (2), 293–307.

- Zarifi, Z., Köhler, A., Ringrose, P., Ottemöller, L., Furre, A-K, Hansteen, F., Jerkins, A., Oye, V., Dehghan Niri, R. and Bakke, R. 2022a. Background seismicity monitoring to prepare for large-scale CO₂ storage offshore Norway. *Seismological Research Letters*, November 22, 2022.
- Zarifi, Z., Ringrose, P., Köhler, A., Oye, V., Ottemöller, L., Bakke, R., Rebel, E., Dehghan Niri, R., Sørensen, M., Jerkins, A., Karlsen, M. and Furre, A-K. 2022b. Background seismicity monitoring prior to CO₂ injection in the Horda Platform: The HNET project. 16th International Conference on Greenhouse Gas Control Technologies, GHGT-16, 23rd–27th October 2022, Lyon, France.